

A STUDY ON SEISMIC BEHAVIOR OF SCOUR-VULNERABLE BRIDGES

A THESIS SUBMITTED TO  
THE GRADUATE SCHOOL OF NATURAL AND APPLIED SCIENCES  
OF  
MIDDLE EAST TECHNICAL UNIVERSITY

BY

HALE SEMA KIZILDUMAN

IN PARTIAL FULFILLMENT OF THE REQUIREMENTS  
FOR  
THE DEGREE OF MASTER OF SCIENCE  
IN  
CIVIL ENGINEERING

AUGUST 2016



Approval of the thesis:

**A STUDY ON SEISMIC BEHAVIOR OF SCOUR-VULNERABLE BRIDGES**

submitted by **HALE SEMA KIZILDUMAN** in partial fulfillment of the requirements for the degree of **Master of Science in Civil Engineering Department, Middle East Technical University** by,

Prof. Dr. Gülbin Dural Ünver  
Dean, Graduate School of **Natural and Applied Sciences** \_\_\_\_\_

Prof. Dr. İsmail Özgür Yaman  
Head of Department, **Civil Engineering** \_\_\_\_\_

Prof. Dr. A. Melih Yanmaz  
Supervisor, **Civil Engineering Dept., METU** \_\_\_\_\_

Assoc. Prof. Dr. Alp Caner  
Co-Supervisor, **Civil Engineering Dept., METU** \_\_\_\_\_

**Examining Committee Members:**

Prof. Dr. M. Altuğ Erberik  
Civil Engineering Dept., METU \_\_\_\_\_

Prof. Dr. A. Melih Yanmaz  
Civil Engineering Dept., METU \_\_\_\_\_

Assoc. Prof. Dr. Alp Caner  
Civil Engineering Dept., METU \_\_\_\_\_

Assoc. Prof. Dr. Ayşegül Askan Gündoğan  
Civil Engineering Dept., METU \_\_\_\_\_

Asst. Prof. Dr. Melih Çalamak  
Civil Engineering Dept., TED University \_\_\_\_\_

**Date:** \_\_\_\_\_ 25.08.2016 \_\_\_\_\_

**I hereby declare that all information in this document has been obtained and presented in accordance with academic rules and ethical conduct. I also declare that, as required by these rules and conduct, I have fully cited and referenced all material and results that are not original to this work.**

Name, Surname: Hale Sema KIZILDUMAN

Signature:

## **ABSTRACT**

### **A STUDY ON SEISMIC BEHAVIOR OF SCOUR-VULNERABLE BRIDGES**

Kızılduman, Hale Sema

M. Sc., Department of Civil Engineering

Supervisor: Prof. Dr. A. Melih Yanmaz

Co-supervisor: Assoc. Prof. Dr. Alp Caner

August 2016, 131 pages

Scour under bridge foundations typically causes serious defects or failures. The studies on seismic behavior of bridges scoured prior to earthquake are very limited. Although earthquakes are not one of the top reasons for bridge failures or damages, when the effects of earthquakes and scour are combined, the structure can become highly vulnerable to failure. In Turkey, during the design process of bridges, the earthquake effects are seriously considered, but the combined effect of scour and earthquake is not normally analyzed. This study aims to evaluate differences of structural behavior proportionally in scoured and not scoured bridges. In this context, a two-span reinforced concrete bridge is selected for this study. For six different flood conditions, water surface profiles are obtained via hydraulic analysis and response spectrum analyses are made for earthquakes with four different return periods. There are two ground structure scenarios studied in analyses; two layers with sand and clay and one layer of sand. The results have shown that the moments

on columns and the fundamental periods of the structure are decreased. As a result, an increase in column capacity is observed to be dependent on the scour depth. On the other side, it is seen that pile capacities decrease and shear force and moments on piles increase due to scour. The stability of the bridge becomes more questionable as the pile load carrying capacity decreases due to loss of skin friction.

**Keywords:** Bridge, bridge scour, earthquake, structural behavior

## ÖZ

### AYAĞI OYULMA EĞİLİMLİ KÖPRÜLERDE DEPREM DAVRANIŞININ İNCELENMESİ ÜZERİNE BİR ÇALIŞMA

Kızılduman, Hale Sema

Yüksek Lisans, İnşaat Mühendisliği Bölümü

Tez Yöneticisi: Prof. Dr. A. Melih Yanmaz

Ortak Tez Yöneticisi: Assoc. Prof. Dr. Alp Caner

Ağustos 2016, 131 sayfa

Köprü ayaklarındaki oyulmalar, köprülerde ciddi hasarlara ya da göçüklere sebep olmaktadır. Depremden önce ayağı oyulmuş olan köprülerin deprem davranışı çalışmaları oldukça sınırlıdır. Deprem ise köprülerin hasar görme ve göçme sebepleri arasında ileri sıralarda olmasa da oyulma ile birleştiğinde yapıyı kolayca zarar görebilir hale getirmektedir. Köprü tasarımları yapılırken deprem dikkate alınıyor olsa da oyulma ve depremin ikili etkisi ülkemizde incelenmemektedir. Bu çalışma, orta ayağı oyulmuş köprülerde deprem performansını inceleyerek değişimleri oransal olarak değerlendirmeyi hedeflemektedir. Bu bağlamda; iki açıklıklı betonarme örnek bir köprü seçilerek analizler onun üzerinden yapılmıştır. Altı farklı dönüş aralığına sahip taşkın için su yüzü profilleri hidrolik analizler sonucunda elde edilmiş ve dört farklı dönüş aralığına sahip deprem altında tepki spektrum analizi yapılmıştır. Analizlerde zeminin iki katmanlı; kum ve kil ve tek katmanlı; sadece kum olduğu senaryolar incelenmiştir. Analiz sonuçları yapı doğal periyotlarının uzadığını ve kolona gelen momentlerin azaldığını göstermektedir. Bunun sonucunda kolon kapasitesinde oyulma miktarına bağlı olarak artış gözlenmiştir. Diğer taraftan,

oyulmadan dolayı kazıkların taşıma gücünde azalma meydana geldiği ve oyulma miktarına bağlı olarak kazıklara gelen kesme kuvveti ve momentlerin arttığı görülmektedir. Yüzey sürtünmesinin kaybına bağlı olarak kazıkların taşıma kapasitesinin azalması ile köprü stabilitesi daha şüpheli duruma gelmektedir.

Anahtar kelimeler: Köprü, köprü ayaklarında oyulma, deprem, yapısal davranış

To my beloved Toygar

## ACKNOWLEDGEMENTS

I would like to express my sincere gratitude to my supervisor Prof. Dr. A. Melih Yanmaz, for his guidance, patience, attention, insightful comments, and useful critiques throughout this study. His guidance and perfectionistic approach encouraged me to do better.

Besides my supervisor, I would like to express my deep appreciation to my Co-Supervisor Assoc. Prof. Dr. Alp Caner for his enthusiastic approach, scientific perspective, suggestions, continuous guidance and invaluable support. He always encouraged me and never withheld his help.

I would like to thank to Ekin Akkaya from DTA Engineering for the information he provided for my thesis study.

I would like to thank to my friend Gülçe Hazal Ak for her sincere friendship and moral support. She never left me alone throughout endless Harry Potter and Lord of the Rings discussions and made me smile whenever I need.

I would like to express my heartfelt gratitude to my friends; Murat Yeğın and Tunç Gökdemir for their encouragement and motivation throughout my research.

I also owe thanks to my friend Çağrı İllez. He is one of the most thoughtful person I have met in my life. I appreciate to him for his delicious foods, warm smile and true friendship.

A special thanks to my childhood friend Tuğba Erten. She is always with me not only as a friend but also as a sister. She is always as close as a phone call. I cannot forget her importance in my life.

I would like to express my deepest appreciations to my family for their sacrifices and unconditional love. Words cannot express how grateful I am to them; especially my parents Nezihe Murat and Muhlis Murat and my intelligent elder brother Ertuğrul Murat. I am very proud of being a part of this family.

Finally, I am deeply thankful to my husband, Toygar Kızılduman. Without his help, patience and understanding, this study would not have been completed. He is always with me at the hardest and most stressful times not only in this thesis period but also in my life. He made everything easier, funnier and possible for me with his love and intelligence. I am the luckiest person in the planet to have him.

# TABLE OF CONTENTS

ABSTRACT.....	v
ÖZ .....	vii
ACKNOWLEDGEMENTS.....	x
TABLE OF CONTENTS.....	xii
LIST OF TABLES.....	xv
LIST OF FIGURES .....	xvii
LIST OF SYMBOLS .....	xxiii
CHAPTERS.....	1
1. INTRODUCTION .....	1
1.1    STATEMENT OF THE PROBLEM.....	1
1.2    OBJECTIVE AND SCOPE OF THE STUDY .....	4
2. LITERATURE REVIEW .....	7
2.1    BACKGROUND .....	7
2.2    REVIEW OF PREVIOUS STUDIES.....	10
2.2.1    Scour Prediction Equations.....	10
2.2.2    Researches on Scoured Bridges Under Seismic Effects .....	14
3. SOFTWARE AND METHODOLOGY .....	21
3.1    SOFTWARE.....	21
3.1.1    HEC-RAS .....	22

3.1.2	LARSA4D .....	22
3.1.3	TASARIM SPEKTRUM-2.....	22
3.1.4	CSiCOL .....	22
3.2	ANALYSIS METHODOLOGY.....	23
3.2.1	Description of the Study Area.....	23
3.2.2	Hydraulic Analysis Methodology.....	24
3.2.3	Structural Analysis Methodology .....	34
4.	ANALYSIS PROCEDURE.....	39
4.1	INTRODUCTION .....	39
4.1.1	Probabilistic Evaluations .....	39
4.2	HYDRAULIC ANALYSIS .....	43
4.2.1	Hydraulic Properties and Computer Model.....	43
4.2.2	Soil Properties.....	44
4.2.3	Scour Calculations .....	46
4.3	STRUCTURAL ANALYSIS .....	47
4.3.1	Description of the Bridge.....	47
4.3.2	Material Properties.....	51
4.3.3	Local Soil Properties.....	51
4.3.4	Structural Computer Model .....	53
4.3.5	Modal Analysis .....	69
4.3.6	Response Spectrum Analysis.....	72
4.4	RESULTS .....	74
4.4.1	Column Demand to Capacity Ratio .....	74
4.4.2	Pile Load Capacity.....	77
4.4.3	Pile M-N Interaction Curve .....	86

4.4.4	Pile Shear Force Check.....	99
5.	CONCLUSION.....	101
	REFERENCES .....	105
	APPENDIX A.....	111
	PILE M-N CURVES .....	111

## LIST OF TABLES

Table 2.1. Pier shape coefficient table (Melville, 1997).....	12
Table 2.2. Bed form coefficient table (Arneson et. al., 2012) .....	13
Table 3.1. Pier nose shape correction factor list (Arneson et. al., 2012).....	30
Table 3.2. Bed condition correction factor list (Arneson et. al., 2012) .....	31
Table 4.1. Probability of earthquake occurrence for return periods: 100 years, 250 years, 475 years and 1000 years .....	41
Table 4.2. Probability of flood occurrence for return periods: 2 years, 5 years, 10 years, 25 years, 50 years and 100 years.....	42
Table 4.3. Joint probability of earthquake and flood events.....	42
Table 4.4. Flood frequency and discharge table .....	43
Table 4.5. Flow velocities and flow depths at corresponding discharges at bridge location.....	44
Table 4.6. Particle $D_{10}$ , $D_{50}$ , $D_{60}$ and $D_{95}$ values .....	44
Table 4.7. Coefficients and inputs that are used in scour calculations .....	46
Table 4.8. Scour depth summary table.....	46
Table 4.9. Material properties of corresponding sections.....	51
Table 4.10. SPT correction factors (Birand et. al., 2011) .....	52
Table 4.11. Uncorrected and corrected N values .....	53
Table 4.12. Member list used in structural model .....	54
Table 4.13. List of SPT results of SK-1 and SK-2.....	61
Table 4.14. Values of $n_h$ ( $\text{kN/m}^3$ ) for sand (Poulos and Davis, 1980).....	63

Table 4.15. Pile spring modulus of subgrade reaction and effective modulus of subgrade reaction list .....	64
Table 4.16. Pile spring stiffness constant according to Winkler’s spring system.....	66
Table 4.17. Column DCR matrix for two layered system .....	75
Table 4.18. Column DCR matrix for one layered system.....	76
Table 4.19. Angle of internal friction values according to Peck and Meyerhof (Gunaratne, 2013) .....	79
Table 4.20. Capacity table for a single pile .....	82
Table 4.21. Ultimate load capacity and axial load table .....	83
Table 4.22. $N_q$ values .....	85
Table 4.23. Acted shear forced for both directions $F_y$ and $F_z$ .....	100

## LIST OF FIGURES

Figure 1.1. Yayakent Bridge view after flood in January, 2016 (Tuna, 2016).....	1
Figure 1.2. Damaged view of Akçaova Bridge in July, 2016 (Sozcu, 2016) .....	2
Figure 1.3. Damaged view of Karşıyaka Bridge in May, 2016 (İleri, 2016).....	2
Figure 1.4. Collapsed view of Çaycuma Bridge after flood in 2012 (Sondevir, 2012)3	
Figure 1.5. Damaged view of the bridge at Devrek due to scour (Yanmaz, 2002) .....	3
Figure 2.1. Free body diagram of a sediment particle (Yanmaz, 2014) .....	8
Figure 2.2. Vortex formation in scour hole (ETH, 2009).....	9
Figure 2.3. Risk curves for different span types (Alipour et al., 2010).....	14
Figure 2.4. Variation of displacement at bridge pier and $d_s/D$ under strong earthquake LA40 and moderate earthquake LA06, respectively (Banerjee and Prasad, 2011)...	16
Figure 2.5 Relation between $D/d_{eq}$ and displacement at top of the pier under earthquakes LA40 and LA06 for 2-span bridge and $d_s/D=0.625$ (Banerjee and Prasad, 2011).....	17
Figure 2.6. Relation between $d_s/D$ and displacement at top of pier for different $D/d_{eq}$ for 2-span bridge (Banerjee and Prasad, 2011).....	17
Figure 2.7. Abutment force-displacement hysteresis curve for ground motion with 50% (Fioklou and Alipour, 2014).....	18
Figure 2.8. Abutment force-displacement hysteresis curve for ground motion with 10% (Fioklou and Alipour, 2014).....	19
Figure 2.9. Abutment force-displacement hysteresis curve for ground motion with 2% (Fioklou and Alipour, 2014).....	19

Figure 3.1. Softwares operation order.....	21
Figure 3.2 Banaz region location on map of Turkey .....	23
Figure 3.3. Bridge and borehole location on satellite view .....	23
Figure 3.4. Hydraulic analysis process .....	24
Figure 3.5. HEC-RAS view of river geometry and cross-sections .....	25
Figure 3.6. HEC-RAS view: bridge geometry definition .....	27
Figure 3.7. HEC-RAS view: velocity distribution for a single section .....	28
Figure 3.8. HEC-18 method scour components figure (Richardson and Davis, 2001) .....	29
Figure 3.9. Velocity component at pile cap elevation (Yanmaz, 2002) .....	34
Figure 3.10. Structural analysis process .....	35
Figure 3. 11. Geometry of a bridge frame view from LARSA 4D finite element model.....	37
Figure 4.1. Sieve analysis test graph at SK-1 .....	45
Figure 4.2. Sieve analysis test results at SK-2 .....	45
Figure 4.3. Scour depth results for two layered system and one layered system .....	47
Figure 4.4. Longitudinal cross-section of Banaz bridge (Dimensions in cm) .....	48
Figure 4.5. Plan view of Banaz bridge (Dimensions in cm).....	49
Figure 4.6. Cross-sectional view of superstructure (Dimensions in cm).....	50
Figure 4.7. 3D view of bridge modeled in LARSA 4D .....	54
Figure 4.8. Cropped model view of the bridge in YZ plane .....	55
Figure 4.9. Precast beam cross-sectional view and dimensions (Dimensions in cm) .....	56
Figure 4.10. Cap beam cross-sectional view and dimensions (Dimensions in cm)...	56
Figure 4.11. Elastomeric bearing cross-sectional view (Dimensions in mm) .....	57
Figure 4.12. Column view and cross-section.....	58

Figure 4.13. Effective stiffness of cracked reinforced concrete circular section (CALTRANS-SDC, 2006).....	59
Figure 4.14. Effective stiffness of cracked reinforced concrete rectangular section (CALTRANS-SDC, 2006).....	59
Figure 4.15. Plan view of pier foundation .....	60
Figure 4.16. Plasticity index and $f_1$ value relation (Stroud,1989).....	62
Figure 4.17. SPT-N value and undrained shear strength relation (Prakash and Sharma, 1990).....	62
Figure 4.18. Winkler’s spring system (Caner, 2014).....	65
Figure 4.19. Foundation layout (Das, 2007).....	67
Figure 4.20 Mode shape 1 and fundamental period of original no scouring case .....	69
Figure 4.21. Mode shape 2 and fundamental period of original no scouring case ....	70
Figure 4.22. Mode shape 3 and fundamental period of original no scouring case ....	70
Figure 4.23. Mode shape 1 and fundamental period of 100-year flood case.....	71
Figure 4.24. Mode shape 2 and fundamental period of 100-year flood case.....	71
Figure 4.25. Mode shape 3 and fundamental period of 100-year flood case.....	72
Figure 4.26. Design spectrums for bridge location for return periods: 100 years, 250 years, 475 years and 1000 years .....	73
Figure 4.27. Unit frictional resistance and effective length of pile representation (Das, 2007).....	78
Figure 4.28. Pressure distribution through the pile for Scenario 1 .....	80
Figure 4.29. Adhesion factor and undrained shear strength relation (Das, 2007) .....	81
Figure 4.30. Axial load and single pile capacity change for different flow rates .....	83
Figure 4.31. Axial load and group pile capacity change for different flow rates .....	84
Figure 4.32 Pressure distribution through the pile for Scenario 2 .....	85
Figure 4.33. Moment change under different conditions for the load combination 8	86

Figure 4.34. No scour case pile M-N interaction diagram for Combination 1 .....	88
Figure 4.35. No scour case pile M-N interaction diagram for Combination 8 .....	88
Figure 4.36. No scour case pile M-N interaction diagram for Combination 9 .....	89
Figure 4.37. $Q_2$ case pile M-N interaction diagram for Combination 1 .....	89
Figure 4.38. $Q_2$ case pile M-N interaction diagram for Combination 8 .....	90
Figure 4.39. $Q_2$ case pile M-N interaction diagram for Combination 9 .....	90
Figure 4.40. $Q_5$ case pile M-N interaction diagram for Combination 1 .....	91
Figure 4.41. $Q_5$ case pile M-N interaction diagram for Combination 8 .....	91
Figure 4.42. $Q_5$ case pile M-N interaction diagram Combination 9 .....	92
Figure 4.43. $Q_{10}$ case pile M-N interaction diagram for Combination 1 .....	92
Figure 4.44. $Q_{10}$ case pile M-N interaction diagram for Combination 8 .....	93
Figure 4.45. $Q_{10}$ case pile M-N interaction diagram for Combination 9 .....	93
Figure 4.46. $Q_{25}$ case pile M-N interaction diagram for Combination 1 .....	94
Figure 4.47. $Q_{25}$ case pile M-N interaction diagram for Combination 8 .....	94
Figure 4.48. $Q_{25}$ case pile M-N interaction diagram for Combination 9 .....	95
Figure 4.49. $Q_{50}$ case pile M-N interaction diagram for Combination 1 .....	95
Figure 4.50. $Q_{50}$ case pile M-N interaction diagram for Combination 8 .....	96
Figure 4.51. $Q_{50}$ case pile M-N interaction diagram for Combination 9 .....	96
Figure 4.52. $Q_{100}$ case pile M-N interaction diagram for Combination 1 .....	97
Figure 4.53. $Q_{100}$ case pile M-N interaction diagram for Combination 8 .....	97
Figure 4.54. $Q_{100}$ case pile M-N interaction diagrams for Combination 9 .....	98
Figure A.1. No scour case pile M-N interaction diagram for Combination 2 .....	111
Figure A.2. No scour case pile M-N interaction diagram for Combination 3 .....	111
Figure A.3. No scour case pile M-N interaction diagram for Combination 4 .....	112
Figure A.4. No scour case pile M-N interaction diagram for Combination 5 .....	112

Figure A.5. No scour case pile M-N interaction diagram for Combination 6 .....	113
Figure A.6. No scour case pile M-N interaction diagram for Combination 7 .....	113
Figure A.7. Q <sub>2</sub> case pile M-N interaction diagram for Combination 2.....	114
Figure A.8. Q <sub>2</sub> case pile M-N interaction diagram for Combination 3.....	114
Figure A.9. Q <sub>2</sub> case pile M-N interaction diagram for Combination 4.....	115
Figure A.10. Q <sub>2</sub> case pile M-N interaction diagram for Combination 5.....	115
Figure A.11. Q <sub>2</sub> case pile M-N interaction diagram for Combination 6.....	116
Figure A.12. Q <sub>2</sub> case pile M-N interaction diagram for Combination 7.....	116
Figure A.13. Q <sub>5</sub> case pile M-N interaction diagram for Combination 2.....	117
Figure A.14. Q <sub>5</sub> case pile M-N interaction diagram for Combination 3.....	117
Figure A.15. Q <sub>5</sub> case pile M-N interaction diagram for Combination 4.....	118
Figure A.16. Q <sub>5</sub> case pile M-N interaction diagram for Combination 5.....	118
Figure A.17. Q <sub>5</sub> case pile M-N interaction diagram for Combination 6.....	119
Figure A.18. Q <sub>5</sub> case pile M-N interaction diagram for Combination 7.....	119
Figure A.19. Q <sub>10</sub> case pile M-N interaction diagram for Combination 2 .....	120
Figure A.20. Q <sub>10</sub> case pile M-N interaction diagram for Combination 3 .....	120
Figure A.21. Q <sub>10</sub> case pile M-N interaction diagram for Combination 4 .....	121
Figure A.22. Q <sub>10</sub> case pile M-N interaction diagram for Combination 5 .....	121
Figure A.23. Q <sub>10</sub> case pile M-N interaction diagram for Combination 6 .....	122
Figure A.24. Q <sub>10</sub> case pile M-N interaction diagram for Combination 7 .....	122
Figure A.25. Q <sub>25</sub> case pile M-N interaction diagram for Combination 2 .....	123
Figure A.26. Q <sub>25</sub> case pile M-N interaction diagram for Combination 3 .....	123
Figure A.27. Q <sub>25</sub> case pile M-N interaction diagram for Combination 4 .....	124
Figure A.28. Q <sub>25</sub> case pile M-N interaction diagram for Combination 5 .....	124
Figure A.29. Q <sub>25</sub> case pile M-N interaction diagram for Combination 6 .....	125

Figure A.30. Q <sub>25</sub> case pile M-N interaction diagram for Combination 7 .....	125
Figure A.31. Q <sub>50</sub> case pile M-N interaction diagram for Combination 2 .....	126
Figure A.32. Q <sub>50</sub> case pile M-N interaction diagram for Combination 3 .....	126
Figure A.33. Q <sub>50</sub> case pile M-N interaction diagram for Combination 4 .....	127
Figure A.34. Q <sub>50</sub> case pile M-N interaction diagram for Combination 5 .....	127
Figure A.35. Q <sub>50</sub> case pile M-N interaction diagram for Combination 6 .....	128
Figure A.36. Q <sub>50</sub> case pile M-N interaction diagram for Combination 7 .....	128
Figure A.37. Q <sub>100</sub> case pile M-N interaction diagram for Combination 2 .....	129
Figure A.38. Q <sub>100</sub> case pile M-N interaction diagram for Combination 3 .....	129
Figure A.39. Q <sub>100</sub> case pile M-N interaction diagram for Combination 4 .....	130
Figure A.40. Q <sub>100</sub> case pile M-N interaction diagram for Combination 5 .....	130
Figure A.41. Q <sub>100</sub> case pile M-N interaction diagram for Combination 6 .....	131
Figure A.42. Q <sub>100</sub> case pile M-N interaction diagram for Combination 7 .....	131

## LIST OF SYMBOLS

$A$	Flow area
$A_b$	Plan area of bearing
$A_g$	Area of gross concrete section
$A_p$	Area of pile tip
$A_s$	Shaft friction area
$A_{st}$	Area of longitudinal bars
$b$	Pier width
$b'$	Width of pier projected normal to approach flow
$b_s^*$	Equivalent pier width
$b_w$	Width of the pile section
$C_B$	Correction for the borehole diameter
$C_R$	Correction factor for rod length
$C_S$	Correction factor for samplers with and without liners
$c_u$	Undrained shear strength soil
$D$	Pile diameter
$d$	Center to center spacing between adjacent piles

$d_{eq}$	Equivalent pile diameter
$D_{10}$	Grain size for which 10% is finer than this size
$D_{16}$	Grain size for which 16% is finer than this size
$D_{50}$	Median sediment size
$D_{60}$	Grain size for which 60% is finer than this size
$D_{84}$	Grain size for which 84% is finer than this size
$D_{95}$	Grain size for which 95% is finer than this size
DC	Dead load
DCR	Demand to capacity ratio
$d_s$	Scour depth
$d_{sp}$	Scour component for the pier stem in flow
$d_{ss}$	Scour component for the pile cap or footing in the flow
E	Elastic modulus of bearing
$EQ_{II}$	Earthquake load according to return period and direction
ER	Hammer energy ratio
$E_s$	Modulus elasticity of reinforcing steel
$f_{av}$	Average unit frictional resistance
$f'_c$	Concrete strength
$F_r$	Froude number
$F_{rc}$	Critical Froude number

$F_y$	Shear force acted in Y direction
$f_y$	Minimum design yield strength of reinforcing steel
$F_z$	Shear force acted in Z direction
$g$	Gravitational acceleration
$G$	Shear modulus of the elastomer
$h_0$	Height of pile cap above bed at the beginning of computations
$h_2$	Height of pile cap after pier stem scour component has been computed
$h_{rt}$	Total thickness of elastomeric layers
$I$	Moment of inertia of bearing
$I_e$	Effective moment of inertia of reinforced concrete section
$I_g$	Gross moment of inertia of reinforced concrete section
$K$	Effective earth coefficient
$K_b$	Bed form factor
$K_d$	Correction factor for sediment size
$k_{eff}$	Reduced modulus subgrade reaction of soil
$k_h$	Modulus of subgrade reaction of soil
$K_H$	Pile spring stiffness constant
$K_{hp}$	Coefficient to account for height of pier stem above bed
$K_i$	Correction factor for flow intensity

$K_o$	Coefficient for pier type
$K_s$	Correction factor for pier shape
$k_s$	Grain roughness of the bed
$k_{sr}$	Rotational stiffness of the bearing
$k_{tr}$	Horizontal stiffness of the bearing
$k_{vr}$	Vertical stiffness of the bearing
$K_w$	Factor accounting for wide pier
$K_{yb}$	Correction factor for flow depth and pier size
$K_z$	Bed armoring factor
$K_\theta$	Correction factor for flow alignment
$l$	Length of pier
$L$	Pile length in soil layer
$L'$	Effective pile length in soil
$M_m$	Maximum bending moment of the bearing
$M_n$	Nominal moment strength
$M_u$	Ultimate moment strength
$n$	Frequency of event
$N$	Measured SPT N value
$n_1$	Number of piles in one row
$n_2$	Number of piles in one column

$N_{60}$	SPT N-value corrected for 60% energy efficiency
$(N_{60})_{ave}$	Average SPT N-value corrected for 60% energy efficiency
$N_c$	Bearing capacity factor for cohesion for deep foundations
$N_s$	Number of particles
$P$	Axial load acted on section
$p$	Perimeter of the cross-section of each pile
$P(E)$	Probability of occurrence of earthquake event
$P(F)$	Probability of occurrence of flood event
$P(J)$	Joint probability of flood and earthquake
$R$	Response modification factor
SSI	Soil structure interaction
$Q$	Flow rate
$Q_{g(u)}$	Ultimate load bearing capacity of the pile group
$Q_p$	Total bearing resistance
$Q_{p,clay}$	Total bearing resistance in cohesive soil
$Q_{p,sand}$	Total bearing resistance in cohesionless soil
$Q_s$	Total shaft resistance
$Q_{s,clay}$	Total shaft resistance in cohesive soil
$Q_{s,sand}$	Total shaft resistance in cohesionless soil
$Q_u$	Ultimate load bearing capacity of each pile without group effect

$T$	Foundation thickness
$t$	Service time
$T_r$	Return period
$u$	Approach flow average velocity
$u_c$	Mean threshold velocity
$u_2$	Adjusted velocity for pile cap computations
$u_f$	Average velocity in the flow zone below the top of the footing
$V_c$	Shear strength provided by concrete
$V_s$	Shear strength provided by steel
$V_u$	Factored shear force at the section
$x$	Number of successful events
$y$	Flow depth directly upstream of the pier
$y_1$	Approach flow depth at the beginning of computations
$y_2$	Adjusted flow depth for pile cap computations
$y_c$	Critical depth
$y_f$	Distance from the bed to the top of the pile cap
$y_n$	Normal depth
$z$	Depth through the soil
$\alpha$	Adhesion factor
$\gamma'$	Effective unit weight of soil

$\gamma_{\text{sat}}$	Saturated specific weight of soil
$\gamma_{\text{water}}$	Specific weight of water
$\Delta$	Relative density
$\delta$	Friction angle between soil and pile
$\Delta_D$	Bridge girder displacement
$\Delta_y$	Bridge girder yield displacement
$\eta$	Group efficiency of piles
$\theta$	Attack angle of flow
$\theta_m$	Maximum design rotation
$\mu_\Delta$	Displacement ductility
$\sigma_g$	Geometric standard deviation of sediment mixture
$\sigma_o'$	Effective vertical stress at the depth under consideration
$\phi$	Internal angle of friction of soil
$\varphi$	Strength reduction factor



# CHAPTER 1

## INTRODUCTION

### 1.1 STATEMENT OF THE PROBLEM

Bridge design is evaluated by considering several aspects, such as structural, hydraulic, economic, and construction.

Scour is a very important phenomenon for river bridges. A study carried out by Wardhana and Hadipiriono (2003) shows that the most important reason of bridge failures in USA is scour with 52.88%. Besides, earthquake causes 3.38% of failures.

Although in Turkish practice earthquake effects are considered during the design process, hydraulic-oriented aspects are generally neglected. There are several examples of hydraulic based damages and failures. A recent example from Turkey, Yayakent Bridge in İzmir had a risk of collapsing due to extreme flood in January, 2016 (See Figure 1.1).



Figure 1.1. Yayakent Bridge view after flood in January, 2016 (Tuna, 2016)

Another example, the deck of Akçaova Bridge in Ordu is damaged and closed to traffic due to an extreme flood in July, 2016 (See Figure 1.2).



Figure 1.2. Damaged view of Akçaova Bridge in July, 2016 (Sozcu, 2016)

Karşıyaka Bridge in Samsun settled, deck broke and bridge operation was closed due to flood in May, 2016 (See Figure 1.3).



Figure 1.3. Damaged view of Karşıyaka Bridge in May, 2016 (İleri, 2016)

Another very hazardous failure example, Çaycuma Bridge which located on Filyos River and collapsed in 2012 resulting 15 deaths (See Figure 1.4). According to a report published by Turkish Association for Bridge and Structural Engineering, failure was happened due to hydraulic reasons (Yanmaz and Caner, 2012).



Figure 1.4. Collapsed view of Çaycuma Bridge after flood in 2012 (Sondevir, 2012)

Another failure example from Devrek, a river bridge as shown in Figure 1.5 highly damaged due to scour in 1998 (Yanmaz, 2002).



Figure 1.5. Damaged view of the bridge at Devrek due to scour (Yanmaz, 2002)

Scour and earthquakes are very destructive events and yet earthquakes increase the probability of failure of scoured bridges.

Scour makes the structure more flexible. As a result of this fundamental periods of the structure elongates and column moments decrease. Although it seems advantageous, the capacity and stability problems at the piles may arise.

This study investigates the coupled effect of scour and earthquake.

## **1.2 OBJECTIVE AND SCOPE OF THE STUDY**

The aim of this study is to propose an assessment guideline for seismic response evaluation of a bridge scoured prior to earthquake. The tasks involved in guideline are as follows:

- To study combined effect of scour and earthquake by using real data.
- Make an overture about occurrence of scour and earthquake at the same time.
- To examine the effect of scour on seismic behavior of bridge.
- To observe the effect of scour on column capacity ratio, pile moment-axial force interaction curve, pile load capacity and pile shear capacity under different earthquake excitations.

In this context, short, a simply supported, two spanned representative river bridge is investigated. Within the scope of this study, seven bridge models are studied under nine different load combinations. Response spectrum analysis is performed for different return periods and following outputs are obtained:

- Change in fundamental period according to scour depth,
- Column demand to capacity ratios ( $M_u/\phi M_n$ ),
- Pile capacity curves,
- Pile load capacity change,
- Pile shear capacity change.

This thesis is composed of five chapters. In the first chapter, the problem is introduced. Then, objective of the thesis is briefly explained and scope of the study is mentioned. The second chapter is devoted to a concise literature review. Background

of HEC-18 method and response spectrum analysis are mentioned shortly. In addition, review of previous studies is given in Chapter 2. The third chapter is about software and analyses methodology. Four softwares and areas of their application are presented. Also, hydraulic and structural analysis methodology is given. The fourth chapter is about the analyses procedure. Hydraulic and structural models, details of analyses and results are presented. In the last chapter, the results are discussed and the conclusions are given.



## CHAPTER 2

### LITERATURE REVIEW

#### 2.1 BACKGROUND

Due to flow action aggradation and degradation occurs on the riverbeds. Scour is usually defined as erosion of the riverbed and transportation of the sediment particles.

Figure 2.1 shows a free body diagram for a soil particle resting on a movable stream bed. Frictional forces between granular soil particles and buoyant weight of the particle resist to move. On the other hand, drag force and lift force tend to remove the soil particle. Particle moves whenever bottom shear stress of the flow is greater than the critical shear stress. At the top, velocity is greater than the velocity at the front. So, pressure at the top is less than the pressure at the front, which creates an inclined force induced by flow from the front of the particle towards the top. This force is decomposed into two components. At the bottom point, pressure is greater than the pressure at the top. Because of the pressure difference, an upward force is developed on the particle and it is called as lift force. Also, a hydrodynamic force, which is called drag force, is acted on the particle by the fluid because of pressure difference between the front and rear sides of the particle. If the disturbing moments around a contact point (Point A in Figure 2.1) is greater than the stabilizing moments, the particle is set the motion (Yanmaz, 2002).

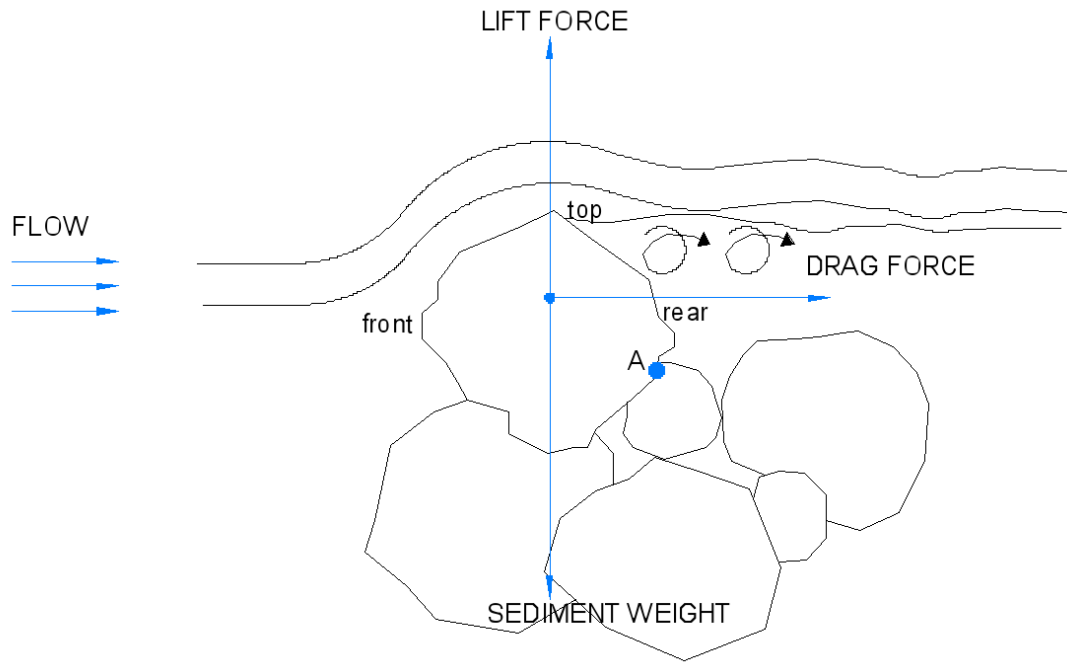


Figure 2.1. Free body diagram of a sediment particle (Yanmaz, 2014)

There are three types of scour: General scour, local scour and contraction scour.

- General scour: General scour can either be short termed or long termed. One or more floods may cause scour in short term. Long term scour can be observed in riverbeds and banks due to the morphological regime of the river. The main reasons of general scour are hydrometeorological, geomorphological and man-made (Yanmaz, 2002).
- Contraction scour: Obstructions may reduce the river cross-section. It increases local velocity and shear stresses. Hence, erosion capacity of the flow increases (Yanmaz, 2002).
- Local scour: Due to some obstruction (i.e. pier, abutment, spurs and embankments) on the riverbed, flow acceleration around the obstacle creates vortices, which starts to erode the riverbed around the base of obstruction. Local scour can be classified as live bed scour or clear water scour.

- Clear water scour: If the bed shear stress due to flow is smaller than critical bed shear stress, it means soil particles on the bed do not move. However due to vortices developed around pier scour is formed (Yanmaz, 2002).
- Live bed scour: If the bed shear stress is greater than critical bed shear stress, then particles at the upstream bed start to move. When it happens not only the vortices in the scour hole is important but also the soil movement at the upstream is important in terms of scour formation. It is called live-bed scour (Yanmaz, 2002).

Bridge piers cause to change in flow velocity and disturbs the flow pattern. Thus, surface roller, horseshoe vortex, and wake vortex are formed (See Figure 2.2). Details of the scouring theory can be found in Yanmaz (2002). Since this study is focused on investigation of bridge behavior due to earthquake motion under scoured bed condition, only brief information on scour mechanism is introduced.

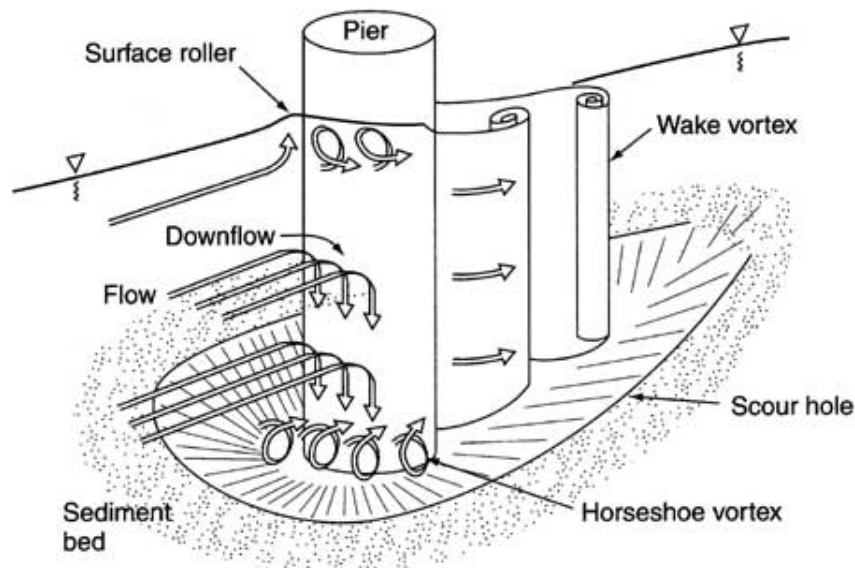


Figure 2.2. Vortex formation in scour hole (ETH, 2009)

## 2.2 REVIEW OF PREVIOUS STUDIES

### 2.2.1 Scour Prediction Equations

Pioneering studies on bridge scouring are introduced in Yanmaz (2002). This study introduces only the recent scour prediction equations that are commonly used in practical applications.

Froelich (1988) developed an equation for live bed condition.

$$d_s = 0.32K_o \left(\frac{b'}{b}\right)^{0.62} \left(\frac{y}{b}\right)^{0.46} F_r^{0.2} \left(\frac{b}{D_{50}}\right)^{0.08} + 1 \quad (2.1)$$

where,

$d_s$ = scour depth (m)

$y$ = flow depth directly upstream of the pier (m)

$b$ = width of pier (m)

$b'$ = width of pier projected normal to approach flow (m)

$$= b \cos \alpha + l \sin \alpha$$

where,  $l$  is the length of pier,  $\alpha$  is the angle of attack of flow with pier axis.

$K_o$ = coefficient for type of pier

$F_r$ = Froude number

$D_{50}$ = median sediment size

Johnson (1992) developed an equation for circular pier and live bed condition.

$$\frac{d_s}{b} = 2.02 \left(\frac{y}{b}\right)^{0.02} F_r^{0.21} \sigma_g^{-0.24} \quad (2.2)$$

where,

$\sigma_g$ =standard deviation of sediment mixture

Abdou (1993) investigates effects of sediment gradations and coarse material fraction on clear water scour condition.

$$\text{For } \sigma_g = 1.38, d_s = 144.5 y F_r^{3.47}$$

$$\text{For } \sigma_g = 2.43, d_s = 38.0 y F_r^{3.03}$$

$$\text{For } \sigma_g = 3.40, d_s = 23.0 y F_r^{3.2}$$

where,

$$\sigma_g = \sqrt{\frac{D_{84}}{D_{16}}} \quad (2.3)$$

Noshi (1993) developed an equation for a steady long-duration flow. He used short-term hydrograph with 2.5, 5.0, 7.5-minute time steps.

$$\left(\frac{d_s}{y}\right)_{5 \text{ min hyd}} = 0.4 \left(\frac{d_s}{y}\right)^{2.44} \sigma_g^{1.58} \quad (2.4)$$

$$\left(\frac{d_s}{y}\right)_{2.5 \text{ min hyd}} = 0.0459 + 0.79 \left(\frac{d_s}{y}\right)_{5 \text{ min hyd}} \quad (2.5)$$

$$\left(\frac{d_s}{y}\right)_{7.5 \text{ min hyd}} = 1.67 \left(\frac{d_s}{y}\right)_{5 \text{ min hyd}}^{1.41} \quad (2.6)$$

$$d_s = y K_g [6.18 F_r - 5.22 F_r^2 - 0.716] \quad (2.7)$$

where,

$$K_g = 2.82 \sigma_g^{-1.33} F_r^{0.849} \quad (2.8)$$

Melville (1997) developed an equation for both live and clear water scour.

$$d_s = K_{yb}K_IK_dK_sK_\theta \quad (2.9)$$

where,

$K_{yb}$ = Correction factor for flow depth and pier size

$K_I$ = Correction factor for flow intensity

$K_d$ = Correction factor for sediment size

$K_s$ = Correction factor for pier shape (See Table 2.1)

$K_\theta$ = Correction factor for flow alignment

$$K_{yb} = 2.4 b \quad \text{for } b/y < 0.7$$

$$K_{yb} = 2.0 \sqrt{yb} \quad \text{for } 0.7 \leq b/y \leq 5.0$$

$$K_{yb} = 4.5 y \quad \text{for } b/y > 5$$

$$K_I = \frac{u}{u_c} \quad (2.10)$$

where  $u$  is mean approach flow velocity and  $u_c$  is mean threshold velocity.

$$K_I = 1.0 \quad \text{for live bed case}$$

$$K_d = 0.57 \log \left( 2.24 \frac{b}{D_{50}} \right) \quad \text{for } b/D_{50} \leq 25$$

$$K_d = 1.0 \quad \text{for } b/D_{50} > 25$$

Table 2.1. Pier shape coefficient table (Melville, 1997)

Pier Shape	$K_s$
Cylindrical	1.0
Round-nose rectangular	1.0
Square	1.1
Pointed nosed	0.9

Sheppard et al. (1998) developed an equation for clear water scour using experimental data.

$$\frac{d_s}{b} = 4.81 \tanh\left(\frac{y}{b}\right) \left[ 1 - 2.87 \left(\frac{u}{u_c}\right) + 1.43 \left(\frac{u}{u_c}\right)^2 \right] \left\{ -0.2 + \log\left(\frac{D_{50}}{b}\right) \exp\left[-0.18 \left(-\log\frac{D_{50}}{b}\right)^{2.09}\right] \right\} \quad (2.11)$$

Richardson and Davis (2001) developed an equation for various pier shapes and both clear water and live bed conditions. This equation is also known as CSU equation or HEC-18 model.

$$\frac{d_s}{b} = 2.0 K_s K_\theta K_b K_z K_w \left(\frac{y}{b}\right)^{0.35} F_r^{0.43} \quad (2.12)$$

where,

$K_b$ = bed form factor (See Table 2.2)

$K_z$ = bed armoring factor

$K_w$ = factor accounting for wide pier for  $y/b < 0.2$

Table 2.2. Bed form coefficient table (Arneson et. al., 2012)

Bed Form	$K_b$
Clear water scouring	1.1
Flat bed and antidunes	1.1
Small dunes	1.1
Medium dunes	1.1-1.2
Large dunes	1.3

$$K_z = 1.0 \quad \text{for } D_{50} < 2 \text{ mm and } D_{95} < 20 \text{ m}$$

$$K_z = 0.4u_R^{0.15} \quad \text{for } D_{50} \geq 2 \text{ mm and } D_{95} \geq 20 \text{ mm}$$

$$\text{Min}(K_z) \approx 0.4 \quad \text{for } u < u_{icD50}$$

$$u_R = \frac{u - u_{icD50}}{u_{cD50} - u_{icD95}} \quad (2.13)$$

$$u_{icDx} = 0.645 \left( \frac{D_x}{b} \right)^{0.053} u_{cDx} \quad (2.14)$$

$$u_{cDx} = 6.19 d_0^{1/6} D_x^{1/3} \quad (2.15)$$

where,  $D_{95}$ = grain size for which 95% is finer than this size and  $D_x$ = grain size for which x% is finer than this size

### 2.2.2 Researches on Scoured Bridges Under Seismic Effects

Alipour et al. (2010) studied on uncertainties associated with design of reinforced concrete bridges considering double action of scour and earthquake. They worked on two rivers to obtain field data. To calculate the scour depth, risk curves which can be seen from Figure 2.3 are prepared for different sets of bridges, which are long-span, medium-span, and short-span bridge. HEC-18 equation has some uncertainties due to parameters. Also flow rate contains some uncertainties. Considering these uncertainties risk curves are obtained at the pier locations for 100-year return period.

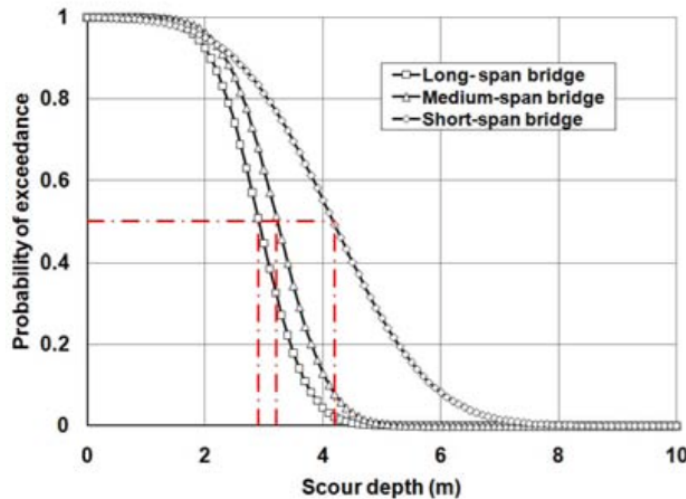


Figure 2.3. Risk curves for different span types (Alipour et al., 2010)

The structural bridge models are created by OpenSees (2009). Soil structure interaction (SSI) is modeled with bi-linear load-deflection springs according to API (1993). Scour is represented in model by removing the springs through the scour depth. Push-over analysis has been carried out to obtain the base shear capacity. As a result of this study, change in shear capacity and natural periods for different probability of occurrence and scour depths are observed. Also to develop fragility curves, nonlinear time-history analysis has been conducted.

Banerjee and Prasad (2011) evaluated the combined effect of earthquake and flood-induced scour on reinforced concrete bridges. They studied two bridges which have two spans and three spans. Total scour depth is taken as the summation of contraction and local scour depths. They used HEC-18 (Richardson and Davis, 2001) method to calculate scour depth. They developed 2D finite element models of bridges by SAP2000 (Computers and Structures Inc.), structural analysis program. SSI is modeled with nonlinear load-deflection springs according to API (2000) recommendation. To represent the scour, pile springs are removed up to scour depth. Bridges are subjected to three sets of earthquakes and nonlinear time history analyses are conducted. Analyses results are evaluated in terms of displacement ductility,

$$\mu_{\Delta} = \frac{\Delta_D}{\Delta_y} \quad (2.16)$$

where,  $\Delta_D$  is bridge girder displacement and  $\Delta_y$  is bridge girder yield displacement.

Also push over analyses are conducted to determine the yield and plastic displacements at the location of plastic hinges on pier. As a result, effect of span number and the ratio of scour depth to pile diameter ( $d_s/D$ ) relation was obtained and this is given in Figure 2.4.

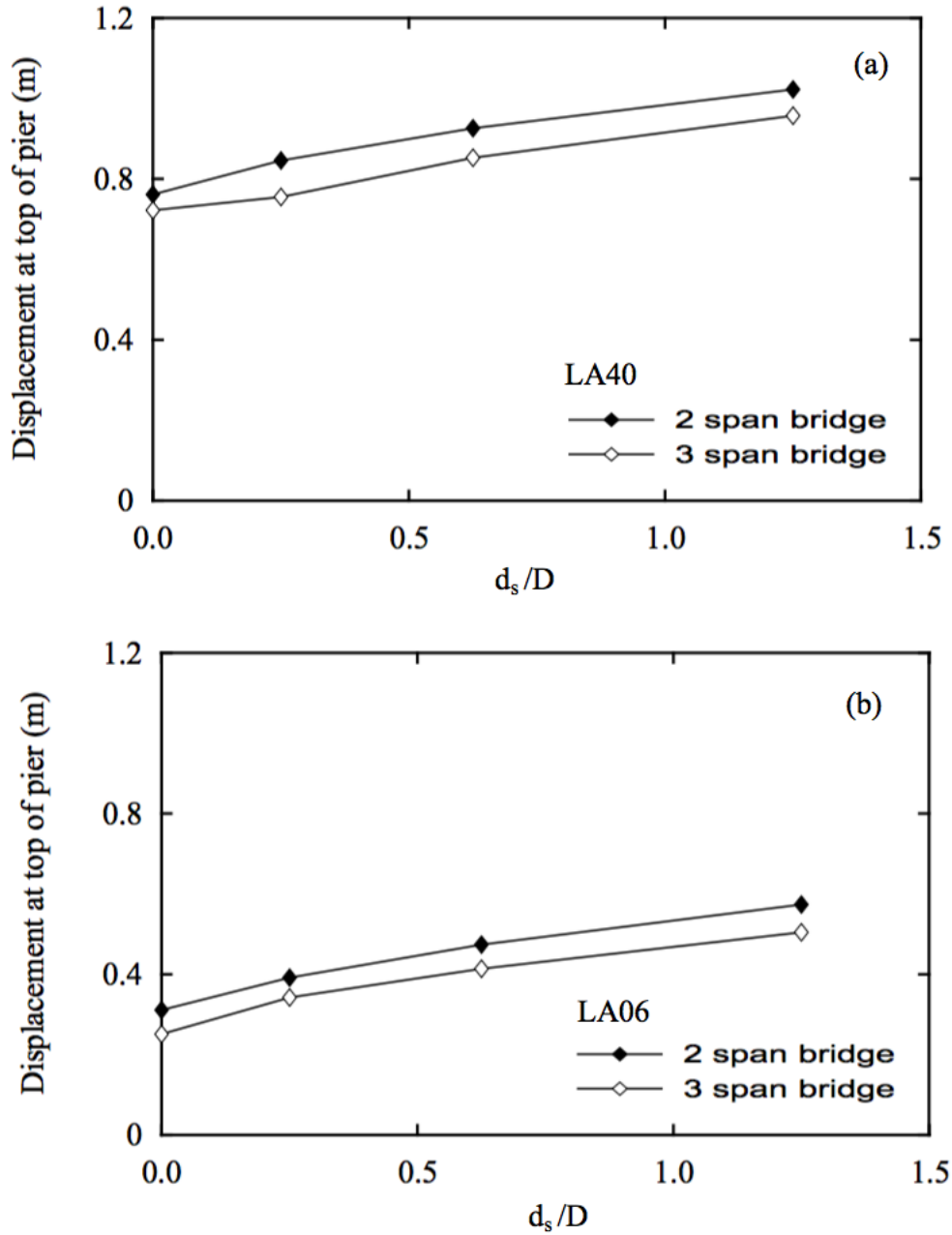


Figure 2.4. Variation of displacement at bridge pier and  $d_s/D$  under (a) strong earthquake LA40 and (b) moderate earthquake LA06, respectively (Banerjee and Prasad, 2011)

Figure 2.5 shows that while pile diameter to equivalent pile diameter,  $d_{eq}$ , ratio increases, displacement at top of the pier increases. Figure 2.6 shows that the bridges, which have greater  $D/d_{eq}$  ratio, also have greater response under combined effect of

scour and earthquake. In addition, for the bridges with  $D/d_{eq}$  ratio is smaller than 1, bridge response does not change significantly.

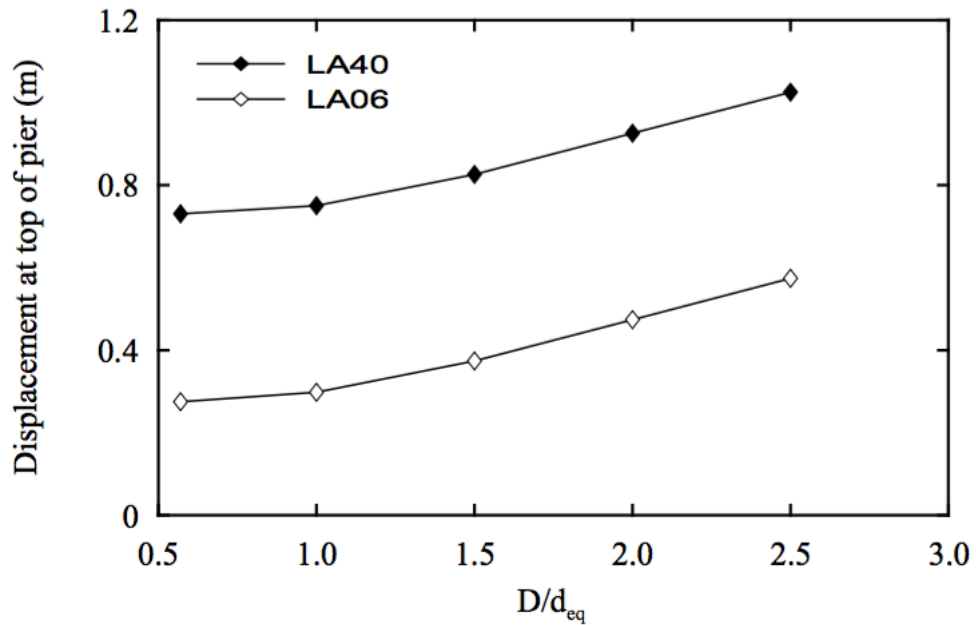


Figure 2.5 Relation between  $D/d_{eq}$  and displacement at top of the pier under earthquakes LA40 and LA06 for 2-span bridge and  $d_s/D=0.625$  (Banerjee and Prasad, 2011)

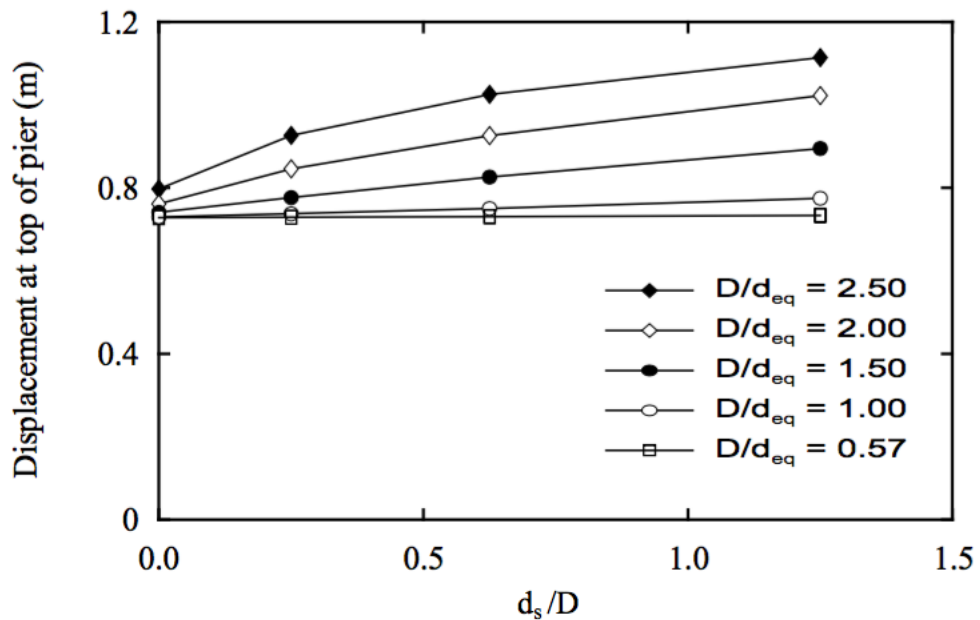


Figure 2.6. Relation between  $d_s/D$  and displacement at top of pier for different  $D/d_{eq}$  for 2-span bridge (Banerjee and Prasad, 2011)

Khan and Amanat (2014) focused on riverbed scouring effect in bridge pile foundation during earthquake. Nine span balanced cantilever box girder Meghna Bridge is studied. Scour depth changes from 0 to 18 m with 3 m increments. Structural analysis was performed with ANSYS (2013) and all material are elastic. For dynamic analysis, response spectrum analysis is executed. Soil structure interaction is represented with linear springs, and pile capacity ratios are obtained using CSiCOL (2005). As a result, considering original no scouring condition, corner pile moment increases 87% for earthquake in parallel direction of traffic and 137% increases for earthquake in perpendicular direction of traffic. Also, pier moments decrease by 59% for earthquake in parallel direction of the traffic and 67% for earthquake in perpendicular direction of the traffic, when no scouring and scoured conditions are compared.

Fioklou and Alipour (2014) aimed to determine the seismic behavior of bridges with deep foundations under effects of scour. Two spans with a total length of 60 m, reinforced concrete bridge was investigated. Three scenarios were modeled which was bridge with no scour (intact), 4 m scour and 8 m scour. Structural 3D model was developed and nonlinear time history analysis was conducted in OpenSees (2009). Material nonlinearity and pile group effects were considered. As a result, foundation performance has an inverse proportion with scour depth. Also abutment force-displacement hysteresis curves were given in Figures 2.6, 2.7 and 2.8 for, 50% probability of exceedance, 10 % probability of exceedance and 2% probability of exceedance in 50 years, respectively.

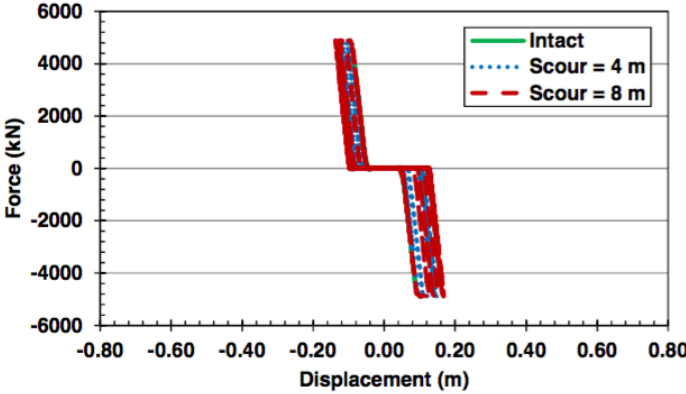


Figure 2.7. Abutment force-displacement hysteresis curve for ground motion with 50% (Fioklou and Alipour, 2014)

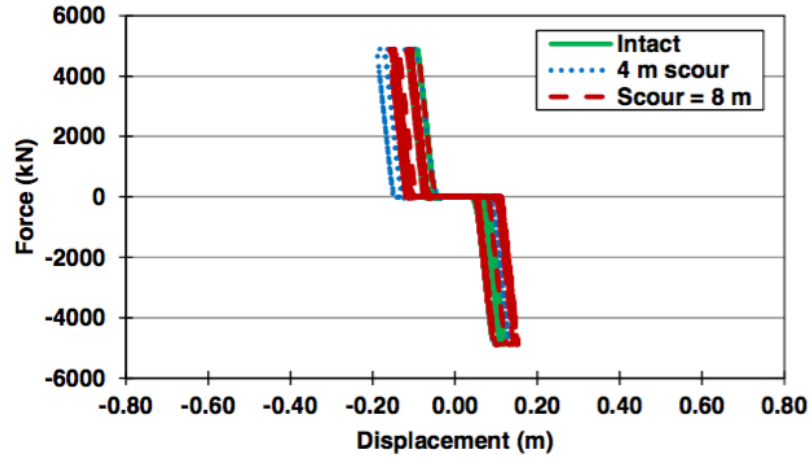


Figure 2.8. Abutment force-displacement hysteresis curve for ground motion with 10% (Fioklou and Alipour, 2014)

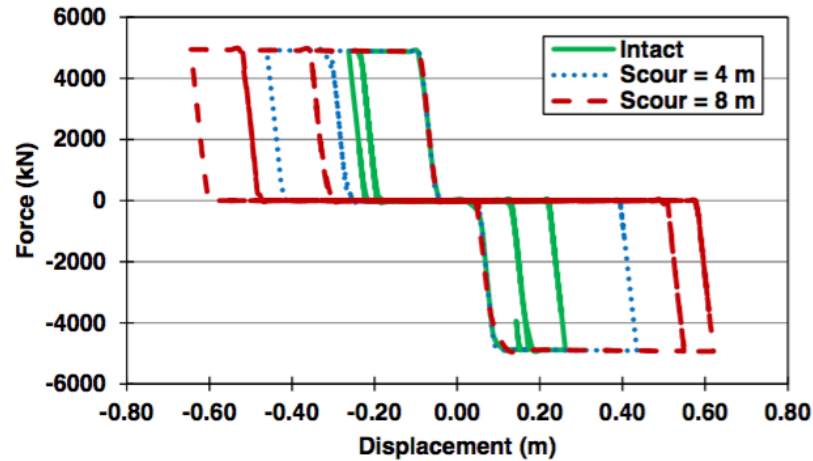


Figure 2.9. Abutment force-displacement hysteresis curve for ground motion with 2% (Fioklou and Alipour, 2014)

Song et al. (2015) studied on earthquake damage potential and critical scour depth of bridges exposed to flood and seismic hazards under lateral seismic load. Bridge bent is modeled as a two-degree-of-freedom system. For earthquake action, response spectrum analysis is performed. Results are evaluated by comparing seismic demand and strength of column and foundation. Davisson (1970) recommendation is used to calculate modulus of subgrade reaction of soil.

In this thesis, a study is conducted to investigate the seismic behavior of scour vulnerable bridges through a case study can be highlighted as follows:

- This study is based on a probabilistic approach.
- The soil-structure interaction and the structural analysis interpretations are considered in the application using different approaches than commonly used in previous studies.
- Various combinations of hydraulic and seismic conditions are evaluated with respect to no-scour case.

## CHAPTER 3

### SOFTWARE AND METHODOLOGY

#### 3.1 SOFTWARE

In this chapter, four different softwares solving different aspects of the problem are utilized to determine the effect of scour on seismic performance of bridges. HEC-RAS (Brunner, 2016) is mainly used to compute scour levels for a given river geometry. The output of HEC-RAS was input into the structural analysis program LARSA 4D (2011) to model the modified soil-structure interaction analysis. The earthquake design spectrum obtained from TASARIM SPEKTRUM-2 (Thiele, 2003) has been input to LARSA 4D (2011) to analyze the representative earthquake effects. The CSiCOL (2005) program has been used to check the adequacy of the design. The brief description of the softwares is found in Figure 3.1.

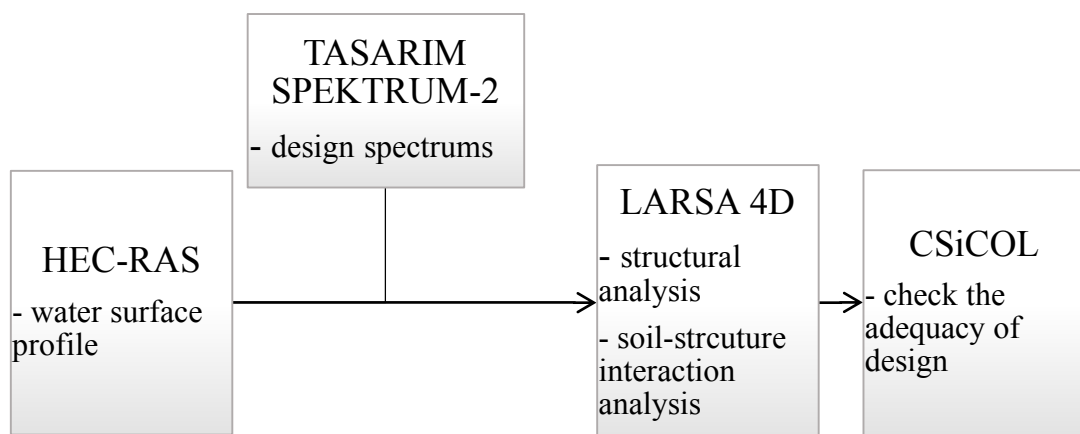


Figure 3.1. Softwares operation order

### **3.1.1 HEC-RAS**

For hydraulic analysis, a software HEC-RAS (Brunner, 2016) version 5.0 (released in February 2016) is used. HEC-RAS (U.S. Army Corps of Engineers' River Analysis System) is developed by Hydrologic Engineering Center. HEC-RAS is capable of carrying out one-dimensional steady flow analysis, one and two-dimensional unsteady flow calculations, sediment transport/mobile bed computations, water temperature/water quality modeling and scour analysis. For 1D analysis, water surface profile is calculated by using the standard step method. For 2D analysis, 2D Diffusion Wave equations or Full 2D St. Venant equations are used by HEC-RAS (Brunner, 2016).

### **3.1.2 LARSA4D**

For structural analysis, LARSA4D (2011) which is developed for the analysis and design of bridges and structures based on the finite element method is used. It is capable of executing influence-based analysis, nonlinear time history analysis, staged construction analysis, eigenvalue analysis, pushover analysis, and moment curvature analysis. Newton-Raphson method is used by the program for iterations (LARSA4D, 2011)

### **3.1.3 TASARIM SPEKTRUM-2**

Tasarım Spektrum-2 (Thiele, 2003) is a free software that can be downloaded from web page of Turkish Association for Bridge and Structural Engineering. It can compute response spectrum functions per bridge site location for different design specifications at different return periods.

### **3.1.4 CSiCOL**

CSiCOL (2005) is a software which allows user to analyze and design reinforced concrete columns in accordance with several design codes. The analysis and design can be carried out for different load combinations by considering sway or non-sway conditions, slenderness effects, and effective length factor for different framing conditions. As an output, the capacity interaction surface, load-moment curves, moment-moment curves, moment-curvature curves, etc. can be obtained.

## 3.2 ANALYSIS METHODOLOGY

In this study, the computations are made by use of four different software. The analysis parameters and the project area are described in the following sections.

### 3.2.1 Description of the Study Area

The study area is located in Banaz region of Uşak city in Turkey. Afyon-Uşak road is divided by Banaz River. The bridge connects these two sides of the river. This study area is specifically selected because of highly vulnerable scour and earthquake conditions.

Figure 3.2 shows Banaz region on Turkey map. Banaz River, bridge location, and borehole area are shown in Figure 3.3.



Figure 3.2 Banaz region location on map of Turkey

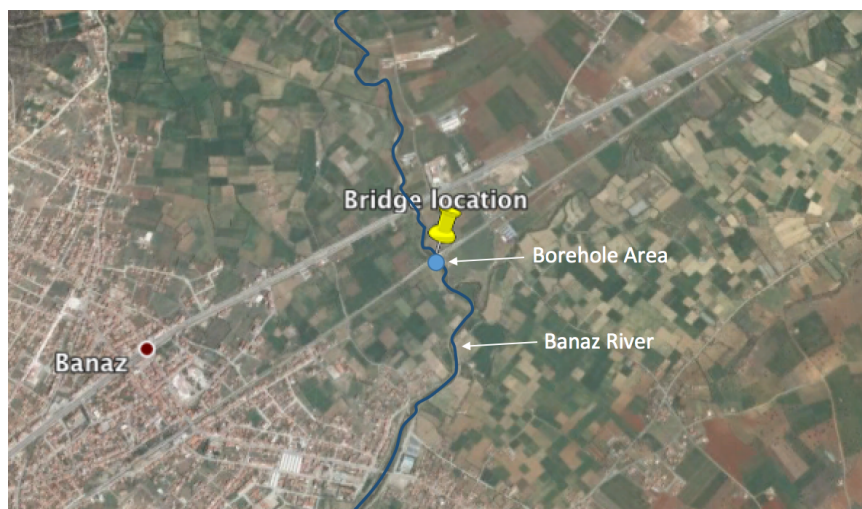


Figure 3.3. Bridge and borehole location on satellite view

The bridge was designed as a two spanned pre-stressed reinforced concrete bridge. Total length is 31.80 m between two abutments. Bridge pier is designed at the middle of the bridge in the flow section.

### 3.2.2 Hydraulic Analysis Methodology

In this part, hydraulic analysis and scour calculations methodology are explained. To obtain the water surface profile and flow velocity, which are needed to calculate scour depth, HEC-RAS (Brunner, 2016) software is used. Plan view of the river reach concerned is close to a straight river. Furthermore, all discharges are confined in the main channel section. Therefore, one dimensional model like HEC-RAS can be used with confidence. Using HEC-18 method, scour depths are calculated for each discharge. Finally, according to scour amount, structural analysis is conducted and details are given in Section 4.2.

The process is briefly explained in a flowchart presented in Figure 3.4.

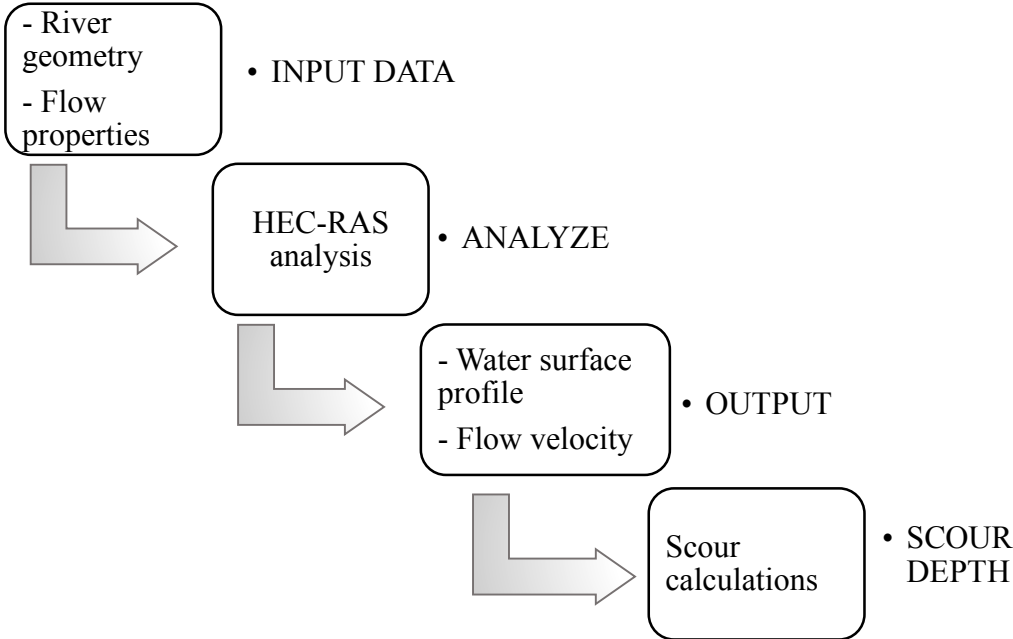


Figure 3.4. Hydraulic analysis process

Detailed procedure for hydraulic analysis is listed as follows:

- 1- Drawing the river geometry: River geometry is drawn according to river map. The plan view of the Banaz River map that has been used for this study and corresponding river geometry drawn is given in Figure 3.5. The average slope of the river at the upstream of the bridge is around 0.0056. At the downstream of the bridge, average river slope is around 0.013. According to the elevations of cross-sections, the program calculates automatically the slope change but for the first iteration it has needed predefined slopes.



Figure 3.5. HEC-RAS view of river geometry and cross-sections

2- Entering cross-section geometric data: For this study, 33 cross-sections have been taken through the river reach. In this study, the river map is limited with 440 m length. The average distance of adjacent cross-sections is 13.3 m, which is sufficient enough for hydraulic modeling. At the expansion and contraction zones and at the bridge location, extra cross-sections are added to observe the change in flow behavior. All cross-sections and map-based data are obtained by a private design company. The coordinates of the cross-sections and distances between them are entered to the program. River station is the station number showing which cross-section is considered. Station indicates the horizontal coordinate and elevation indicates the vertical coordinate. Reach lengths are the distances between two adjacent cross-sections in terms of left overbank, channel, and right overbank. Manning's roughness coefficient is selected as 0.030, which is assumed to be suitable considering local conditions.

Left and right banks are indicated on "Main Channel Bank Stations" part and contraction and expansion coefficients can be described in "Cont/Exp Coefficient" part of the program.

3- Defining flow profiles: Several flow profiles can be described in the program. These profiles include flow properties, flow rates, flow boundary conditions, etc. For each profile, flow depths and flow velocities are calculated by the program. For this study, 7 profiles have been defined for the floods and all profiles have the same properties except the flow rate. Flow rate is changed from 20.9 m<sup>3</sup>/s with 2-year return period flood event to 243.4 m<sup>3</sup>/s with 100-year return period flood event.

4- Defining bridge geometry: Bridge geometry should be defined for two reasons. First, it is a geometric change in river geometry. Second, it causes a contraction in river. Depending on contraction amount and place of contraction, water surface profile changes. Thus, scour amount is directly affected. To define the bridge geometry, upstream and downstream cross-sections of the bridge must be defined. After that, new river station between

them is defined. Using deck and pier modules, point locations of the bridge are entered to the new defined cross-section (See Figure 3.6).

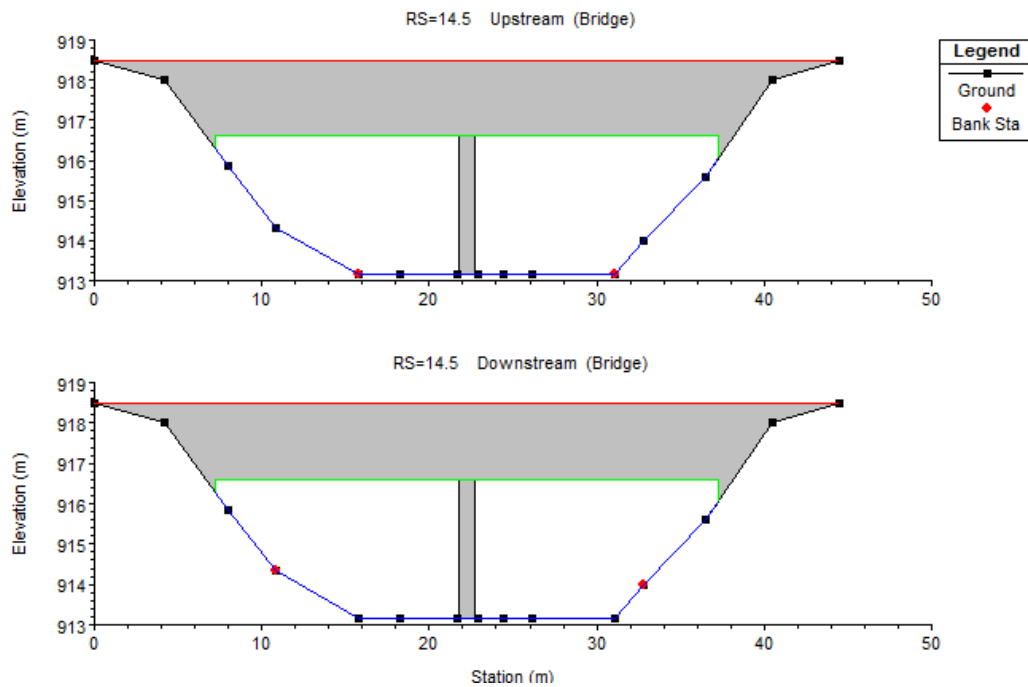


Figure 3.6. HEC-RAS view: bridge geometry definition

- 5- Analysis and determination of water surface profile: Water surface profile shows the depth of flow throughout the reach of analysis. It is specified depending on the position of actual flow depth, to the normal depth,  $y_n$ , and critical depth,  $y_c$ . Normal depth is calculated by Manning's Equation. Critical depth is defined as the depth of flow for which the specific energy is at minimum.

Subcritical flow is downstream controlled flow and Froude number is smaller than 1.0. Supercritical flow is upstream controlled flow and Froude number is greater than 1.0. For the critical state, Froude number equals to 1.0 (Sturm, 2009).

As a result of the analysis, water surface profile is obtained and for every cross-section, velocity distribution is achieved (See Figure 3.7).

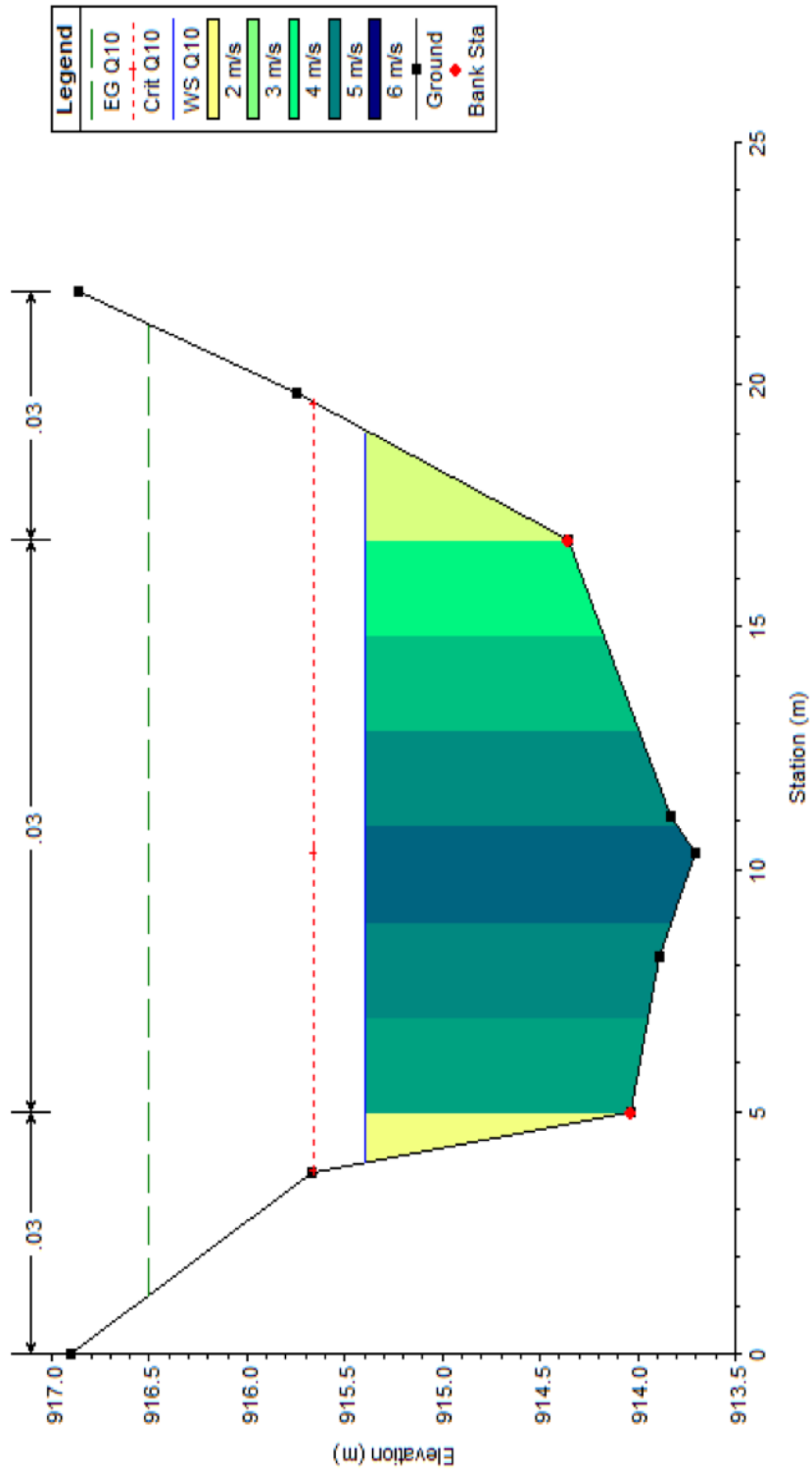


Figure 3.7. HEC-RAS view: velocity distribution for a single section

- 6- Determine soil properties: To calculate the scour depth, some soil data are required.  $D_{10}$  (mm),  $D_{50}$  (mm),  $D_{60}$  (mm) and  $D_{95}$  (mm) values of soil which are determined according to sieve analysis test results are used. These are the sediment sizes for which the percentage indicated in the subscript is smaller than that size.
- 7- Scour calculation: HEC-18 method (Richardson and Davis, 2001) is used for scour calculations. This method is not applicable for silt and clay particles. According to Yanmaz (2002), scouring is very slow in clay and rocky riverbeds. No major scour is expected on bridge foundation during an average flood. So, in the scope of this study clay erosion will not be considered. Scour components for deep foundation are shown in Figure 3.8.

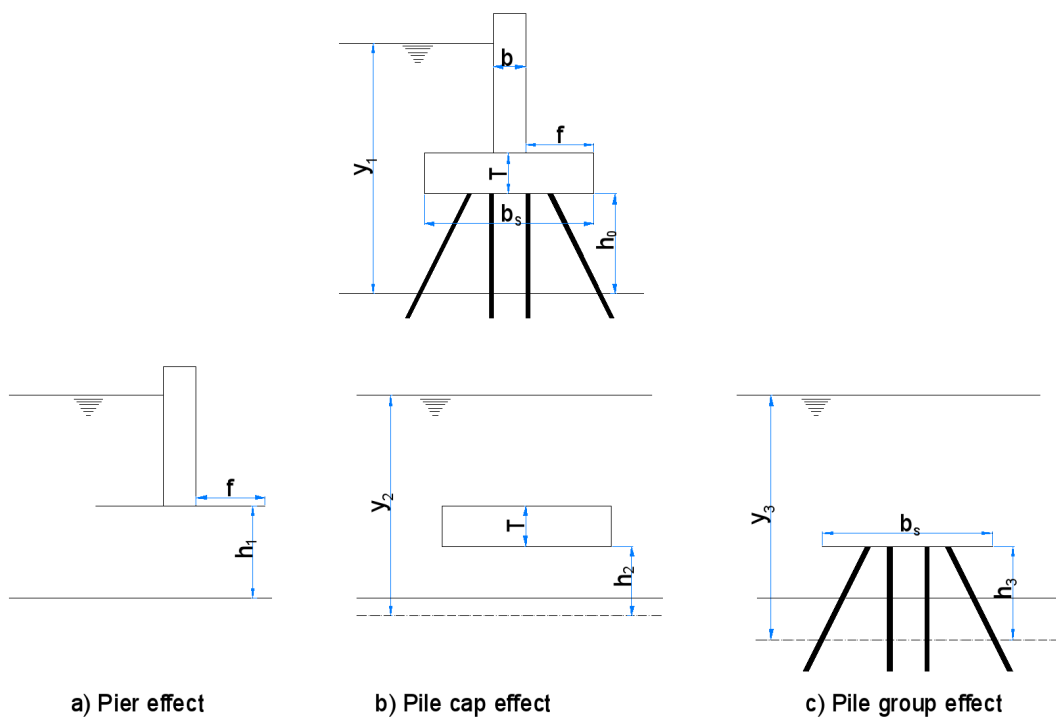


Figure 3.8. HEC-18 method scour components figure (Richardson and Davis, 2001)

The scour depth due to pier is calculated by given Equation 3.1.

$$\frac{d_{sp}}{y_1} = K_{hp} \left[ 2.0 K_s K_\theta K_b K_z \left( \frac{b}{y_1} \right)^{0.65} \left( \frac{u_1}{\sqrt{gy_1}} \right)^{0.43} \right] \quad (3.1)$$

where;

$d_{sp}$  : scour component for the pier in the flow

$y_1$  : approach flow depth at the beginning of computations

$K_{hp}$  : coefficient to account for height of pier stem above bed and shielding effect by pile cap overhang distance “F” in front of pier stem

$$K_{hp} = \left( 0.4075 - \frac{0.0669f}{b} \right) - \left( 0.4271 - \frac{0.0778f}{b} \right) \frac{h_1}{b} + \left( 0.1615 - \frac{0.0455f}{b} \right) \left( \frac{h_1}{b} \right)^2 - \left( 0.0269 - \frac{0.012f}{b} \right) \left( \frac{h_1}{b} \right)^3 \quad (3.2)$$

$K_s$  : correction factor for pier nose shape (See Table 3.1)

Table 3.1. Pier nose shape correction factor list (Arneson et. al., 2012)

Shape of Pier Nose	$K_s$
Square Nose	1.1
Round Nose	1.0
Circular Cylinder	1.0
Sharp Nose	0.9
Group of cylinders	1.0

$K_\theta$ : correction factor for angle of attack (Richardson and Davis, 2001)

$$K_\theta = \left[ \cos\theta + \frac{L_p}{b} \sin\theta \right]^{0.65} \quad (3.3)$$

$K_b$  : correction factor for bed condition (See Table 3.2)

Table 3.2. Bed condition correction factor list (Arneson et. al., 2012)

Bed Form	$K_b$
Clear water scouring	1.1
Flat bed and antidunes	1.1
Small dunes	1.1
Medium dunes	1.1-1.2
Large dunes	1.3

$K_z$  : Grain size correction factor

$$K_z = [1 - 0.89(1 - u_R)^2]^{0.5} \quad (3.4)$$

where,

$$u_R = \frac{u - u_{icD50}}{u_{cD50} - u_{icD95}} \quad (3.5)$$

$$u_{icDx} = 0.645 \left(\frac{D_x}{b}\right)^{0.053} u_{cDx} \quad (3.6)$$

$$u_{cDx} = 6.19 d_0^{1/6} D_x^{1/3} \quad (3.7)$$

$b$  : pier width, (m)

$u_1$  : approach velocity used at the beginning of computations, (m/s)

$g$  : gravitational acceleration, (m/s<sup>2</sup>)

- Pier and pile cap geometries are different. This difference should be corrected by  $K_{hp}$  (See Equation 3.2).
- Pier shape affects the turbulence level around the pier and this effect can cause decrease or increase in scour depth. For this reason, a shape factor,  $K_s$ , should be taken into account.

- Except the circular piers, all pier shapes are affected by the approach angle of the flow. This alignment pronounces vortices in the flow and this can be expressed by a correction factor,  $K_{\theta}$ .
- Bed forms, such as ripples, dunes, antidunes, etc. also effect the scour depth. Therefore, bed form factor,  $K_b$ , should be considered.
- Bed armoring effect related with the particle size distribution of the soil. It is indicated with bed armoring factor,  $K_z$ .

Before calculating the scour depth due to pile cap, depth and velocity parameters must be corrected (Richardson and Davis, 2001).

$$y_2 = y_1 + \frac{d_{sp}}{2} \quad (3.8)$$

$$h_2 = h_0 + \frac{d_{sp}}{2} \quad (3.9)$$

$$u_2 = u_1 \left( \frac{y_1}{y_2} \right) \quad (3.10)$$

where;

$y_2$ : adjusted flow depth for pile cap computations, (m) (See Figure 3.9)

$h_2$ : height of pile cap after pier stem scour component has been computed, (m)

$h_0$ : height of the pile cap above bed at the beginning of computations, (m)

$u_2$ : adjusted velocity for pile cap computations, (m/s)

If the elevation of the pile cap is above the scoured river bed, then following formula is used for calculating the scour depth due to pile cap.

$$\frac{d_{ss}}{y_2} = 2.0K_sK_{\theta}K_bK_z \left( \frac{b_s^*}{y_2} \right)^{0.65} \left( \frac{u_2}{\sqrt{gy_2}} \right)^{0.43} \quad (3.11)$$

$$\frac{b_s^*}{b} = \exp \left[ -2.7057 + 0.51 \ln \left( \frac{T}{y_2} \right) - 2.783 \left( \frac{h_2}{y_2} \right)^3 + \frac{1.751}{\exp \left( \frac{h_2}{y_2} \right)} \right] \quad (3.12)$$

where;

$d_{ss}$  : scour component for the pier cap or footing in the flow, (See Figure 3.9)

$b_s^*$  : equivalent pier width

$b$  : column width

$T$  : foundation thickness

If the elevation of the pile cap is below the river bed, then following formula is used for calculating the scour depth due to pile cap.

$$\frac{d_{ss}}{y_f} = 2.0K_sK_\theta K_b K_z \left( \frac{b_s}{y_f} \right)^{0.65} \left( \frac{u_f}{\sqrt{g y_f}} \right)^{0.43} \quad (3.13)$$

$$y_f = h_1 + \frac{d_{sp}}{2} \quad (3.14)$$

$$\frac{u_f}{u_2} = \frac{\ln \left( 10.93 \frac{y_f}{k_s} + 1 \right)}{\ln \left( 10.93 \frac{y_2}{k_s} + 1 \right)} \quad (3.15)$$

where;

$d_{ss}$  : scour component for the pier cap or footing in the flow, (m)

$y_f$  : distance from the bed to the pile cap's top elevation, (m)

$u_f$  : average velocity in the flow zone below the top of the footing, (m/s)

$k_s$  : grain roughness of the bed, (m)

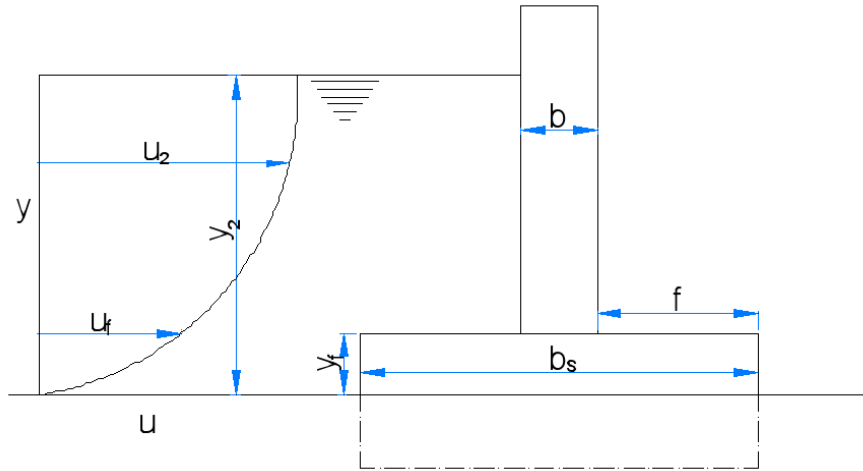


Figure 3.9. Velocity component at pile cap elevation (Yanmaz, 2002)

### 3.2.3 Structural Analysis Methodology

In this part, structural analysis methodology is explained. Just after the scour depths are obtained for each flow rate ( $Q_2$ ,  $Q_5$ ,  $Q_{10}$ ,  $Q_{25}$ ,  $Q_{50}$ ,  $Q_{100}$ ), structural analysis is conducted. While modeling the scoured bridge, pile springs are removed from scoured sections. Design spectrum values (time versus acceleration) are obtained for different return periods from Tasarım Spektrum-2 (Thiele, 2003) and copied to the LARSA 4D (2011). Thus, LARSA 4D (2011) draws the spectrums. Finally, response spectrum analysis is carried out and frame reactions are computed. After that, design checks by using CSiCOL (2005) and comparisons are performed for column and piles.

The process is briefly explained in a flowchart presented in Figure 3.10.

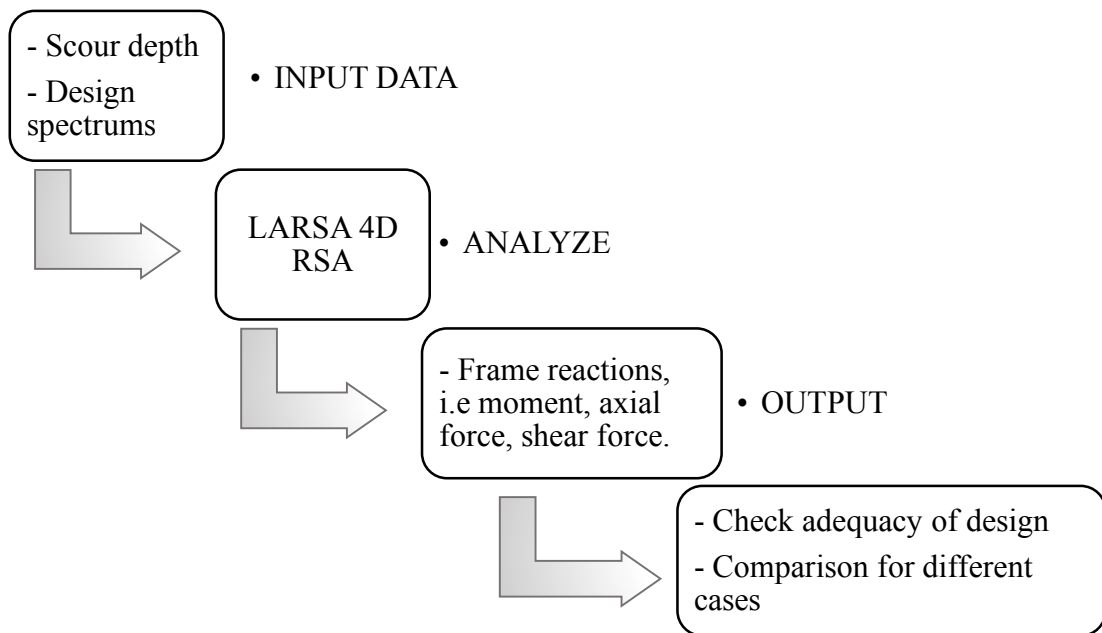


Figure 3.10. Structural analysis process

Detailed process of structural analysis is described below:

1- Material properties: In LARSA 4D (2011) materials can be defined as time dependent, inelastic or isotropic material which means the behavior of material does not depend on the direction of loading or the orientation of the material (LARSA 4D, 2011). In this study, two types of concrete which have 25 MPa and 40 MPa compressive strength and a rigid material are defined as isotropic material. It is assumed that materials show linearly elastic behavior, time dependency and inelasticity are not considered.

Name of the materials; modulus of elasticity, poisson ratio, shear modulus, and unit weights are defined. Since thermal loading will not be considered, coefficient of thermal expansion is neglected.

2- Section properties: Section properties are defined using section composer module of the LARSA 4D (2011). Section areas, shear areas, torsional constants and moment of inertias  $I_{yy}$  and  $I_{zz}$  are calculated by the program automatically.

Plastic section moduli  $Z_{yy}$  and  $Z_{zz}$ , ductility and residual strength are not considered because preferred analysis type is elastic analysis. These properties are used for inelastic analysis, such as time history analysis, etc.

- 3- Spring properties: Spring elements are defined in both lateral directions through the piles to represent the soil-pile interaction. Also to represent the elastomeric bearings, spring elements are used. Linear springs are preferred for the analysis.

Elastomeric bearings on pier and abutments are represented with linear springs which are three translational and two rotational. Spring stiffness' are calculated according to AASHTO (2002) by the following formula:

Translational elastomeric bearing stiffness in longitudinal and transverse direction,  $k_{tr}$ :

$$k_{tr} = G \frac{A_b}{h_{rt}} \quad (3.16)$$

where,

$k_{tr}$  : horizontal stiffness of the elastomeric bearing, (kN/m)

$G$  : shear modulus of the elastomer, (kN/m<sup>2</sup>)

$A_b$  : plan of area bearing, (m<sup>2</sup>)

$h_{rt}$  : total thickness of elastomeric layers, (m)

Translational elastomeric bearing stiffness in vertical direction,  $k_{vr}$ :

$$k_{vr} = E \frac{A_b}{h_{rt}} \quad (3.17)$$

where,

$k_{vr}$  : vertical stiffness of the elastomeric bearing, (kN/m)

$E$  : elastic modulus of elastomer, (kN/m<sup>2</sup>)

$A_b$  : plane area of bearing, (m<sup>2</sup>)

$h_{rt}$  : total thickness of elastomeric layers, (m)

Rotational elastomeric bearing stiffness in longitudinal and transverse direction,  $k_{sr}$  :

$$k_{sr} = \frac{M_m}{\theta_m} \quad (3.18)$$

$$M_m = 0.5EI \frac{\theta_m}{h_{rt}} \quad (3.19)$$

where,

$k_{sr}$  : rotational stiffness of the elastomeric bearing, (kN/m)

$M_m$ : maximum bending moment of bearing (kN.m-rad)

$\theta_m$  : maximum design rotation, (rad)

$E$  : elastic modulus of bearing, (kN/m<sup>2</sup>)

$I$  : moment of inertia of bearing, (m<sup>4</sup>)

$h_{rt}$  : total thickness of elastomeric layers, (m)

- 4- Defining geometry: While defining geometric model of the bridge, frame, shell and spring elements have been used. Deck is modeled with shell elements. Girders, column, cap beam, foundation and piles are modeled with frame elements. Bearings and soil behavior are represented with spring elements. Abutments are modelled with pin supports at both ends of the bridge. A sample geometric model of a bridge is shown Figure 3.11:

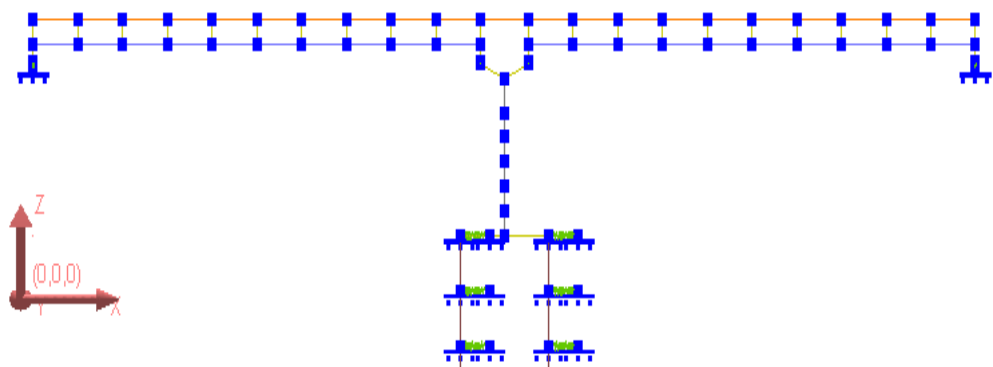


Figure 3. 11. Geometry of a bridge frame view from LARSA 4D finite element model

- 5- Response spectrum function: Response spectrum function is determined according to coordinates of the bridge. In order to obtain the response spectra curve, Tasarım Spektrum-2 (Thiele, 2003) is used. Response modification factor (R) has been taken as unity.
  
- 6- Response spectrum analysis (RSA): For this study, design is based on peak responses of the forces and displacements. Although RSA does not give exact solutions, it is accurate enough for design applications. The RSA can be performed using natural frequencies and mode shapes of the structure which are already calculated in eigenvalue analysis.  
In this analysis CQC (complete quadratic combination) modal combination rule which is based on A. Der Kiureghian formulation is used (LARSA 4D, 2011).
  
- 7- Evaluating the results: CSiCOL (2005) is used for column design check, demand to capacity ratio (DCR). Cross-section of the column is formed, material properties, clear cover, and design standard are chosen. Top and bottom forces are entered to the program and **demand** to capacity ratios are obtained as output. This ratio should be smaller than unity for the safety. If the ratio is greater than one, it indicates that the design should be changed.

## CHAPTER 4

### ANALYSIS PROCEDURE

#### 4.1 INTRODUCTION

In this chapter, hydraulic and structural analyses procedures are presented. Hydraulic analyses were executed by HEC-RAS (Brunner, 2016) software. LARSA 4D (2011) finite element analysis and design software is used for structural analyses. Three-dimensional models were formed and response spectrum analyses have been conducted.

Probabilistic evaluations of flood and earthquake events, hydraulic analysis procedure and results, scour calculations, and structural analyses and results are presented.

##### 4.1.1 Probabilistic Evaluations

In Turkish practice, service life of a bridge like in this study is usually selected as 75 years. During this period, bridges may be exposed to extreme events, such as flood and earthquake. Since this study focuses on the seismic behavior of flood imposed and consequently scoured bridges, detailed probability distribution investigation has not been conducted.

By using the local data, poisson and binomial distributions can be checked whether assumed distributions fit the real ones or not. For this study, general assumptions like poisson, and binomial distributions are used. It should be noted that poisson and binomial distributions are represented by mathematical expressions and, therefore, they are not site specific. Normally with the use of relevant local data, their

applicability need to be verified. However, this verification is not conducted in this study. Flood probability distribution may differ according to the river location, annual precipitation, basin type and size, soil properties, etc. Earthquake probability distribution may differ according to ground properties, the shortest distance to fault zone and earthquake region, etc. So, for the studies that focus on probabilistic evaluation, distribution type should be confirmed by local data.

Probability of occurrence of earthquake:

Earthquake probability distribution is assumed to follow poisson distribution in common practice (General Directorate of Highways, 2015). Probability of an earthquake can be calculated by Equation 4.1. The probabilities for 100-year, 250-year, 475-year, and 1000-year earthquake events are given in Table 4.1.

$$P(E) = \frac{(e^{-nt})(nt)^x}{x!} \quad (4.1)$$

where,

P(E)= probability of occurrence of earthquake events

n= frequency of event

t= service time of the bridge, which is taken as 75 years

x= number of occurrences of events

$$P(E) = 1 - P(E = 0) \quad (4.2)$$

P(E=0) stands for non-occurrence of an earthquake event. When P(E=0), the x value is equal to 0.

$$\text{Therefore, } P(E = 0) = e^{-nt} \quad (4.3)$$

Table 4.1. Probability of earthquake occurrence for return periods: 100 years, 250 years, 475 years and 1000 years

<b>Return Period, T (Year)</b>	<b>n (1/T)</b>	<b>n t</b>	<b>P (E=0)</b>	<b>P (E )</b>
<b>100</b>	0.010	0.75	0.47	0.53
<b>250</b>	0.004	0.30	0.74	0.26
<b>475</b>	0.002	0.16	0.85	0.15
<b>1000</b>	0.001	0.08	0.93	0.07

Probability of occurrence of flood:

Flood probability distribution is assumed to follow binomial distribution. The probability has been calculated and given for the events which have 2 years, 5 years, 10 years, 25 years, 50 years, and 100 years of return periods in Table 4.2.

$$P(F) = \frac{t!}{[(t-x)!x!]} n^x(1-n)^{t-x} \quad (4.4)$$

where, P(F)= probability of occurrence of flood events

$$P(F) = 1 - P(F = 0) \quad (4.5)$$

P(F=0) stands for non-occurrence of a flood event. When P(F=0), the x value is equal to 0.

$$\text{Therefore, } P(F = 0) = (1 - n)^t \quad (4.6)$$

Table 4.2. Probability of flood occurrence for return periods: 2 years, 5 years, 10 years, 25 years, 50 years and 100 years

<b>Return Period, T (Year)</b>	<b>n (1/T)</b>	<b>P (F=0)</b>	<b>P (F)</b>
<b>2</b>	0.500	2.60E-23	1.00
<b>5</b>	0.200	5.40E-08	1.00
<b>10</b>	0.100	3.70E-04	1.00
<b>25</b>	0.040	4.70E-02	0.95
<b>50</b>	0.020	2.20E-01	0.78
<b>100</b>	0.010	4.70E-01	0.53

For independent flood and earthquake events, their joint probability of occurrence is given by:

$$P(J) = P(E) P(F) \quad (4.7)$$

The probability of occurrence of two events, flood and earthquake, is shown in Table 4.3. Probability of exceedance above 15% is marked with blue. 15% is assumed as enough for design considerations.

Table 4.3. Joint probability of earthquake and flood events

<b>RETURN PERIODS - EARTHQUAKE</b>				
<b>P(J)</b>	<b>100</b>	<b>250</b>	<b>475</b>	<b>1000</b>
<b>2</b>	0.530	0.260	0.150	0.070
<b>5</b>	0.530	0.260	0.150	0.070
<b>10</b>	0.530	0.260	0.150	0.070
<b>25</b>	0.505	0.248	0.143	0.067
<b>50</b>	0.413	0.203	0.117	0.055
<b>100</b>	0.281	0.138	0.080	0.037

## 4.2 HYDRAULIC ANALYSIS

In order to determine water surface profile and to calculate flow velocities, geometric characteristics of the river and discharges for each return period are introduced to HEC-RAS model.

After the analysis, water surface profiles are obtained for the related reach of Banaz River, which covers upstream and downstream parts of the bridge. Finally, flow velocities and flow depths at pier location are used for scour calculations.

### 4.2.1 Hydraulic Properties and Computer Model

Geometric characteristics of Banaz River are defined in HEC-RAS (Brunner, 2016) according to satellite view and topographical map. Firstly, river reach is drawn and then the x and y coordinates of the cross-sections are entered to the program as station and elevation, respectively. Mean river slopes are 0.0056 and 0.013 at upstream and at downstream part, respectively. There are six flood profiles which are defined according to their return periods. Flood discharge values are given in Table 4.4. Since the slopes are already known, the normal depth is selected for flow boundary conditions of all profiles. Since, both subcritical and supercritical flows were observed in the studied river, the flow regime is selected as mixed flow.

Table 4.4. Flood frequency and discharge table

<b>Qi</b>	<b>Return Period, Tr (years)</b>	<b>Discharge (m<sup>3</sup>/s)</b>
Q <sub>2</sub>	2	20.9
Q <sub>5</sub>	5	51.1
Q <sub>10</sub>	10	83.6
Q <sub>25</sub>	25	136.3
Q <sub>50</sub>	50	183.3
Q <sub>100</sub>	100	243.4

Flow velocities and corresponding flow depths are calculated by HEC-RAS (Brunner, 2016). For each profile, velocities and flow depths at bridge location are given in Table 4.5.

Table 4.5. Flow velocities and flow depths at corresponding discharges at bridge location

<b>Q<sub>i</sub></b>	<b>Flow Velocity (m/s)</b>	<b>Flow Depth (m)</b>
Q <sub>2</sub>	1.55	0.84
Q <sub>5</sub>	2.21	1.14
Q <sub>10</sub>	4.35	1.25
Q <sub>25</sub>	5.26	1.47
Q <sub>50</sub>	5.93	1.70
Q <sub>100</sub>	6.58	1.97

#### 4.2.2 Soil Properties

Geological investigation of Banaz Bridge was conducted in 2014. In order to determine soil characteristics, two boreholes were drilled (SK-1 and SK-2) in the river. Sieve analysis test is performed for both boreholes. Sieve analyses results are given in Figures 4.1 and 4.2. The average D<sub>10</sub>, D<sub>50</sub>, and D<sub>60</sub> values which are used in scour analysis are given in Table 4.6.

Table 4.6. Particle D<sub>10</sub>, D<sub>50</sub>, D<sub>60</sub> and D<sub>95</sub> values

	<b>SK-1</b>	<b>SK-2</b>	<b>AVERAGE</b>
<b>D<sub>10</sub> (mm)</b>	0.1	-	0.1
<b>D<sub>50</sub> (mm)</b>	3	5	4
<b>D<sub>60</sub> (mm)</b>	5.5	9	7.25
<b>D<sub>95</sub> (mm)</b>	25	21	23

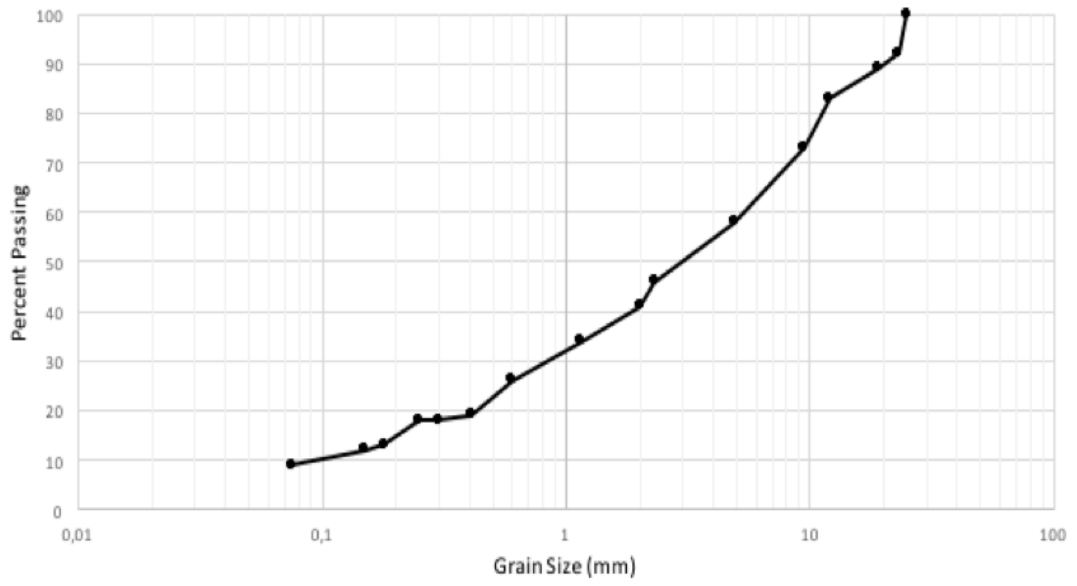


Figure 4.1. Grain size distribution at SK-1

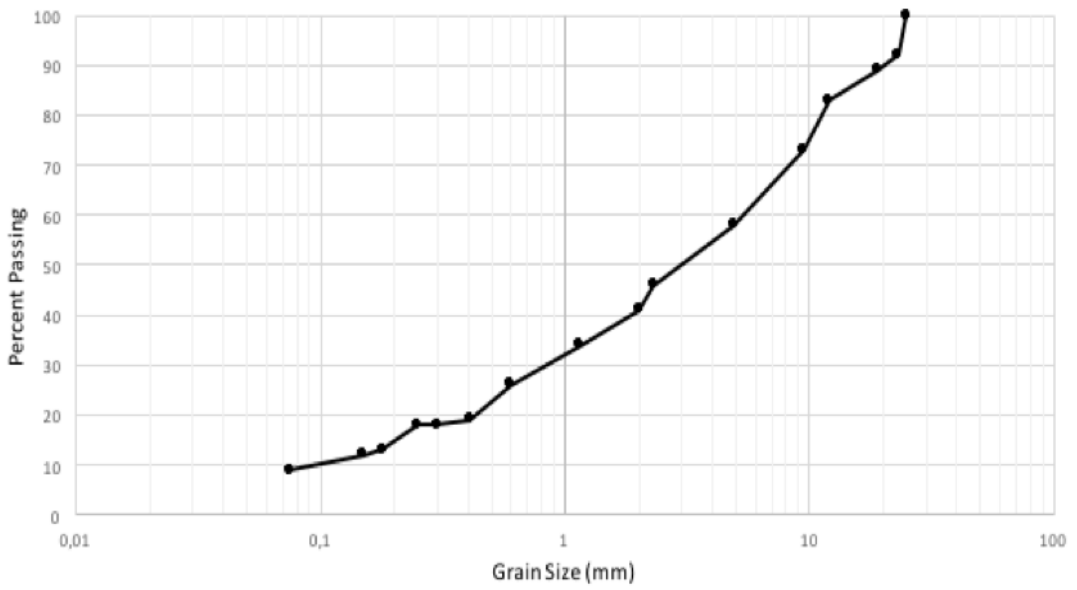


Figure 4.2. Grain size distribution at SK-2

### 4.2.3 Scour Calculations

HEC-18 method is used to calculate the scour depths. The inputs and coefficients that are considered in scour calculations are given in Table 4.7.

Table 4.7. Coefficients and inputs that are used in scour calculations

Input		Coefficient			
b =	1.0 m	K <sub>hp</sub> =	0.475	K <sub>b</sub> =	1.1
h <sub>1</sub> =	-0.65 m	K <sub>s</sub> =	1.0	K <sub>z</sub> =	0.632
θ =	8°	K <sub>θ</sub> =	1.208		
L =	2.5 m				

Total scour depth ( $d_{st}$ ) is sum of the pier and pile cap components.

$$d_{st} = d_{sp} + d_{ss} \quad (4.8)$$

The scour values ( $d_{sp}$ ,  $d_{ss}$  and  $d_{st}$ ) calculated for each discharge are presented in Table 4.8.

Table 4.8. Scour depth summary table

	Q <sub>2</sub>	Q <sub>5</sub>	Q <sub>10</sub>	Q <sub>25</sub>	Q <sub>50</sub>	Q <sub>100</sub>
<b>d<sub>sp</sub> (m)</b>	0.58	0.74	0.13	1.29	1.41	1.52
<b>d<sub>ss</sub> (m)</b>	2.02	2.97	4.54	5.36	5.93	6.36
<b>d<sub>st</sub> (m)</b>	2.60	3.71	4.67	6.65	7.34	7.88

Figure 4.3 shows the total scour depth for two scenarios.

Scenario-1: Below 6 meters from the riverbed, scour amount can be neglected. Because the soil type changes from sand to clay below 6 meters from the riverbed. According to Yanmaz (2002), scouring is very slow in clayey and rocky riverbeds.

So no major scour is expected on bridge foundations during an average flood. This scenario is indicated with orange bars in Figure 4.3.

Scenario-2: This scenario evaluates the influence of different soil types on the structure. For this scenario, soil type is assumed as sand. In this circumstances, scouring continues without limited first 6 meters. It is indicated with blue bars in Figure 4.3.

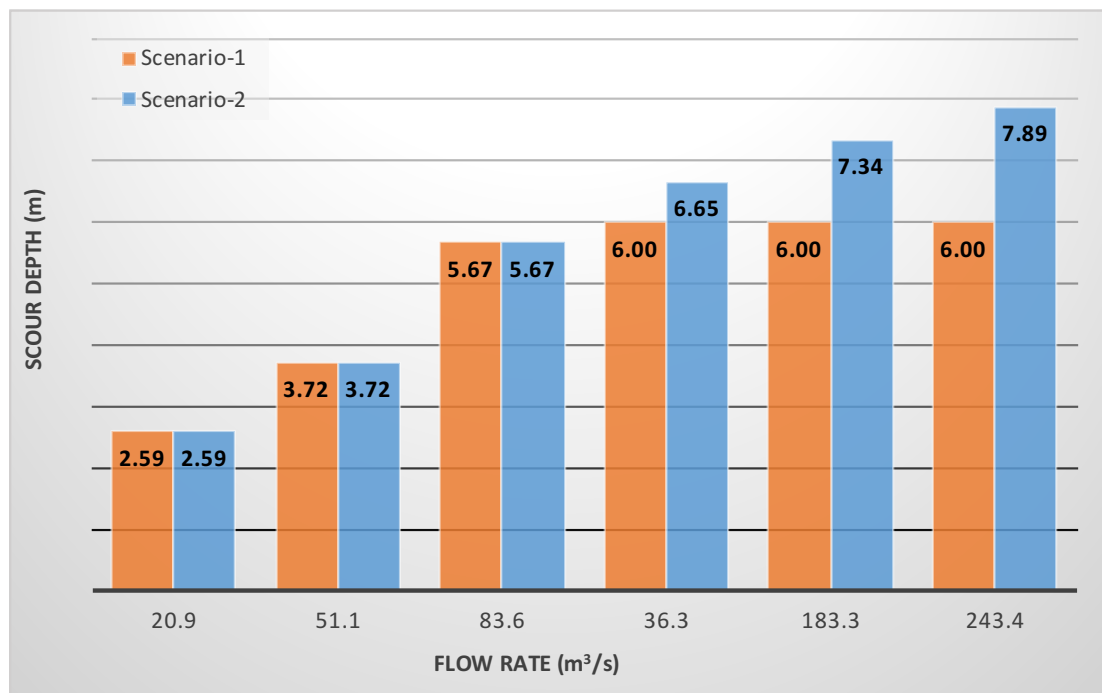


Figure 4.3. Scour depth results for two layered system and one layered system

## 4.3 STRUCTURAL ANALYSIS

### 4.3.1 Description of the Bridge

The bridge has two equally spaced spans. The girder length is 15.10 m between two bearings axes. Total length of the bridge is 31.80 m from center to center of bearings at two abutments. The plan and section of the bridge is shown in Figure 4.4 and Figure 4.5, respectively.



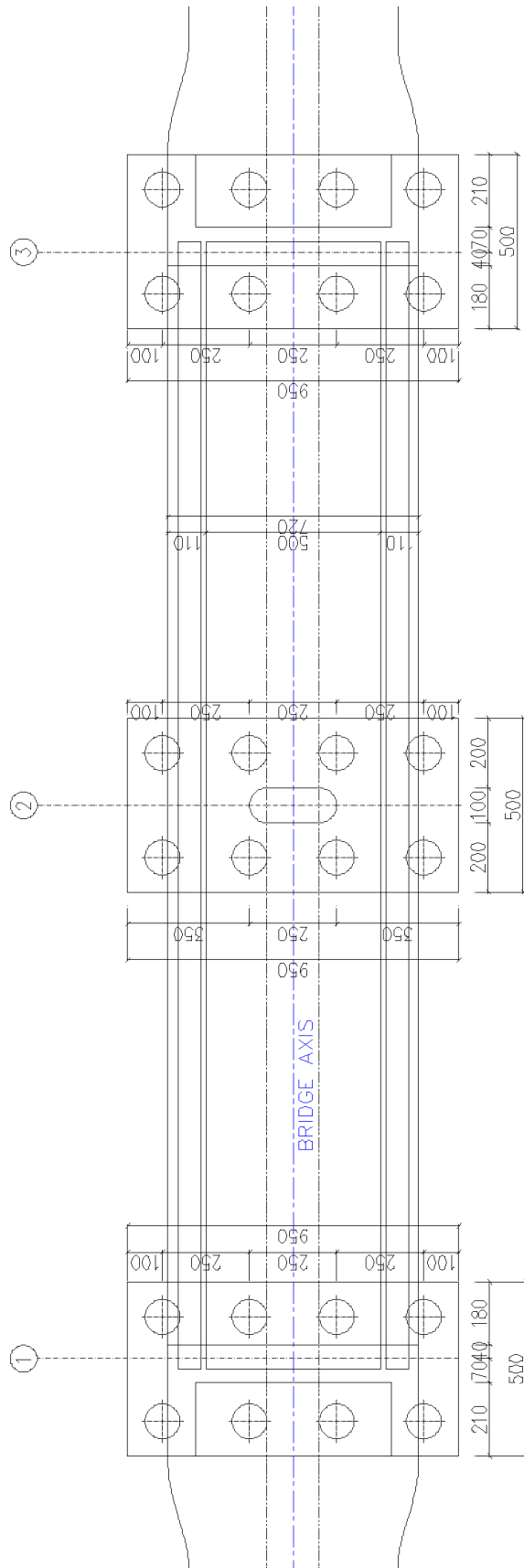


Figure 4.5. Plan view of Banaz bridge (Dimensions are in cm)



The net column height is 2.90 meters. The column width and length are 1 m and 2.5 m, respectively. There are 8 piles with two rows under each 1.5 m-thick foundation. Each pile has 1.0 m diameter and spaced 2.5 m in vertical direction and 3.0 m in horizontal direction with the adjacent pile.

### 4.3.2 Material Properties

The material properties which are used in design for each section are listed in Table 4.9.

Deck unit weight is selected as 55 kN/m<sup>3</sup> to include the effect of ballast weight to concrete unit weight. Rigid members are defined as massless because in the model they are used to provide only adequate and realistic connection between members as much as possible. For the reinforcing steel minimum design yield strength is  $f_y = 420$  MPa and modulus of elasticity is  $E_s = 200000$  MPa.

Table 4.9. Material properties of corresponding sections

<b>Material Section</b>	<b>Modulus of Elasticity (N/mm<sup>2</sup>)</b>	<b>Compressive Strength (MPa)</b>	<b>Poisson Ratio</b>	<b>Shear Modulus (N/mm<sup>2</sup>)</b>	<b>Unit Weight (kN/m<sup>3</sup>)</b>
<b>Deck</b>	34000	25	0.2	12823.8	55
<b>Girder</b>	34000	40	0.2	14533.6	25
<b>Cap Beam</b>	34000	25	0.2	12823.8	25
<b>Column</b>	34000	25	0.2	12823.8	25
<b>Foundation</b>	34000	25	0.2	12823.8	25
<b>Rigid</b>	34000	25	0.2	12823.8	0

### 4.3.3 Local Soil Properties

According to local soil properties, spring stiffness constants and pile capacities are determined. There are two layers around the piles. These layers are clayey sandy gravel at the upper part and sand-silt-clay mixture at the lower part. The upper part continues through six meters below the riverbed and then sand-silt-clay mixture starts and continues along the piles.

While specifying the soil properties, uncorrected standard penetration test (SPT) results are considered to find out the related parameters of spring stiffness constants and pile capacities. First, SPT blow counts, N values, are corrected by Equation 4.9.

$$N_{60} = N \frac{ER}{0.6} C_B C_S C_R \quad (4.9)$$

where,

$N_{60}$  = SPT N-value corrected for 60% energy efficiency and field procedures

N = Measured SPT N-value

ER = Hammer energy ratio

$C_B$  = Correction factor for the borehole diameter

$C_S$  = Correction factor for samplers with and without liners

$C_R$  = Correction factor for rod length

In Turkish practice ER is usually taken as 0.45 per Sivrikaya and Toğrol (2006).

Table 4.10. SPT correction factors (Birand et. al., 2011)

Factor	Equipment Variables	Correction
Borehole diameter factor, $C_B$	65 - 115 mm	1.00
	150 mm	1.05
	200 mm	1.15
Sampling method factor, $C_S$	Standart sampler	1.00
	Sampler without liner	1.20
Rod length factor, $C_R$	3 m to 4 m	0.75
	4 m to 6 m	0.85
	6 m to 10 m	0.95
	10 m to 30 m	1.00

Uncorrected and corrected N values are listed in Table 4.11.

Table 4.11. Uncorrected and corrected N values

Depth (m)	N	N <sub>60</sub>	
1.50-1.95	50	47	CLAYEY SANDY GRAVEL
3.50-3.95	30	28	
5.00-5.45	34	32	
7.00-7.45	37	35	SAND SILT CLAY MIXTURE
9.50-9.95	50	47	
11.00-11.45	41	39	
13.00-13.45	32	30	
15.00-15.45	33	31	
17.00-17.45	37	35	
19.00-19.45	39	37	
20.50-20.95	41	39	
22.00-22.45	39	37	
24.00-24.45	45	43	
26.00-26.45	37	35	
27.50-27.95	40	38	
25.99-30.00	37	35	

#### 4.3.4 Structural Computer Model

LARSA 4D (2011), which is mentioned in Chapter 3, is used to form 3 dimensional finite element models of the bridge and to analyze them. Three dimensional finite element models are shown in Figure 4.7 and Figure 4.8. The bridge is modeled as a whole to reflect the real behavior as much as possible. The deck is modeled with shell elements using four nodes. Girders, cap beam, column, foundation and piles are modeled with beam elements. Elastomeric bearings and soil are represented by linear springs. Rigid elements are massless and almost infinitely rigid. They are used to provide adequate connection between members. Since the foundation is assumed as rigid, rigid elements are also used in foundation modelling. The list of members which are used in the model are given in Table 4.12.

Table 4.12. Member list used in structural model

<b>Member</b>	<b>Structural Model</b>
Deck	Plate
Prestressed Beam	Frame
Bearing	Spring
Cap Beam	Frame
Column	Frame
Foundation	Frame (Rigid)
Pile	Frame
Soil	Spring

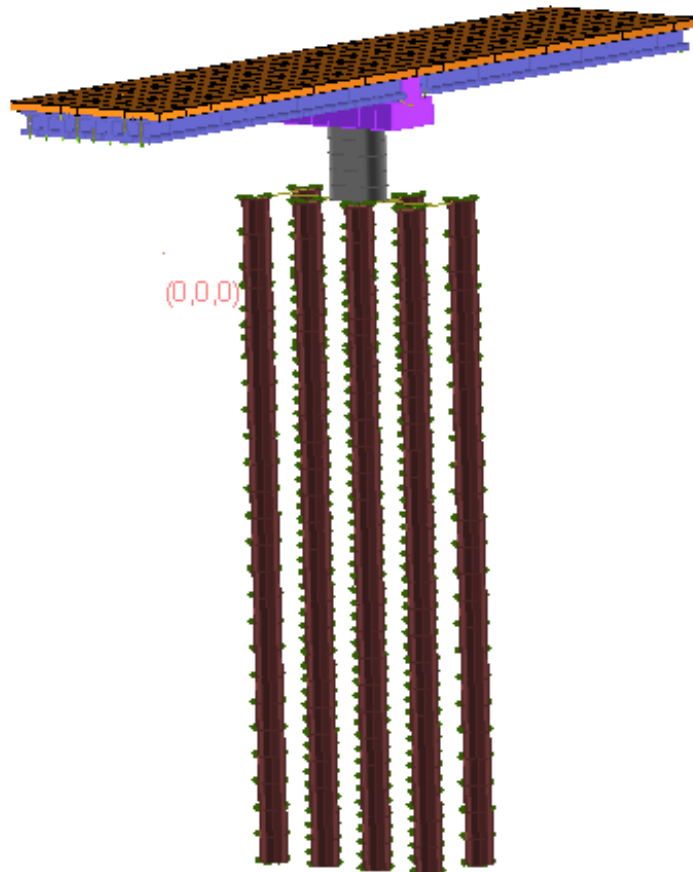


Figure 4.7. 3D view of bridge modeled in LARSA 4D

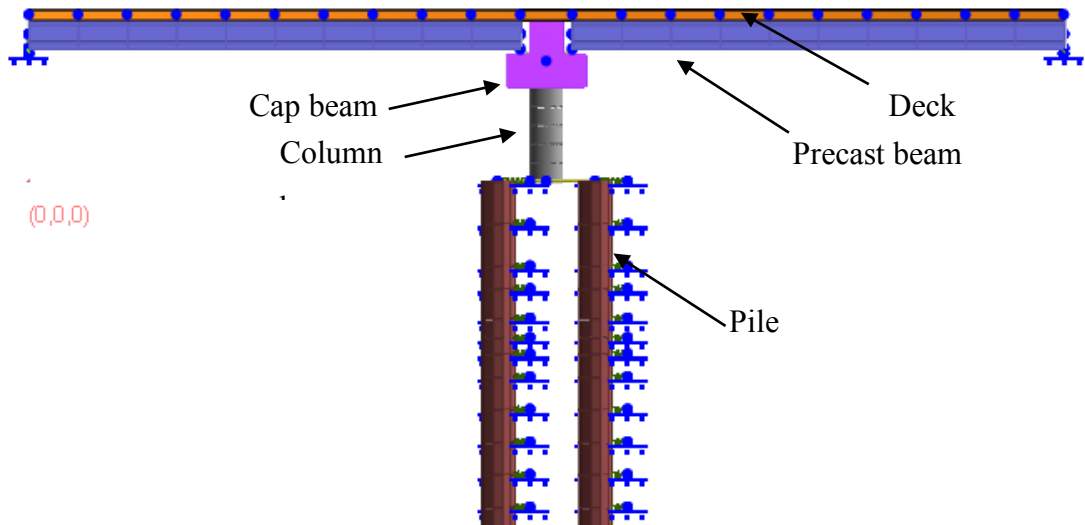


Figure 4.8. Cropped model view of the bridge in YZ plane

#### 4.3.4.1 Superstructure

Superstructure is composed of deck, girders, cap beam, and elastomeric bearings. All members are reinforced concrete except elastomeric bearings.

**Deck:** Deck is formed with ballast and 30 cm-thick precast concrete. In the model, deck is modeled as 30 cm-thick shell members. Deck and ballast are modeled together. Girder and deck members are connected with rigid frame members from center of the deck to the center of the girder in order to reflect the real behavior as much as possible.

**Girder:** Girders are modeled with I-type beam elements which are common in Turkish practice. In the system, 8 girders carry the slab and distribute loads to the supports and cap beam. Each girder is connected to elastomeric bearings at the ends via rigid beam elements. Thus rigid beam elements directly transfer the end reactions to the bearings. Dimensions of the girders in cm are shown in Figure 4.9.



directions which are translational and rotational. In Y-direction, no displacement is expected due to shear keys. Stiffness coefficient is taken as  $10^5$  kN/m besides the calculated values because of the reason mentioned above. The abutments are shown as support in the model. Calculated elastomeric bearing stiffness constants are listed below. The calculation method is explained in Chapter 3.

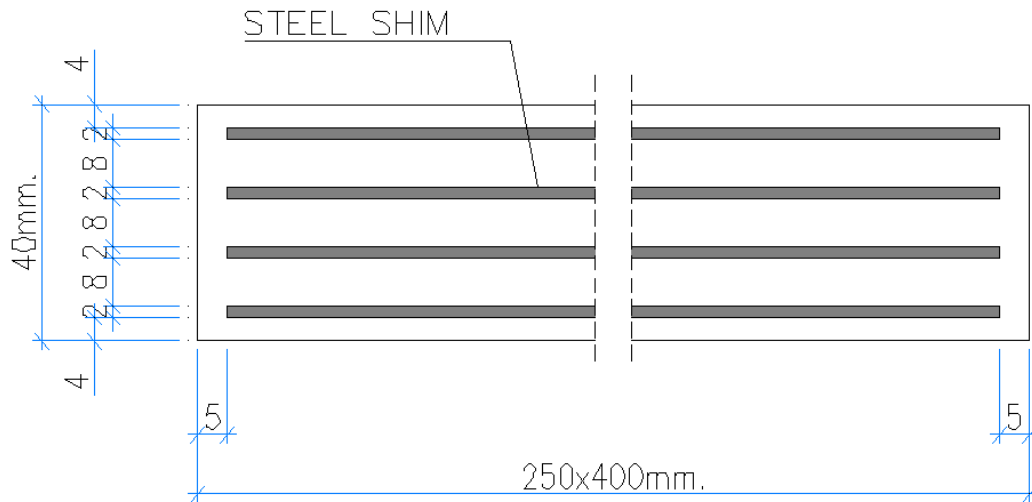


Figure 4.11. Elastomeric bearing cross-sectional view (Dimensions are in mm)

Longitudinal translational stiffness,  $k_{tr} = 3125$  kN/m

Transverse translational stiffness,  $k_{tr} = 100000$  kN/m

Vertical translational stiffness,  $k_{vr} = 378130$  kN/m

Longitudinal rotational stiffness,  $k_{sr} = 2514$  kN.m/rad

Transverse rotational stiffness,  $k_{wr} = 984$  kN.m/rad

#### 4.3.4.2 Substructure

Substructure consists of column, foundation, and piles.

**Column:** Column is modeled as 2.9 m-thick linear elastic beam element and connected to cap beam via rigid beam. Concrete cover of the columns is 5 cm in longitudinal direction, 18 mm diameter bars have been used with 10 cm spacing. Also in transverse direction, 18 mm diameter bars have been used. The cross-sections of the column are presented in Figure 4.12.

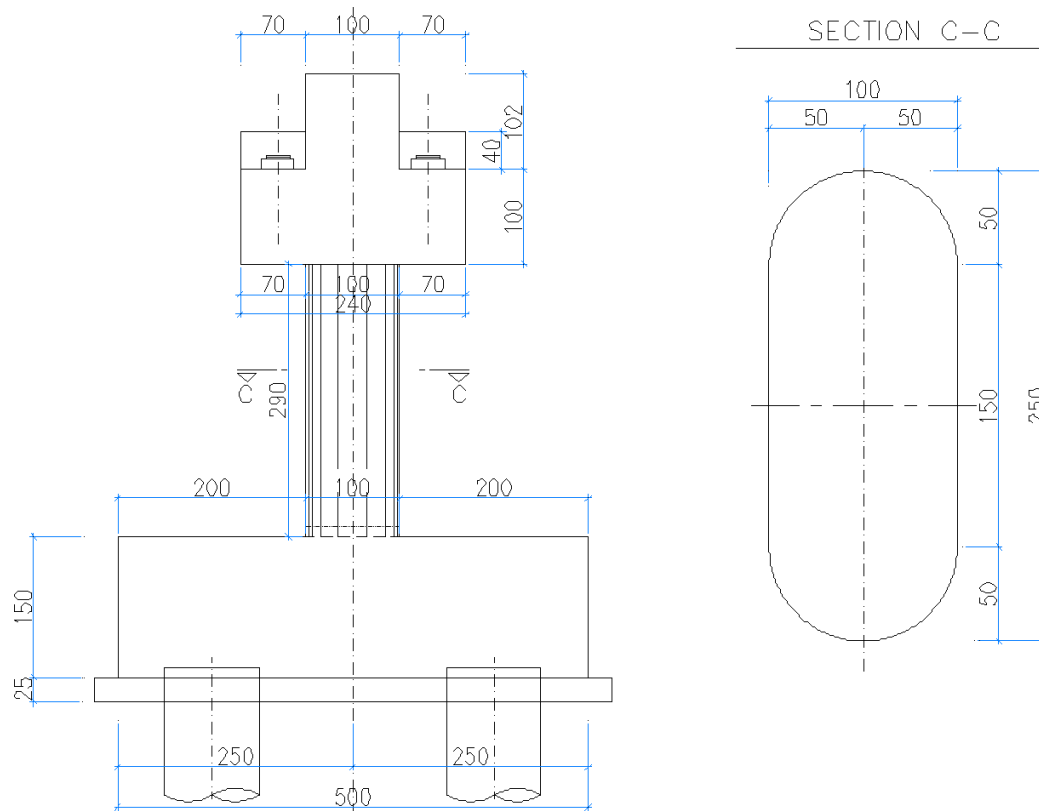


Figure 4.12. Column view and cross-section (Dimensions are in cm)

According to CALTRANS-SDC (2006) effective stiffness of cracked reinforced concrete is reduced with a ratio. For this study, this ratio is chosen based on graphs given in Figures 4.13 and 4.14. The column shape is rectangular with rounded nose. These graphs give the  $I_e/I_g$  ratio as 0.035 according to  $A_{st}/A_g$  and  $P/f'_c A_g$  values.

Herein,

$I_e$  : Effective moment of inertia of reinforced concrete section

$I_g$  : Gross moment of inertia of reinforced concrete section

$A_{st}$ : Area of longitudinal bars

$A_g$ : Area of gross concrete section

$P$  : Axial load acted on section

$f'_c$ : Concrete strength

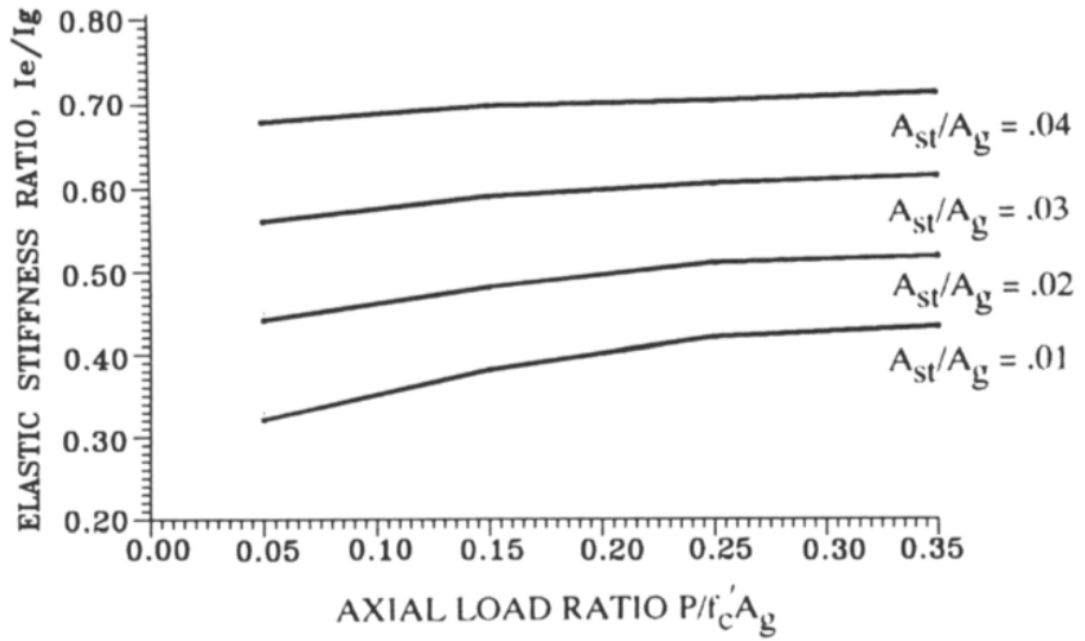


Figure 4.13. Effective stiffness of cracked reinforced concrete circular section (CALTRANS-SDC, 2006)

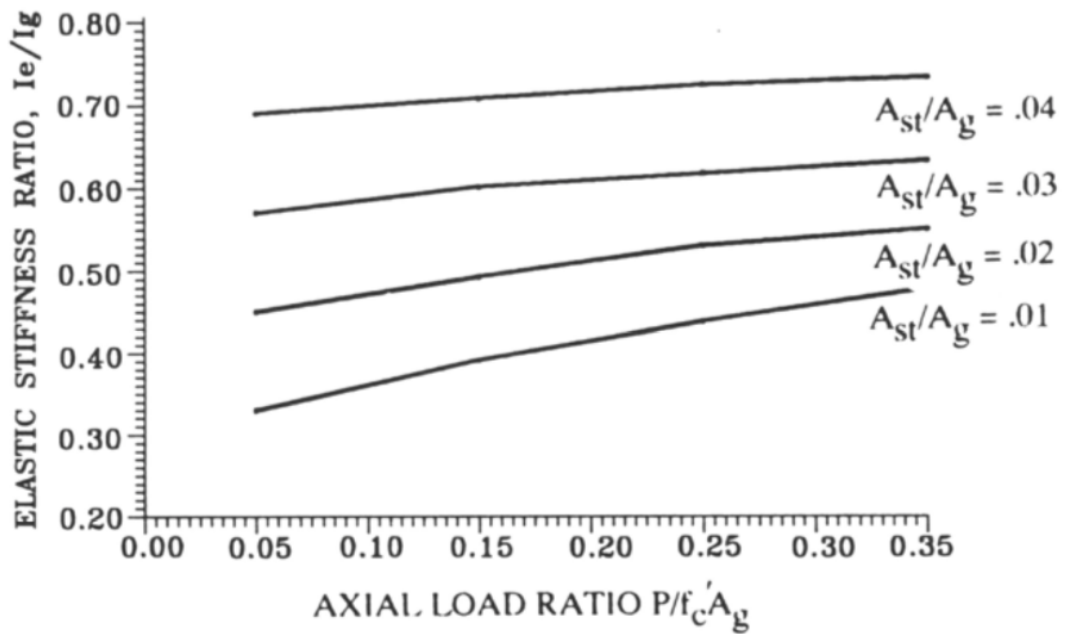


Figure 4.14. Effective stiffness of cracked reinforced concrete rectangular section (CALTRANS-SDC, 2006)

**Pile Cap:** 1.5 m-thick pile cap is selected and modeled with rigid beam elements such that it directly distributes the column load to the group of piles.

**Pile:** In this system, 8 piles under the foundation carry the load transferred. As it can be seen from the Figure 4.15, center to center spacing between adjacent piles is 2.5 m in horizontal direction and 3.0 m in vertical direction.

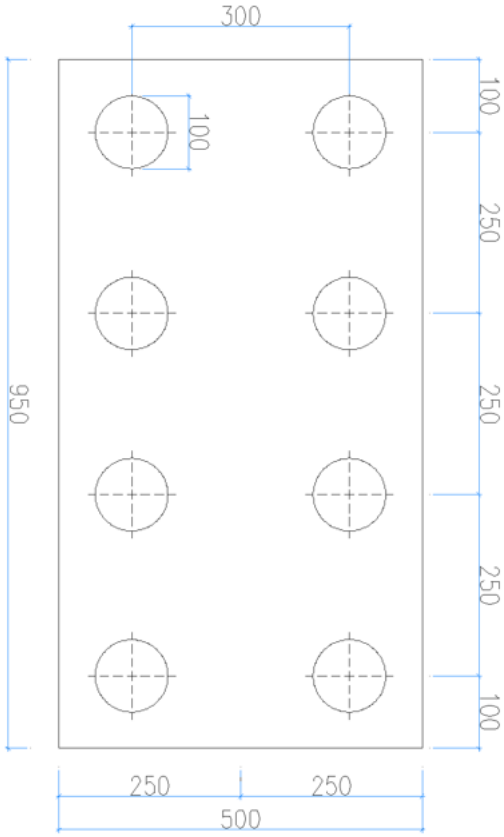


Figure 4.15. Plan view of pier foundation

**Pile springs:** To understand the soil behavior, SPT (Standard Penetration Test) results and geological profile are examined. There are two boring holes at the two sides of the bridge, namely SK-1 and SK-2. SPT N30 values, which stands for blow count, are shown in Table 4.13.

Table 4.13. List of SPT results of SK-1 and SK-2

SK-1		SK-2	
Depth (m)	N30	Depth (m)	N30
1.50-1.95	50+	3.50-3.95	30
3.50-3.95	30	5.50-5.95	30
5.00-5.45	34	7.50-7.95	37
7.00-7.45	37	9.50-9.95	37
9.50-9.95	50+	11.00-11.45	40
11.00-11.45	41	13.00-13.45	38
13.00-13.45	32	15.00-15.45	46
15.00-15.45	33	16.50-16.95	33
17.00-17.45	37	18.50-18.95	41
19.00-19.45	39	20.00-20.45	46
20.50-20.95	41	22.00-22.45	44
22.00-22.45	39	24.00-24.45	37
24.00-24.45	45	25.50-25.95	29
26.00-26.45	37	27.50-27.95	40
27.50-27.95	40	29.55-30.00	43
25.99-30.00	37		

In the piles, to represent the soil structure interaction, linear springs are used. There are several empirical equations for the modulus of subgrade reaction,  $k_h$ .

**Modulus of subgrade reaction of clayey soil:**

In this study, Skempton's (1951) equation which is given in Equation 4.10 is used. According to Skempton,  $k_h$  value is assumed to be independent of depth for clayey soil.

$$k_h = (80 - 320) \frac{c_u}{D} \quad (4.10)$$

For this study, average of 80 and 320 is taken and Equation 4.11 is used for the clay part of soil (Poulos and Davis, 1980). Therefore,

$$k_h = (200) \frac{c_u}{D} \quad (4.11)$$

where,

$c_u$ = undrained shear strength, 152 kPa

D= pile diameter, 1 m

While selecting the undrained shear strength of the clay, three approaches have been used and the average value is taken.

- Stroud’s recommendation (Prakash and Sharma, 1990):

$$c_u = f_1 N_{60} = 127 \text{ kN/m}^2 \tag{4.12}$$

where,

$$f_1 = 4.9 \text{ (See Figure 4.16)}$$

$$(N_{60})_{ave} = 26$$

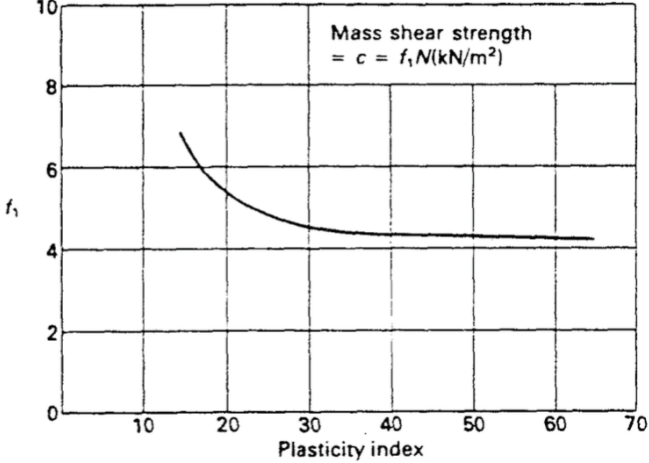


Figure 4.16. Plasticity index and  $f_1$  value relation (Stroud,1989)

- Sowers’s recommendation (Prakash and Sharma, 1990):

$$c_u = 170 \text{ kN/m}^2 \text{ (See Figure 4.17)}$$

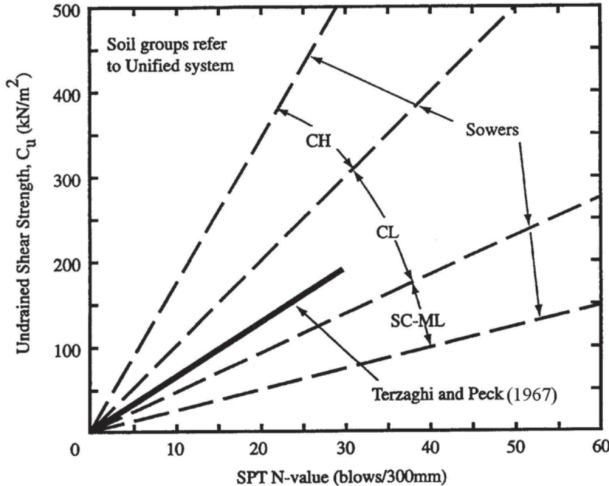


Figure 4.17. SPT-N value and undrained shear strength relation (Prakash and Sharma, 1990)

- Terzaghi and Peck's recommendation (Poulos and Davis, 1980):

$$c_u = \frac{q_u}{2} \text{ kN/m}^2 \quad (4.13)$$

where,

$$q_u = \frac{N_{60}}{12.5} \quad (4.14)$$

**Modulus of subgrade reaction of sandy soil:**

According to Poulos and Davis (1980), the modulus of subgrade reaction can be calculated as shown in Equation 4.15.

$$k_h = n_h \frac{z}{D} \quad (4.15)$$

where,

$$n_h = 11964 \text{ kN/m}^3 \text{ (See Table 4.14), } z = \text{depth (m)}$$

Table 4.14. Values of  $n_h$  ( $\text{kN/m}^3$ ) for sand (Poulos and Davis, 1980)

Relative Density	Loose	Medium	Dense
Range of Values of A	35188 - 105563	105563 - 351876	351876 - 703752
Adopted Values of A	70375	211126	527814
$n_h$ , dry or moist sand	2463	7389	19705
$n_h$ , submerged sand	1408	4926	11964

According to The Canadian Foundation Engineering Manual (Canadian Geotechnical Society, 2006), for spacing less than eight meters, the modulus of subgrade reaction of pile groups and the single-pile subgrade reaction ratios are recommended as: 0.70, 0.4, 0.25 for 6D spacing, 4D spacing and 3D spacing, respectively.

Also Davisson (1970) recommended that for 3D spacing group, the reduction factor is 0.25. Therefore, reduction factor is taken as 0.25.

$$k_{eff} = 0.25 k_h \quad (4.16)$$

where,

$k_{eff}$  = reduced modulus of subgrade reaction, (kN/m<sup>3</sup>)

$k_h$  = modulus of subgrade reaction, (kN/m<sup>3</sup>)

Calculated modulus of subgrade reactions and effective modulus of subgrade reactions of the soil are given according to depth in Table 4.15.

Table 4.15. Pile spring modulus of subgrade reaction and effective modulus of subgrade reaction list

Depth (m)	N	N <sub>60</sub>		k <sub>h</sub> (kN/m <sup>3</sup> )	k <sub>eff</sub> (kN/m <sup>3</sup> )
1.50-1.95	50	47	CLAYEY SANDY GRAVEL	23330	5832
3.50-3.95	30	28		47258	11814
5.00-5.45	34	32		65204	16301
7.00-7.45	37	35	SAND SILT CLAY ALTERATION	43706	10927
9.50-9.95	50	47		59063	14766
11.00-11.45	41	39		48431	12108
13.00-13.45	32	30		37800	9450
15.00-15.45	33	31		38981	9745
17.00-17.45	37	35		43706	10927
19.00-19.45	39	37		46069	11517
20.50-20.95	41	39		48431	12108
22.00-22.45	39	37		46069	11517
24.00-24.45	45	43		53156	13289
26.00-26.45	37	35		43706	10927
27.50-27.95	40	38		47250	11813
25.99-30.00	37	35		43706	10927

Winkler's spring system is used while assigning spring stiffness constants. According to Winkler, spring stiffness constant depends on the depth of soil, the spacing between the springs, and the modulus of subgrade reaction (Caner, 2014) (See Equation 4.17).

$$K_H = z_i L_i k_{eff} \quad (4.17)$$

where,

$z_i$  = soil depth from the riverbed for  $i^{\text{th}}$  spring (See Figure 4.18)

$L_i$  = spacing between the springs at the depth  $z_i$  (See Figure 4.18)

The system and calculated spring stiffness constants are given in Figure 4.18 and Table 4.16.

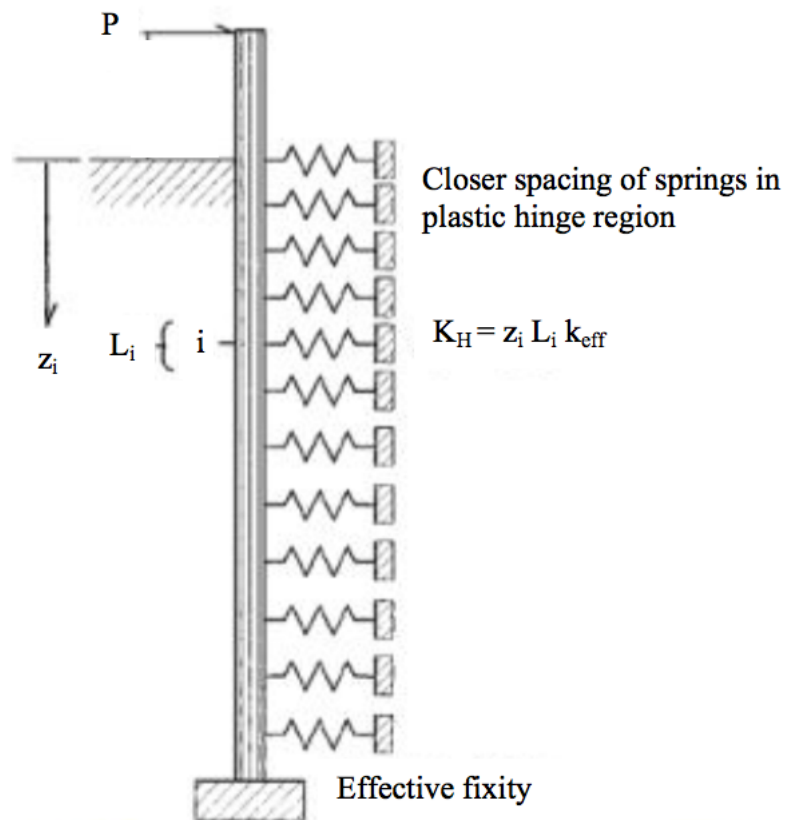


Figure 4.18. Winkler's spring system (Caner, 2014)

Table 4.16. Pile spring stiffness constant according to Winkler's spring system

$l_i$ (m)	$k_{eff}$ (kN/m <sup>3</sup> )	$z_i$ (m)	$K_{pi}$ (kN/m)
0.65	9600	2.15	13416
1.3	10000	3.45	44850
1	11000	4.75	52250
0.8	11800	5.45	51448
0.75	13000	6.35	61912,5
0.55	14000	6.95	53515
0.6	16300	7.45	72861
0.85	15000	8.15	72850
1	7500	9.15	68625
1	7500	10.15	76125
1	7500	11.15	83625
1	7500	12.15	91125
1	7500	13.15	98625
1	7500	14.15	106125
1	7500	15.15	113625
1	7500	16.15	121125
1	7500	17.15	128625
1	7500	18.15	136125
1	7500	19.15	143625
1	7500	20.15	151125
1	7500	21.15	158625
1	7500	22.15	166125
1	7500	23.15	173625
1	7500	24.15	181125
1	7500	25.15	188625

Yüksekol (2007) has made an iterative procedure to find out the effective moment of inertia ( $I_e$ ) of a pile section. Yüksekol (2007) has compared the results with the general assumption of taking the effective moment of inertia as half of the gross moment of inertia ( $I_g$ ) of a pile section,  $I_e = 0.5I_g$ . As a result, Yüksekol (2007) found out that there is no significant difference between the iterative process and the general assumption mentioned above. Therefore, the effective moment of inertia of the pile section is calculated with the general assumption for the studied bridge.

Pile load capacity:

According to Caltrans-SDC (2006), if the center to center spacing of adjacent piles is equal to or greater than  $3D$ , the group effect may be neglected for dynamic analyses. On the other hand, according to Das (2007), when center to center spacing is taken as  $2.5D$ , efficiency is calculated as  $0.955$ . For  $3D$  spacing, group efficiency is  $1.56$ . To be on the safe side, group efficiency is taken as  $0.955$ . Foundation layout presented by Das (2007) is shown in Figure 4.19.

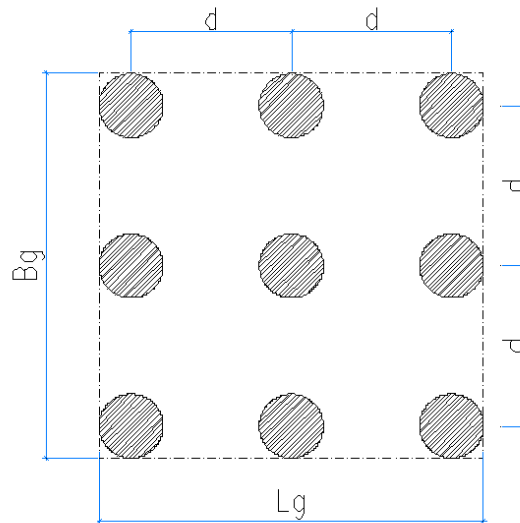


Figure 4.19. Foundation layout (Das, 2007)

Number of piles in group =  $n_1 n_2$

$$Lg = (n_1 - 1)d + 2\left(\frac{D}{2}\right) \tag{4.18}$$

$$Bg = (n_2 - 1)d + 2\left(\frac{D}{2}\right) \tag{4.19}$$

Note:  $L_g \geq B_g$

$$\eta = \frac{Q_{g(u)}}{\Sigma Q_u} = \frac{f_{av}[2(n_1 + n_2 - 2)d + 4D]L}{p n_1 n_2 L f_{av}} = \frac{2(n_1 + n_2 - 2)d + 4D}{p n_1 n_2} \quad (4.20)$$

where,

$\eta$  = group efficiency

$n_1$  = number of piles in one row

$n_2$  = number of piles in one column

$d$  = center to center spacing between adjacent piles, (m)

$D$  = pile diameter, (m)

$p$  = perimeter of the cross-section of each pile, (m)

In practice, if  $\eta < 1$  then,

$$Q_{g(u)} = \eta \Sigma Q_u \quad (4.21)$$

where,

$\eta$  = group efficiency

$Q_{g(u)}$  = ultimate load-bearing capacity of the group pile, (kN)

$Q_u$  = ultimate load-bearing capacity of each pile without group effect, (kN)

If  $\eta > 1$  then,

$$Q_{g(u)} = \Sigma Q_u \quad (4.22)$$

For the sake of simplicity,  $\eta$  is assumed as 0.955 for both directions while calculating the load capacity of piles. Concrete cover of the piles is selected as 7.5 cm.

### 4.3.5 Modal Analysis

Under earthquake excitation to measure the dynamic response of the structure, modal analysis has been conducted. As a result of the modal analysis, for each scour condition which are no scour case and 100-year flood case, different fundamental periods of the structure have been obtained. Fundamental periods and mode shapes can be seen in the Figures 4.20-4.25.

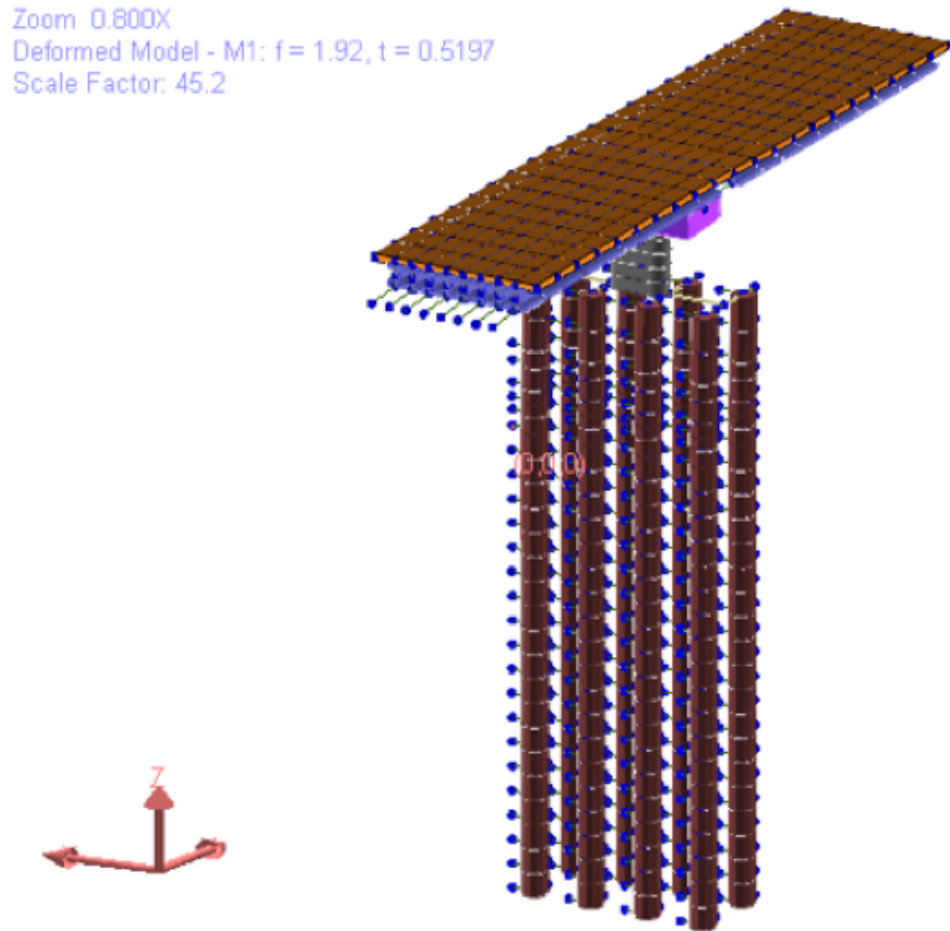


Figure 4.20 Mode shape 1 and fundamental period of original no scouring case

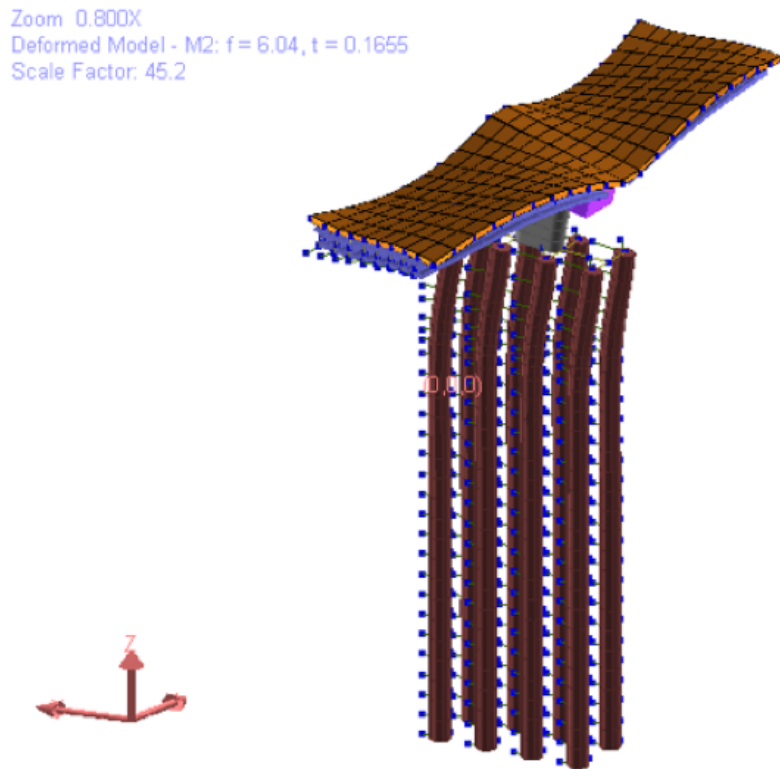


Figure 4.21. Mode shape 2 and fundamental period of original no scouring case

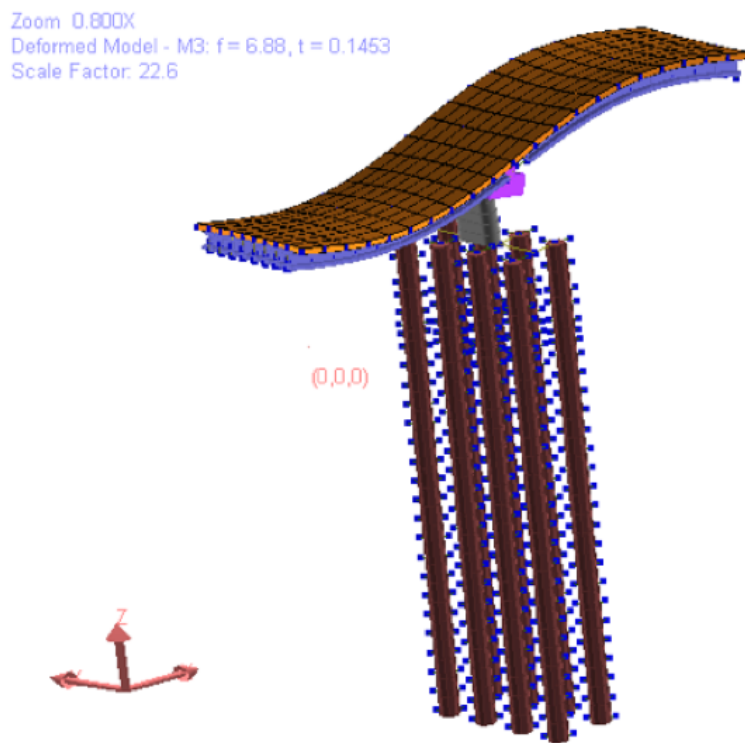


Figure 4.22. Mode shape 3 and fundamental period of original no scouring case

Zoom 0.800X  
Deformed Model - M1:  $f = 1.83$ ,  $t = 0.5475$   
Scale Factor: 64.

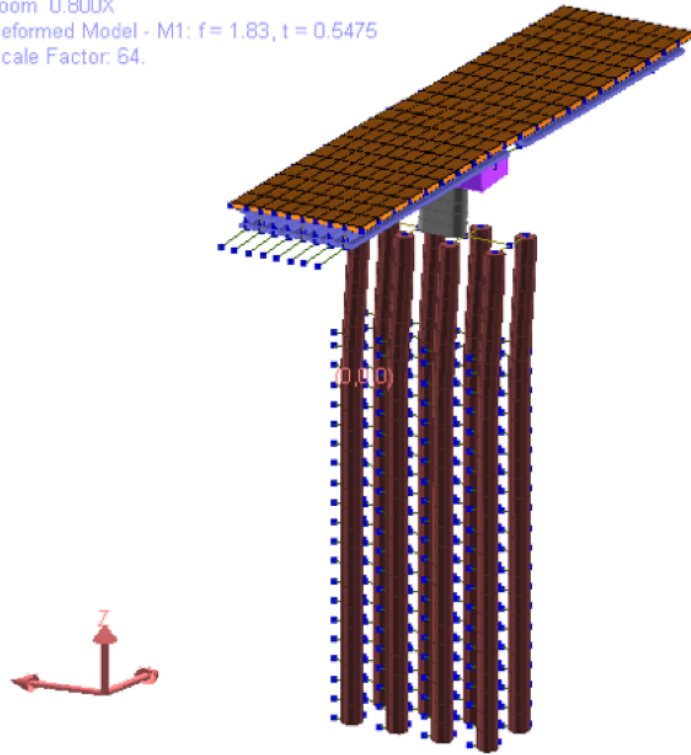


Figure 4.23. Mode shape 1 and fundamental period of 100-year flood case

Zoom 0.800X  
Deformed Model - M2:  $f = 5.02$ ,  $t = 0.1993$   
Scale Factor: 22.6

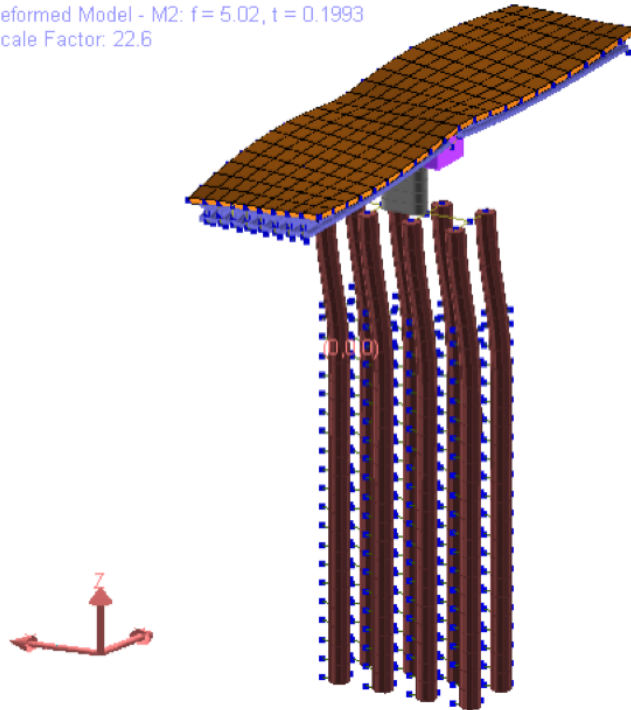


Figure 4.24. Mode shape 2 and fundamental period of 100-year flood case

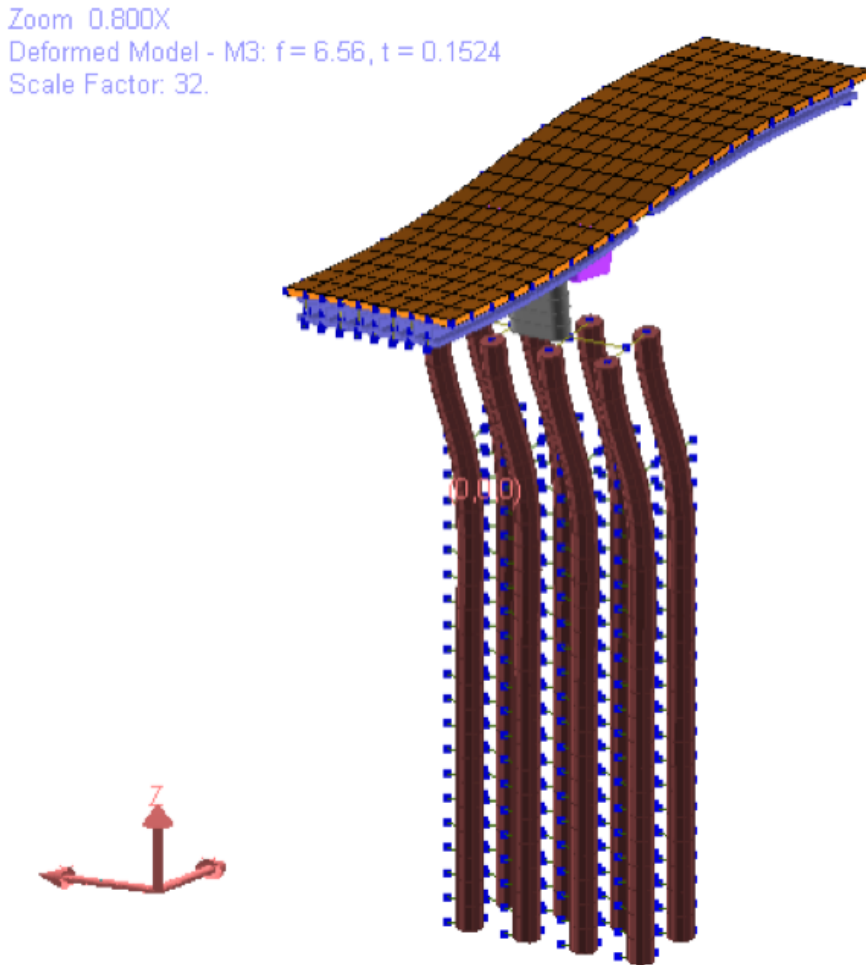


Figure 4.25. Mode shape 3 and fundamental period of 100-year flood case

#### 4.3.6 Response Spectrum Analysis

Complete quadratic combination (CQC), which is a load combination method is applied to combine for maximums of each mode. Total mass participation has to be greater than 90%. In order to ensure this rule, 100 modes have been computed. In the analyses, 4 different response spectrum functions, which have the return periods 100-year, 250-year, 475-year, and 1000-year, are used in the response spectrum functions. The response spectrum functions are presented in Figure 4.26.

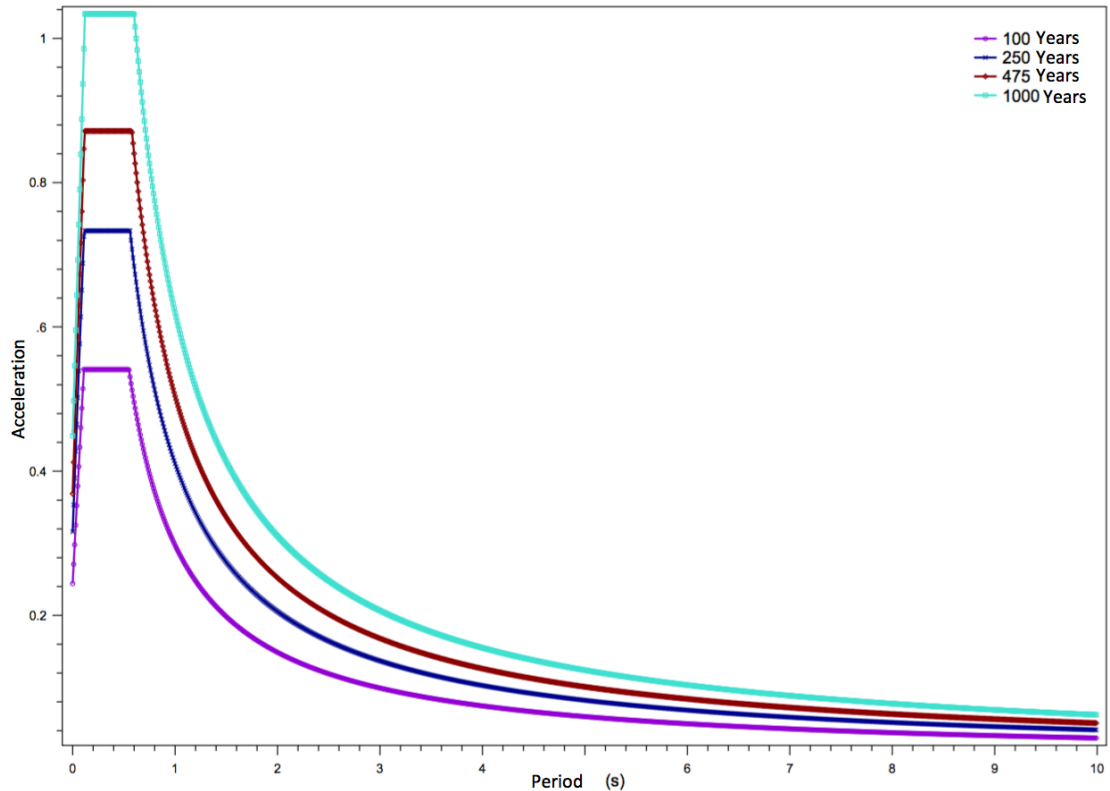


Figure 4.26. Design spectra for bridge location for return periods: 100 years, 250 years, 475 years and 1000 years

**Loads:** Within the scope of this study, dead load and earthquake loads are considered. Dead load is directly included by the program according to the defined unit weight and sectional characteristics. So there is no need to consider extra load assignment. The loads are expressed by:

DC : Dead load

EQ<sub>IJ</sub>: Earthquake load according to return period and direction

where, I: indicates return period, and J: indicates direction

**Load Combinations:** 9 load combination are investigated in this study.

Loading Combination 1: 1.0 DC

Loading Combination 2: 1.0 DC + 1.0 EQ<sub>100X</sub> + 0.3 EQ<sub>100Y</sub>

Loading Combination 3: 1.0 DC + 1.0 EQ<sub>100Y</sub> + 0.3 EQ<sub>100X</sub>

Loading Combination 4:  $1.0 \text{ DC} + 1.0 \text{ EQ}_{250\text{X}} + 0.3 \text{ EQ}_{250\text{Y}}$

Loading Combination 5:  $1.0 \text{ DC} + 1.0 \text{ EQ}_{250\text{Y}} + 0.3 \text{ EQ}_{250\text{X}}$

Loading Combination 6:  $1.0 \text{ DC} + 1.0 \text{ EQ}_{475\text{X}} + 0.3 \text{ EQ}_{475\text{Y}}$

Loading Combination 7:  $1.0 \text{ DC} + 1.0 \text{ EQ}_{475\text{Y}} + 0.3 \text{ EQ}_{475\text{X}}$

Loading Combination 8:  $1.0 \text{ DC} + 1.0 \text{ EQ}_{1000\text{X}} + 0.3 \text{ EQ}_{1000\text{Y}}$

Loading Combination 9:  $1.0 \text{ DC} + 1.0 \text{ EQ}_{1000\text{Y}} + 0.3 \text{ EQ}_{1000\text{X}}$

## 4.4 RESULTS

The results of the analyses are presented for two scenarios:

- **Scenario-1:** Soil consists of two layers which are sand and clay.
- **Scenario-2:** Soil consists of only one type of layer which is sand.

### 4.4.1 Column Demand to Capacity Ratio

DCR ( $M_u/\phi M_n$ ) should be smaller than 1.0. If the ratio is greater than 1.0, it indicates that the structure capacity is not enough.  $M_u$  is the ultimate moment strength,  $M_n$  is the nominal moment strength and  $\phi$  is the strength reduction factor which is equal to 0.9. For this study, all the results are smaller than 1.0. For different scour levels, capacity change in column can be observed from Table 4.17. Structure gains flexibility and natural period increases as the foundation gets scoured. As it is given in the Table 4.17 and Table 4.18, column DCR increases up to 21% and 31% for Scenario-1 and Scenario-2, respectively, in which  $\Delta$  stands for percent difference between un-scoured and scoured condition.

Table 4.17. Column DCR matrix for two layered system

<b>DCR</b> <b>(<math>M_u/\phi M_n</math>)</b>	<b>NO SCOUR</b>	<b>Q<sub>2</sub></b>	<b>Q<sub>5</sub></b>	<b>Q<sub>10</sub></b>	<b>Q<sub>25</sub></b>	<b>Q<sub>50</sub></b>	<b>Q<sub>100</sub></b>	<b>Δ</b>
<b>COMB 1</b>	0.10	0.10	0.10	0.10	0.10	0.10	0.10	0.0%
<b>COMB 2</b>	0.57	0.56	0.54	0.51	0.48	0.48	0.48	9.0%
<b>COMB 3</b>	0.41	0.40	0.36	0.32	0.27	0.27	0.27	14.0%
<b>COMB 4</b>	0.76	0.75	0.72	0.69	0.66	0.66	0.66	10.0%
<b>COMB 5</b>	0.54	0.53	0.47	0.42	0.37	0.37	0.37	17.0%
<b>COMB 6</b>	0.87	0.86	0.82	0.79	0.76	0.76	0.76	11.0%
<b>COMB 7</b>	0.62	0.61	0.54	0.48	0.42	0.42	0.42	20.0%
<b>COMB 8</b>	0.89	0.87	0.84	0.81	0.77	0.77	0.77	12.0%
<b>COMB 9</b>	0.64	0.62	0.55	0.49	0.43	0.43	0.43	21.0%

Table 4.18. Column DCR matrix for one layered system

<b>DCR</b> <b>(<math>M_u/\phi M_n</math>)</b>	<b>NO SCOUR</b>	<b>Q<sub>2</sub></b>	<b>Q<sub>5</sub></b>	<b>Q<sub>10</sub></b>	<b>Q<sub>25</sub></b>	<b>Q<sub>50</sub></b>	<b>Q<sub>100</sub></b>	<b>Δ</b>
<b>COMB 1</b>	0.10	0.10	0.10	0.10	0.10	0.10	0.10	0.0%
<b>COMB 2</b>	0.57	0.56	0.54	0.51	0.48	0.46	0.44	13.0%
<b>COMB 3</b>	0.41	0.40	0.36	0.32	0.27	0.24	0.21	20.0%
<b>COMB 4</b>	0.76	0.75	0.72	0.69	0.66	0.63	0.61	15.0%
<b>COMB 5</b>	0.54	0.53	0.47	0.42	0.37	0.32	0.28	26.0%
<b>COMB 6</b>	0.87	0.86	0.82	0.79	0.76	0.73	0.70	17.0%
<b>COMB 7</b>	0.62	0.61	0.54	0.48	0.42	0.36	0.32	30.0%
<b>COMB 8</b>	0.89	0.87	0.84	0.81	0.77	0.74	0.71	18.0%
<b>COMB 9</b>	0.64	0.62	0.55	0.49	0.43	0.37	0.33	31.0%

#### 4.4.2 Pile Load Capacity

For Scenario-1, single pile load capacity in group changes from 5362 kN to 5269.9 kN. So, it decreases 1.7%. Axial load acting on a single pile changes from 1981 kN to 2308 kN with an increase of 16.5%.

For Scenario-2, single pile capacity in group changes from 11170.6 kN to 11078.6 kN. So, it decreases 0.8%. Axial load acting on a single pile changes from 1981 kN to 2389 kN with an increase of 20.6%.

Pile group capacity depends on the skin friction capacity and end bearing capacity of the pile. Sum of the skin friction capacity and the end bearing capacity of a pile gives the pile capacity for a single pile,  $Q_u$ :

$$Q_u = Q_s + Q_p \quad (4.23)$$

where,

$Q_s$ = Total skin friction resistance, (kN)

$Q_p$ = Total bearing resistance, (kN)

#### Scenario-1:

##### Frictional resistance in cohesionless soil:

Frictional resistance in sand,  $Q_{s,sand}$  is given by:

$$Q_{s,sand} = \Sigma p \Delta L f = p L f_{av} \quad (4.24)$$

where,

$p$ = perimeter of pile, (m)

$L$ = pile length in sand layer, (m)

$f_{av}$ = average unit frictional resistance, (kN/m<sup>2</sup>)

After a certain depth, unit frictional resistance does not change. This depth is called critical depth.

Critical depth,  $L' \approx 15D$  (See Figure 4.27)

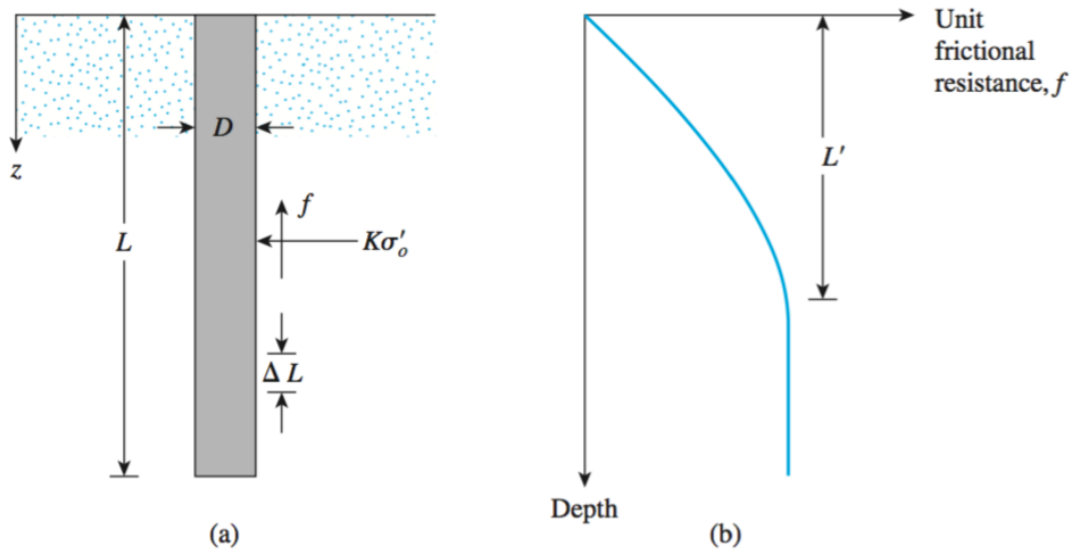


Figure 4.27. Unit frictional resistance and effective length of pile representation  
(Das, 2007)

For  $z = 0$  to  $L'=15$  m

Unit frictional resistance:

$$f = K \sigma'_o \tan \delta \quad (4.25)$$

where,

$K$  = effective earth coefficient

$\sigma'_o$  = effective vertical stress at the depth under consideration, ( $\text{kN/m}^2$ )

$\delta$  = soil-pile friction angle, (deg)

$$K = 1 - \sin \phi \quad (4.26)$$

where,  $\phi$  = angle of internal friction for soil

Hatanaka and Uchida (1996) recommend an equation for the relation between  $N$  value and internal angle of friction (See Equation 4.27).

$$\phi = \sqrt{20N} + 20 \quad (4.27)$$

Average N-value is used. For the simplicity,  $N = 31$  is taken.

Peck's and Meyerhof's correlations between SPT-N and  $\phi$  values are given in Table 4.19 (Gunaratne, 2013).

Table 4.19. Angle of internal friction values according to Peck and Meyerhof (Gunaratne, 2013)

SPT-N	Density of Sand	According to Peck $\phi$ (°)	According to Meyerhof $\phi$ (°)
< 4	Very loose	< 29	< 30
4 - 10	Loose	29 - 30	30 - 35
10 - 30	Medium	30 - 36	35 - 40
30 - 50	Dense	36 - 41	40 - 45
> 50	Very Dense	> 41	> 45

Therefore, considering three different recommendations  $\phi$  value is assumed as  $40^\circ$ .

Effective vertical stress at a particular depth  $z$ ,

$$\sigma'_o = z \gamma' \quad (4.28)$$

where,  $z$ = depth, (m)

$$\gamma' = \gamma_{sat} - \gamma_{water} \quad (4.29)$$

saturated unit weight of soil ( $\gamma_{sat}$ ) is assumed as  $21 \text{ kN/m}^3$ . Then,  $\gamma' = 11 \text{ kN/m}^3$  is obtained. Effective vertical stress distribution is shown in Figure 4.28. Average effective vertical stress,  $(\sigma'_o)_{av}$  is found by dividing the total effective stress area to the length.

$$(\sigma'_o)_{av} = \frac{A}{L} = 44.8 \text{ kN/m}^2 \quad (4.30)$$

where,

A= total effective stress area, 172.6 kN/m (See Figure 4.28)

L= considered length, 3.85 m (See Figure 4.28)

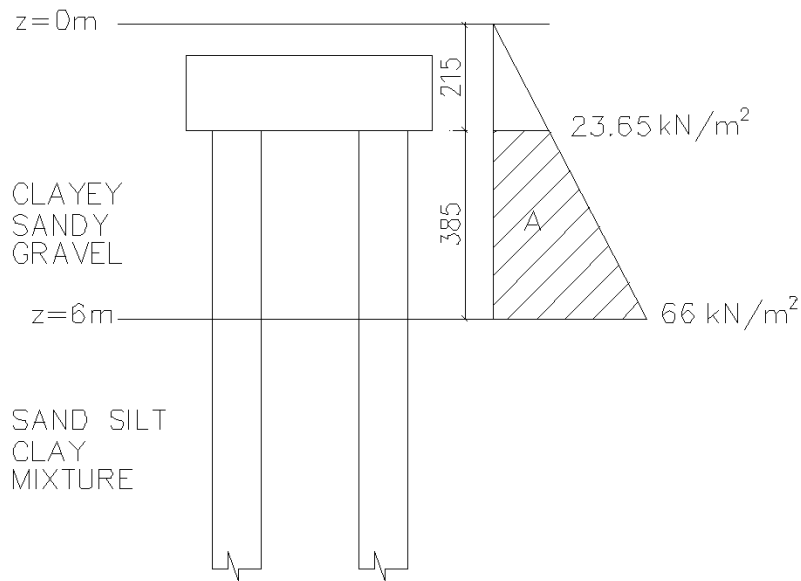


Figure 4.28. Pressure distribution through the pile for Scenario 1

Average unit skin friction,  $f_{av}$

$$f_{av} = K (\sigma'_o)_{av} \tan \delta = 8.1 \text{ kN/m}^2 \quad (4.31)$$

where,

$$\tan \delta = \tan \left( \frac{2}{3} \phi \right) = 0.502 \quad (4.32)$$

For sandy soil, calculated total friction resistances for each case (no scour,  $Q_2$ ,  $Q_5$ ,  $Q_{10}$ ,  $Q_{25}$ ,  $Q_{50}$  and  $Q_{100}$ ) are given in Table 4.20.

Frictional resistance in cohesive soil:

While calculating frictional resistance in clay,  $\alpha$  method has been used (Das, 2007).

$$Q_{s,clay} = \alpha c_u A_s \quad (4.33)$$

where,

$\alpha$ = adhesion factor, 0.4 (See Figure 4.29)

$c_u$ = undrained shear strength, 152 kN/m<sup>2</sup>

$A_s$ = shaft friction area, m<sup>2</sup>

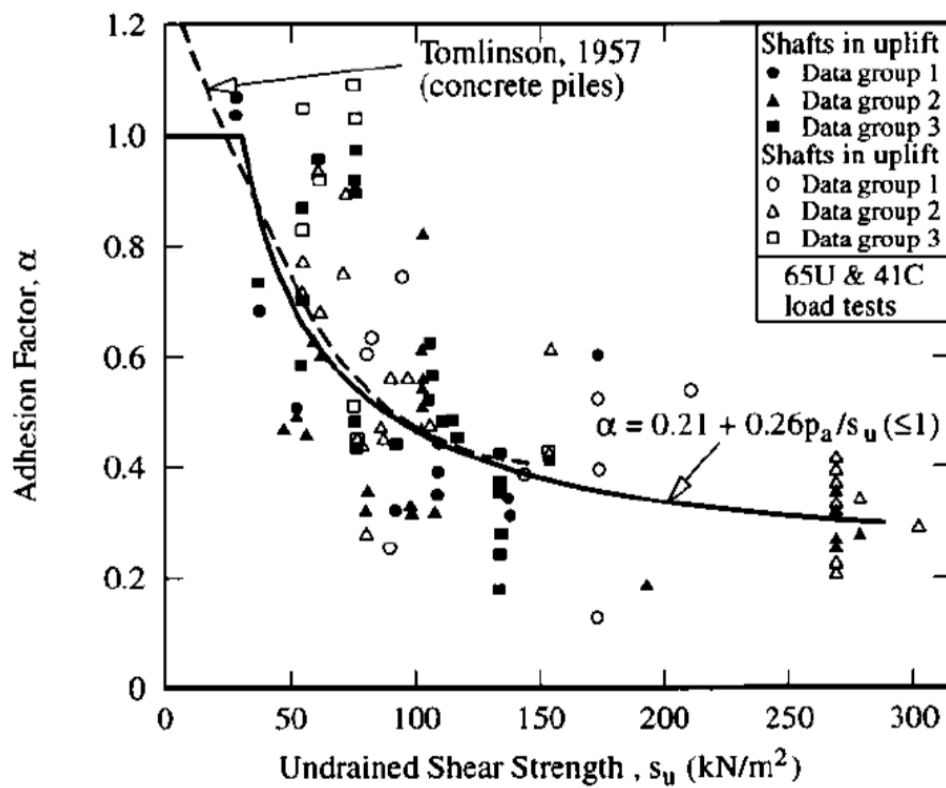


Figure 4.29. Adhesion factor and undrained shear strength relation (Das, 2007)

For clayey soil, calculated total friction resistances for each case (no scour,  $Q_2$ ,  $Q_5$ ,  $Q_{10}$ ,  $Q_{25}$ ,  $Q_{50}$  and  $Q_{100}$ ) are given in Table 4.20.

End bearing resistance:

For the piles in saturated clay, end bearing resistance can be calculated from (Das, 2007).

$$Q_p \approx N_c c_u A_p \quad (4.34)$$

where,

$N_c$ = bearing capacity factor for cohesion for deep foundations, 9

$c_u$ = undrained shear strength, kN/m<sup>2</sup>

$A_p$ = area of pile tip, m<sup>2</sup>

End bearing resistance and total capacity of a single pile, which is calculated according to Equations 4.33-4.35, is presented in summary table, Table 4.20.

Table 4.20. Capacity table for a single pile

Case Name	Skin Friction for Sand $Q_{s,sand}$ (kN)	Skin Friction for Clay $Q_{s,clay}$ (kN)	Total Skin Friction $Q_s$ (kN)	End Bearing Resistance $Q_p$ (kN)	Total Capacity $Q_u$ (kN)
No Scour	97.2	4443.8	4541.0	1074.4	5615.5
Q <sub>2</sub>	85.8	4443.8	4529.7	1074.4	5604.1
Q <sub>5</sub>	57.8	4443.8	4501.6	1074.4	5576.1
Q <sub>10</sub>	33.6	4443.8	4477.4	1074.4	5551.8
Q <sub>25</sub>	0.0	4443.8	4443.8	1074.4	5518.2
Q <sub>50</sub>	0.0	4443.8	4443.8	1074.4	5518.2
Q <sub>100</sub>	0.0	4443.8	4443.8	1074.4	5518.2

As indicated in section 4.3.4.2 for a group of piles, group efficiency should be taken into account. So, the total load capacity should be reduced by multiplying it with the

group efficiency factor, which is 0.955. Pile ultimate group capacity and applied axial loads which are obtained from structural analysis are given Table 4.21.

Table 4.21. Ultimate load capacity and axial load table

Case Name	Total Capacity $Q_u$ (kN)	Pile Group Capacity $(Q_u)_g$ (kN)	Axial Load (kN)
No Scour	5615.5	5362.8	1981.0
$Q_2$	5604.1	5351.9	2046.0
$Q_5$	5576.1	5325.1	2165.7
$Q_{10}$	5551.8	5302.0	2241.2
$Q_{25}$	5518.2	269.9	2308.0
$Q_{50}$	5518.2	5269.9	2355.6
$Q_{100}$	5518.2	5269.9	2389.1

Figure 4.30 and Figure 4.31 show the change of single pile capacity and group pile capacity according to corresponding axial load.

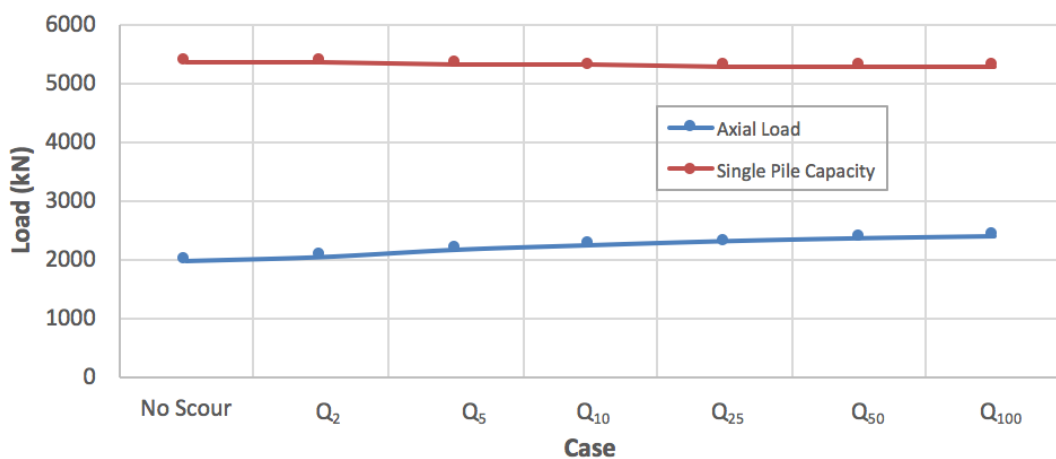


Figure 4.30. Axial load and single pile capacity change for different flow rates

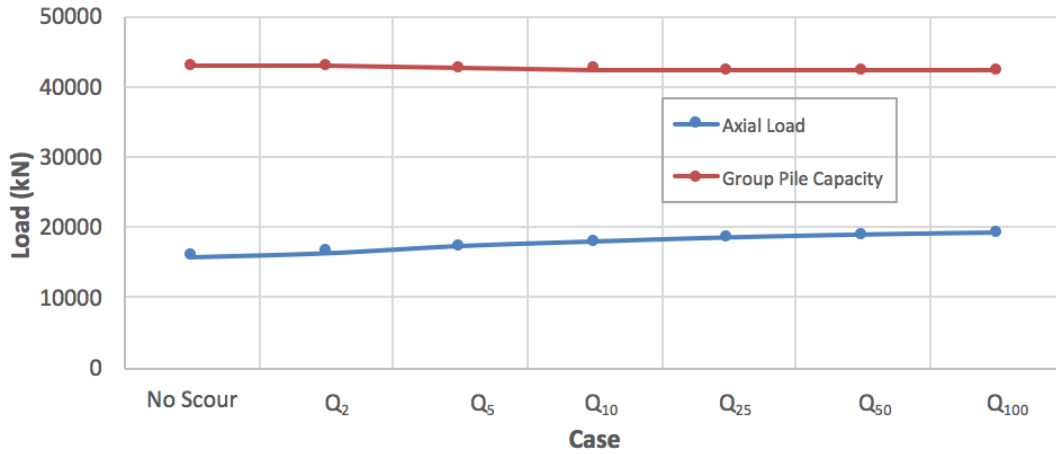


Figure 4.31. Axial load and group pile capacity change for different flow rates

**Scenario-2:**

If the whole pile system in the sand and the soil had the same properties with the first layer, then capacity would be as follows:

$Q_{s,sand}$ :

For  $z = 0$  to  $L'=15$  m

$$f = K \sigma'_o \tan \delta \tag{4.35}$$

For  $z=L'$  to  $L$

$$f = f_{z=L'} \tag{4.36}$$

The pressure distribution through the pile is shown in Figure 4.32.

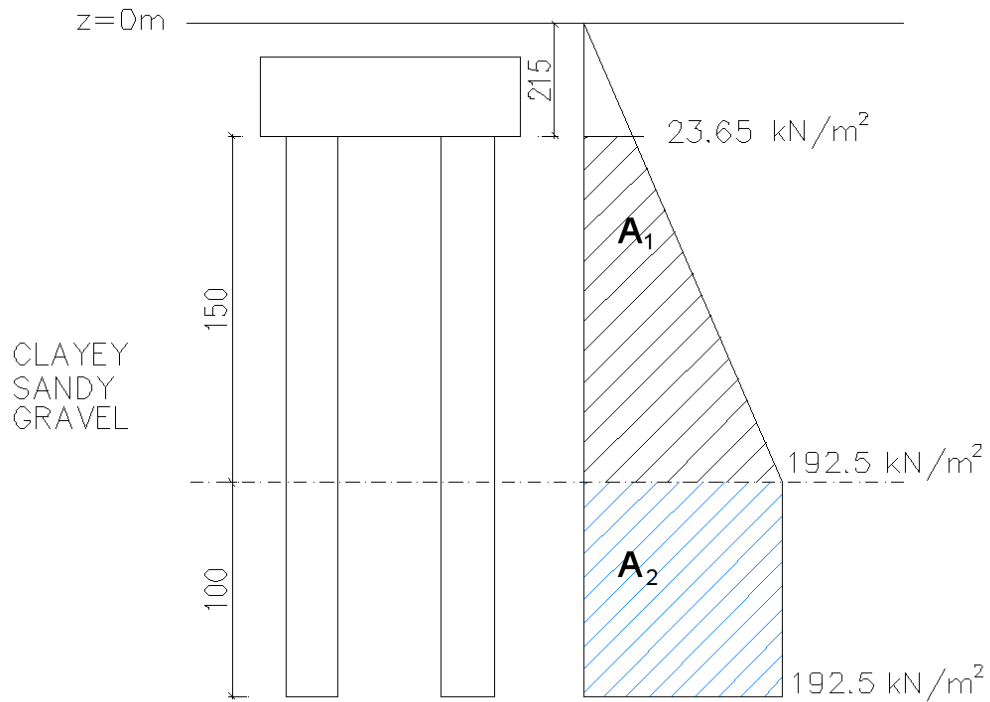


Figure 4.32 Pressure distribution through the pile for Scenario 2

$$A_1 = 1621.1\text{ kN/m}^2$$

$$A_2 = 1925\text{ kN/m}^2$$

$$(\sigma_0)'_{av1} = 108.1\text{ kN/m}^2$$

$$(\sigma_0)'_{av2} = 192.5\text{ kN/m}^2$$

$$f_1 = 19.5\text{ kN/m}^2$$

$$f_2 = 34.8\text{ kN/m}^2$$

$$Q_{s,sand1} = 920.8\text{ kN}$$

$$Q_{s,sand2} = 1093.0\text{ kN}$$

$$Q_{s,sand} = 920.8 + 1093 = 2013.8\text{ kN}$$

$$Q_{p,sand} = N_q(\sigma_0)'_{z=L} A_p = 9066.8\text{ kN}$$

where,

$N_q$ = bearing capacity factor for deep foundations, see Table 4.22.

Table 4.22.  $N_q$  values

$\phi$ (°)	20	25	28	30	32	34	36	38	40	42	45
$N_q$ (driven)	8	12	20	25	35	45	60	80	120	160	230
$N_q$ (bored)	4	5	8	12	17	22	30	40	60	80	115

Calculated total capacity of a single pile ( $Q_u$ ) is 11170.6 kN. In Scenario-1 the  $Q_u$  is equal to 5615.5 kN for no scour condition.

**4.4.3 Pile M-N Interaction Curve**

To understand how the moment changes from no scour condition to  $Q_{100}$  condition, maximum moments that are obtained as a result of analyses, are observed. Load combination 8 gives the maximum moments through the piles. For Combination 8, the moment changes from 451 kN.m to 1214 kN.m. So 169% moment increase is observed and presented in Figure 4.33.

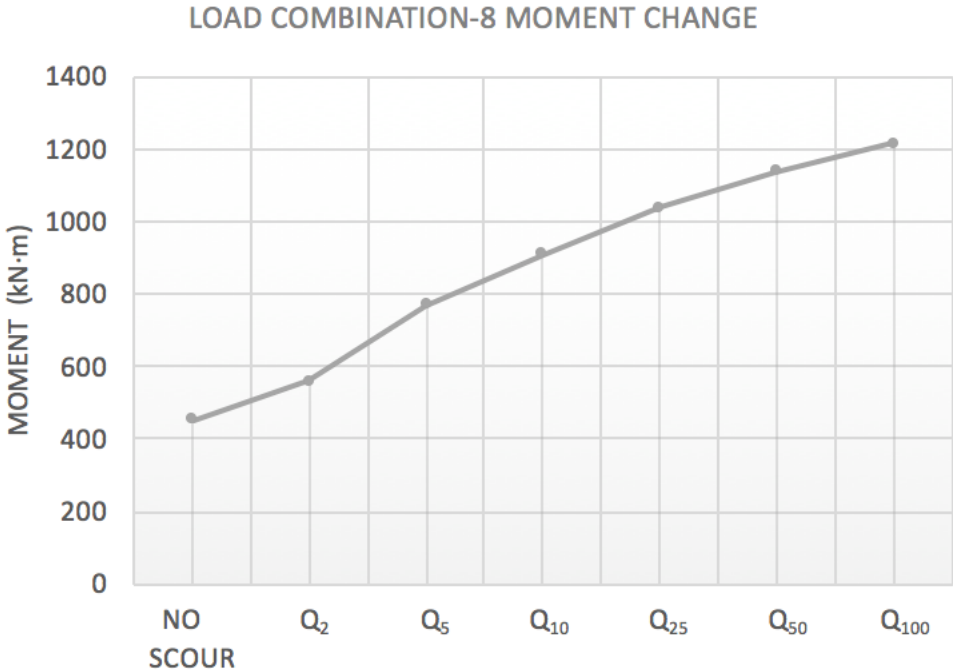


Figure 4.33. Moment change under different conditions for the load combination 8

Pile M-N interaction curves for both directions (weak and strong) are presented in Figures 4.34 – 4.54. For each condition (no scour,  $Q_2$ ,  $Q_5$ ,  $Q_{10}$ ,  $Q_{25}$ ,  $Q_{50}$ ,  $Q_{100}$ ) three load combination, which are combination 1, combination 8 and combination 9, are selected. The reason for this selection is that they are the extremes of the analysis. While the load combination 1 gives the most secure result, combination 8 and combination 9 give the most unsafe situation. Combination 8 and combination 9 are subjected to the same response spectrum function however, the combination 8

governs in the weak direction of the system. The other M-N interaction diagrams of the piles for the load combination 2, 3, 4, 5, 6, 7 are given in Appendix A.

In the graphs (See Figures 4.34 – 4.54), the interaction curve, which is green, indicates the moment-axial load capacity of the pile section. The blue dots indicate the MY-N loads and the red dots indicate the MZ-N loads, which the piles are subjected to. If the dots are within the interaction curve, it means that the section is safe in terms of flexure. As the dots approach to the interaction boundary, the section approaches its flexure capacity. If the dots are located outside the interaction curve, flexure capacity of the pile section is exceeded.

In the light of above explanation,

- Combination 1: Since the bridge geometry is symmetric and the spring stiffness are small when they are close to riverbed, pile reactions do not change significantly for no scour and scoured conditions.
- Combination 8: This is the most crucial combination for the bridge. From the no scour case to the  $Q_{100}$  case, pile reactions gets closer to the boundary. If the total pile number was less or the pile section was smaller, the pile foundation might fail.
- Combination 9: This is an important combination in terms of flexure capacity of the piles. Pile reactions gets close to the M-N curve from no scour case to  $Q_{100}$  case. The difference between the results of combination 8 and combination 9 occurs due to the direction of the earthquake.

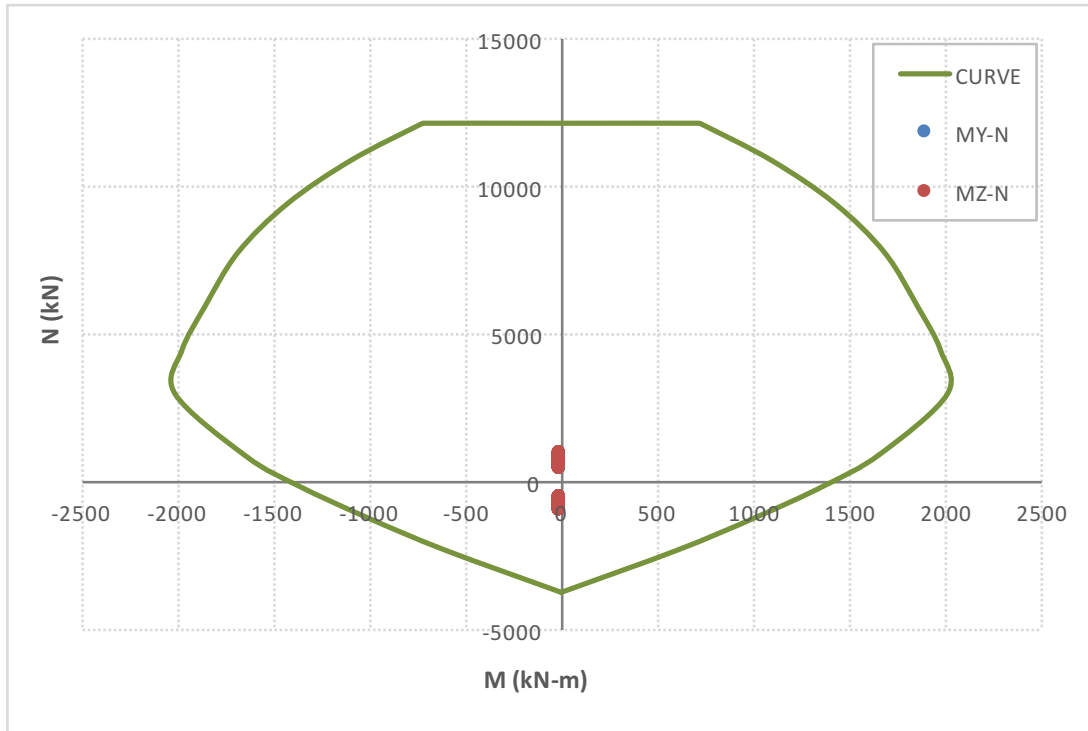


Figure 4.34. No scour case pile M-N interaction diagram for Combination 1

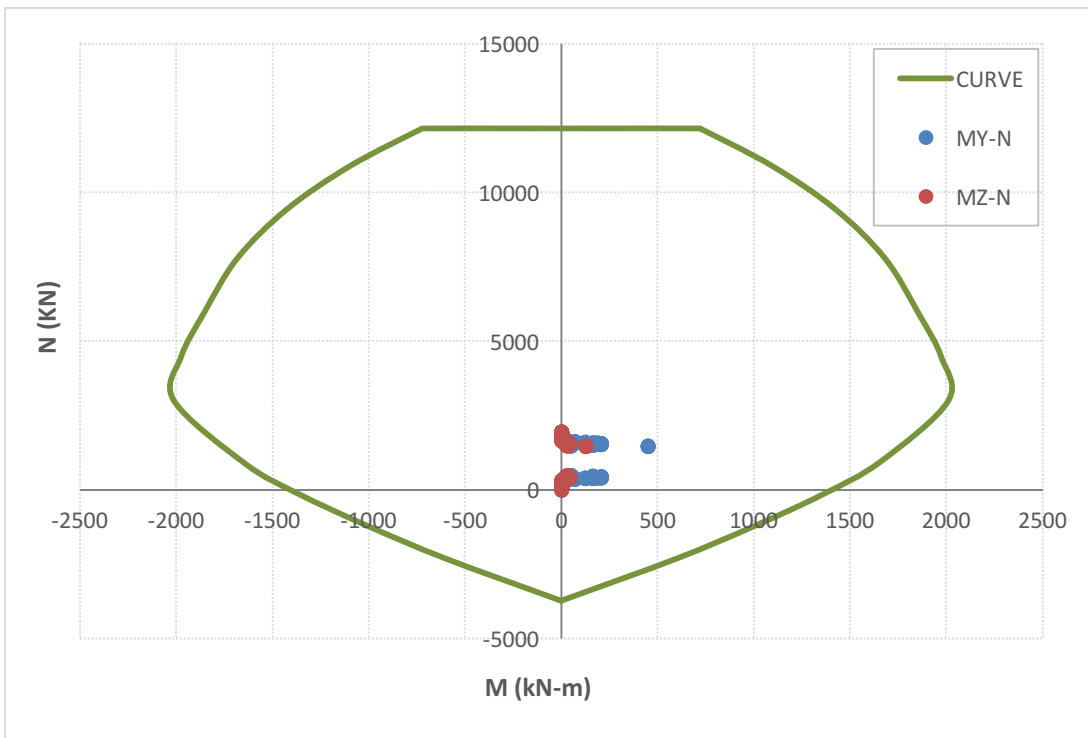


Figure 4.35. No scour case pile M-N interaction diagram for Combination 8

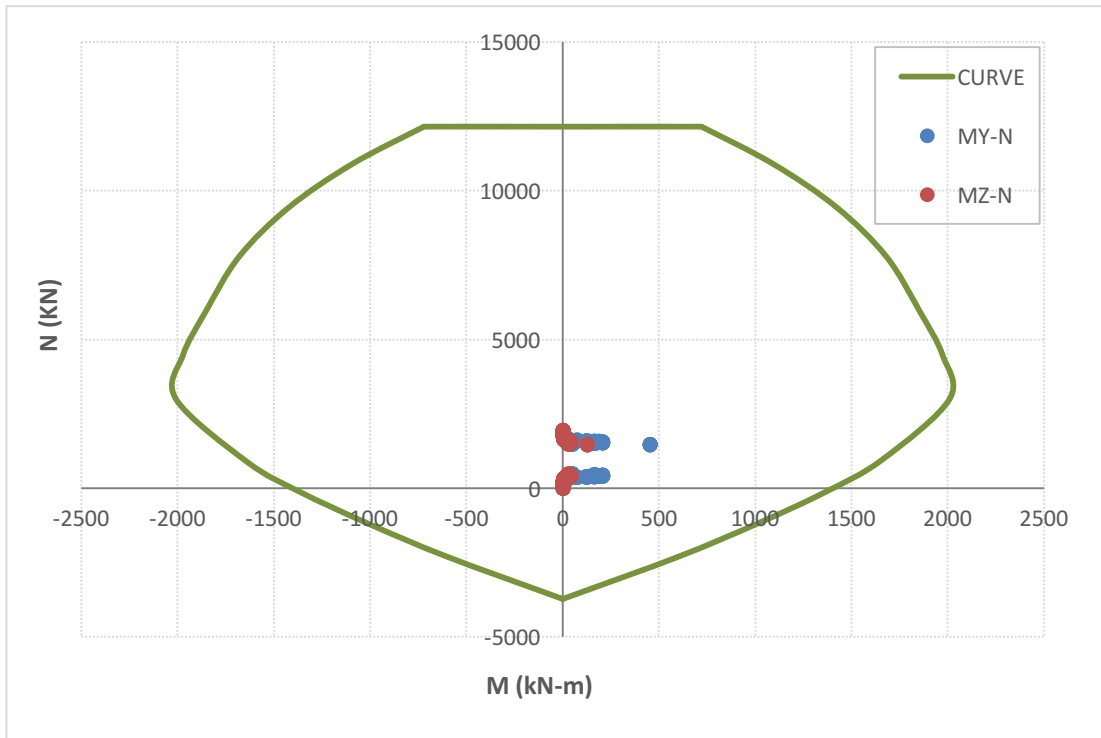


Figure 4.36. No scour case pile M-N interaction diagram for Combination 9

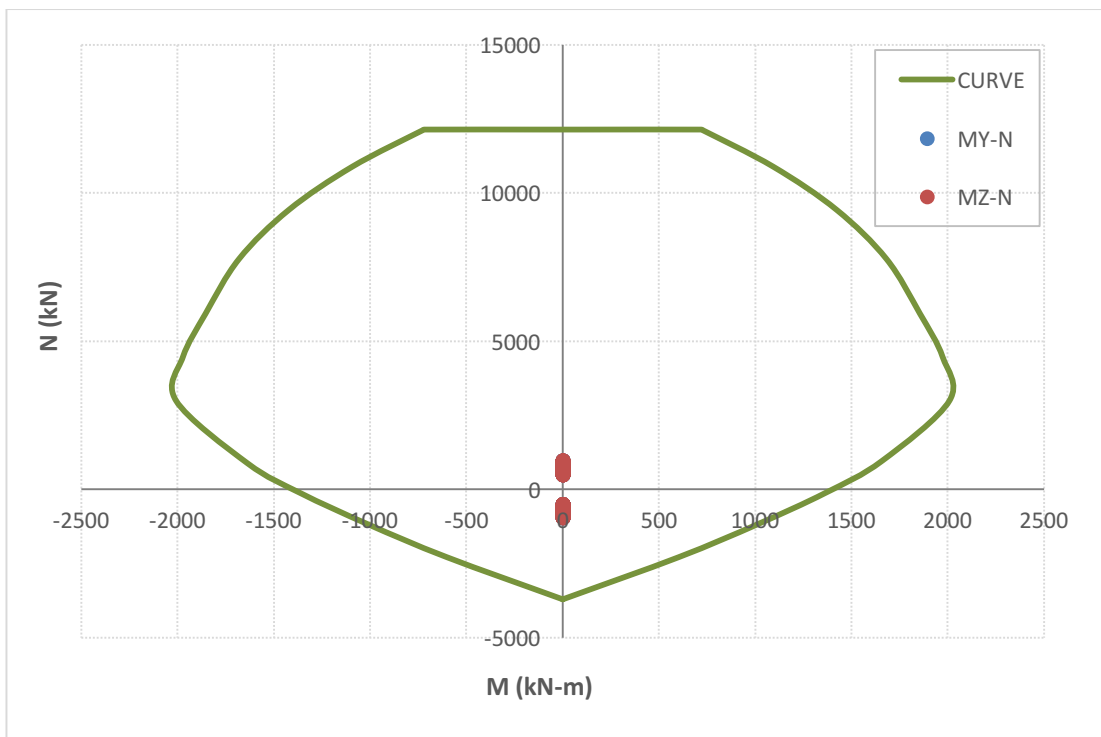


Figure 4.37. Q<sub>2</sub> case pile M-N interaction diagram for Combination 1

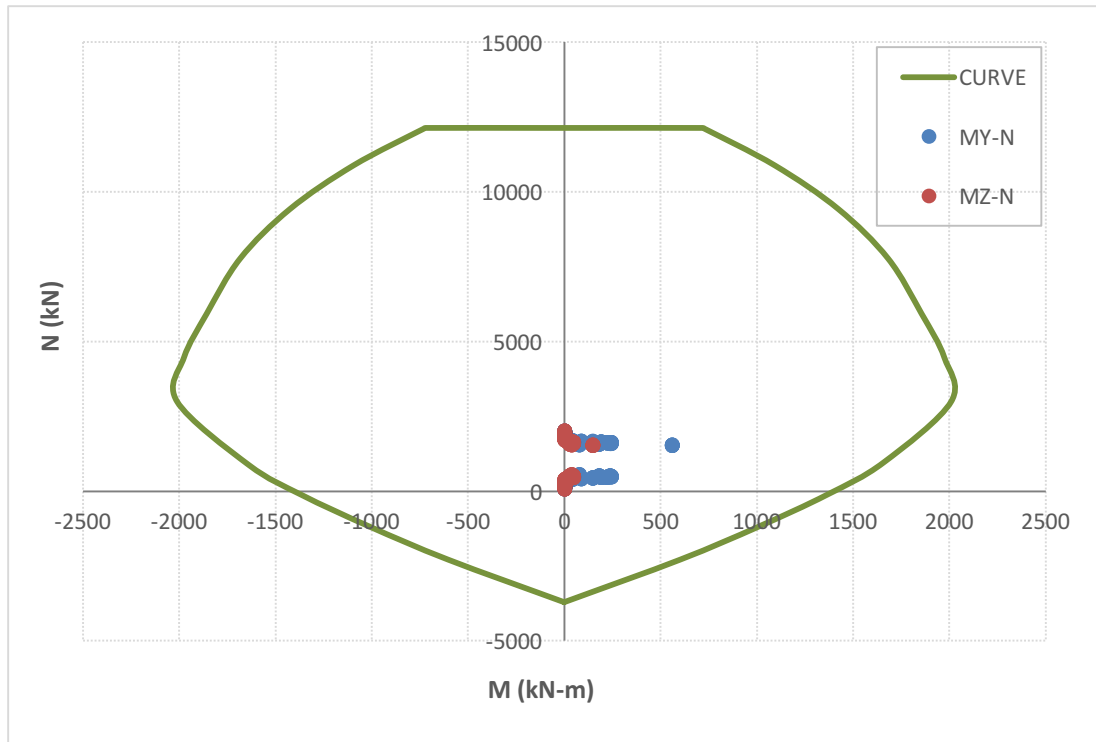


Figure 4.38. Q<sub>2</sub> case pile M-N interaction diagram for Combination 8

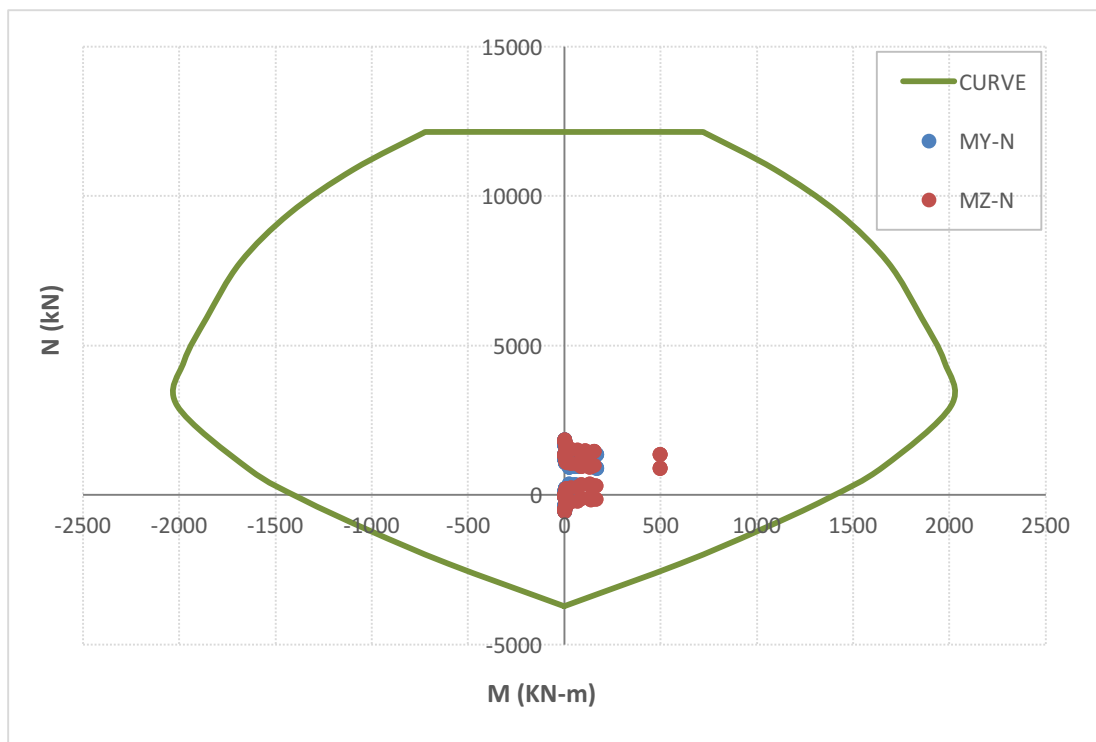


Figure 4.39. Q<sub>2</sub> case pile M-N interaction diagram for Combination 9

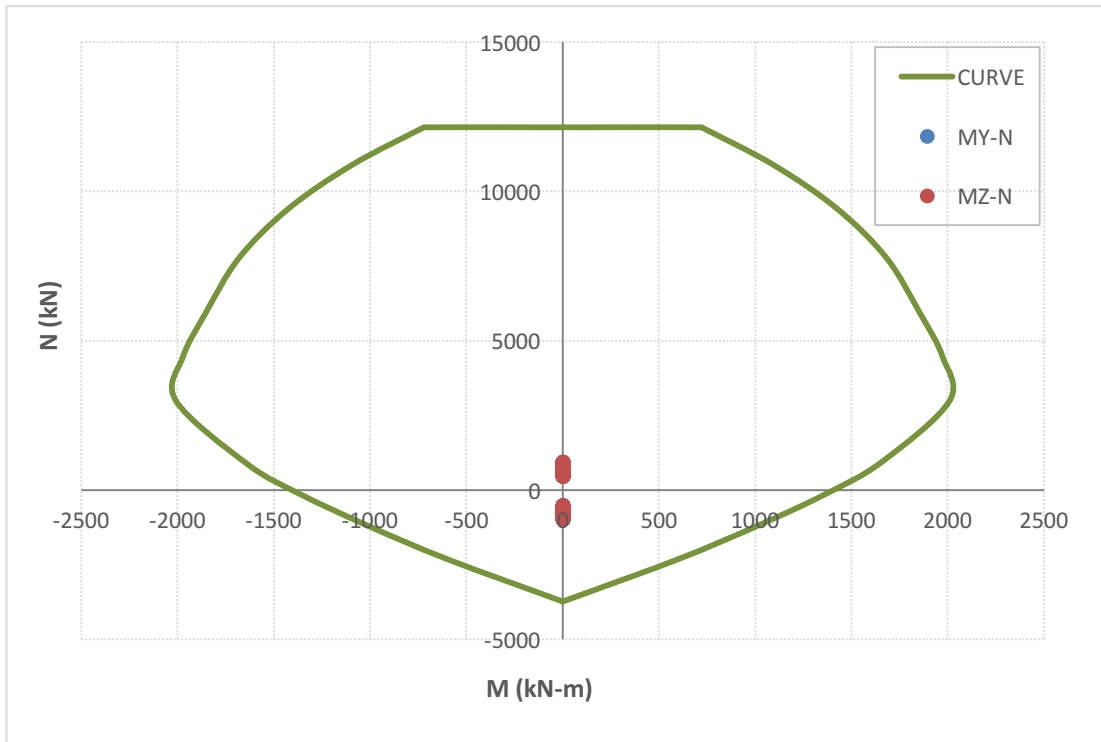


Figure 4.40. Q<sub>5</sub> case pile M-N interaction diagram for Combination 1

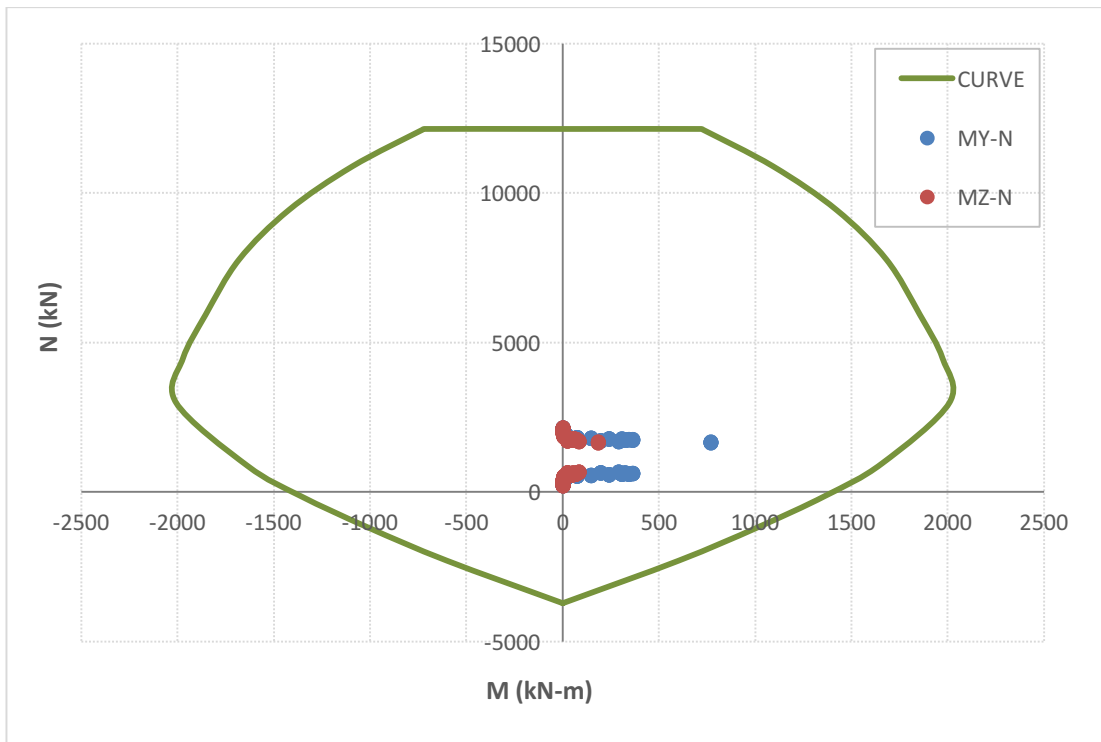


Figure 4.41. Q<sub>5</sub> case pile M-N interaction diagram for Combination 8

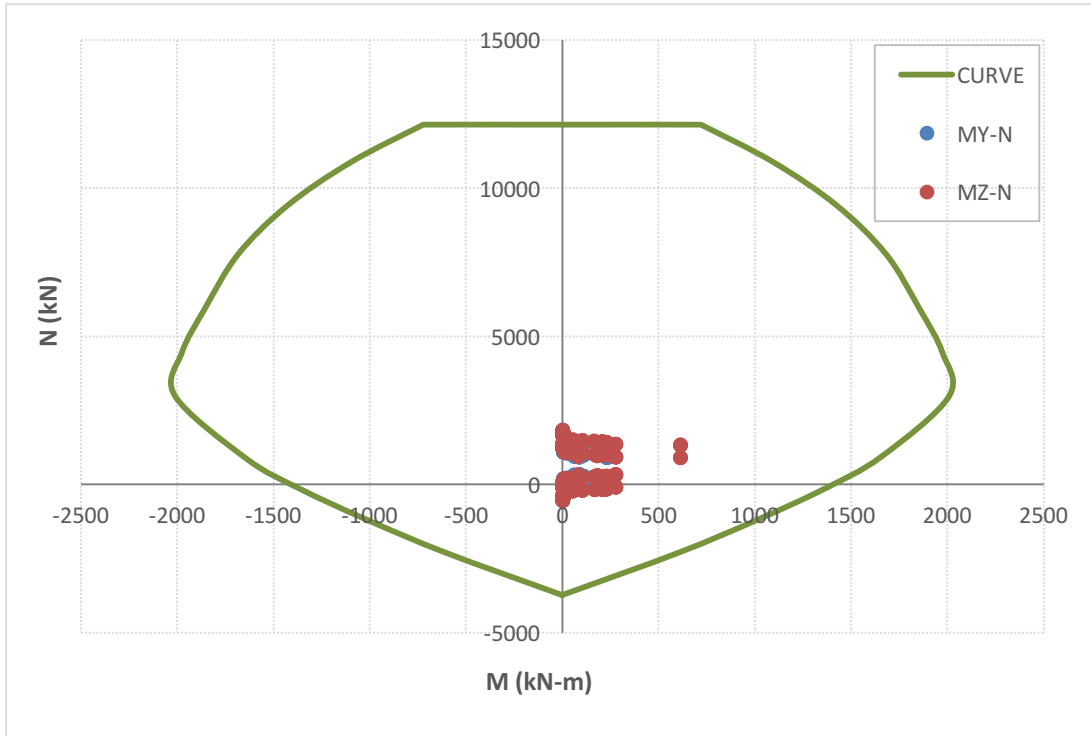


Figure 4.42. Q<sub>5</sub> case pile M-N interaction diagram Combination 9

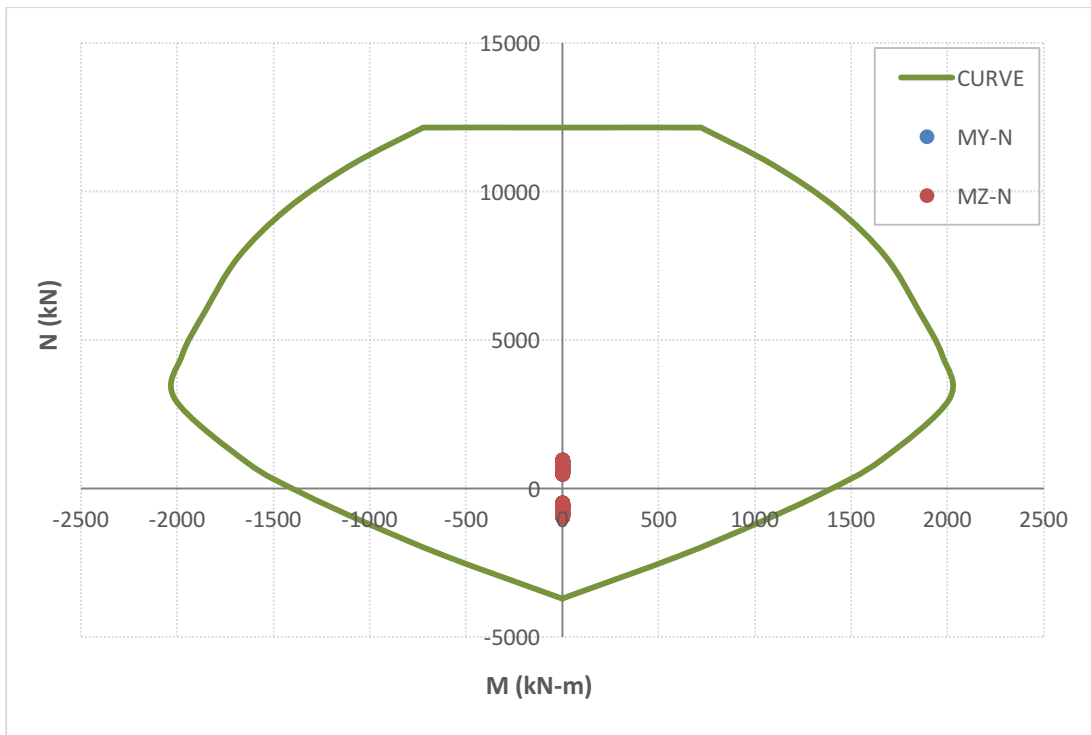


Figure 4.43. Q<sub>10</sub> case pile M-N interaction diagram for Combination 1

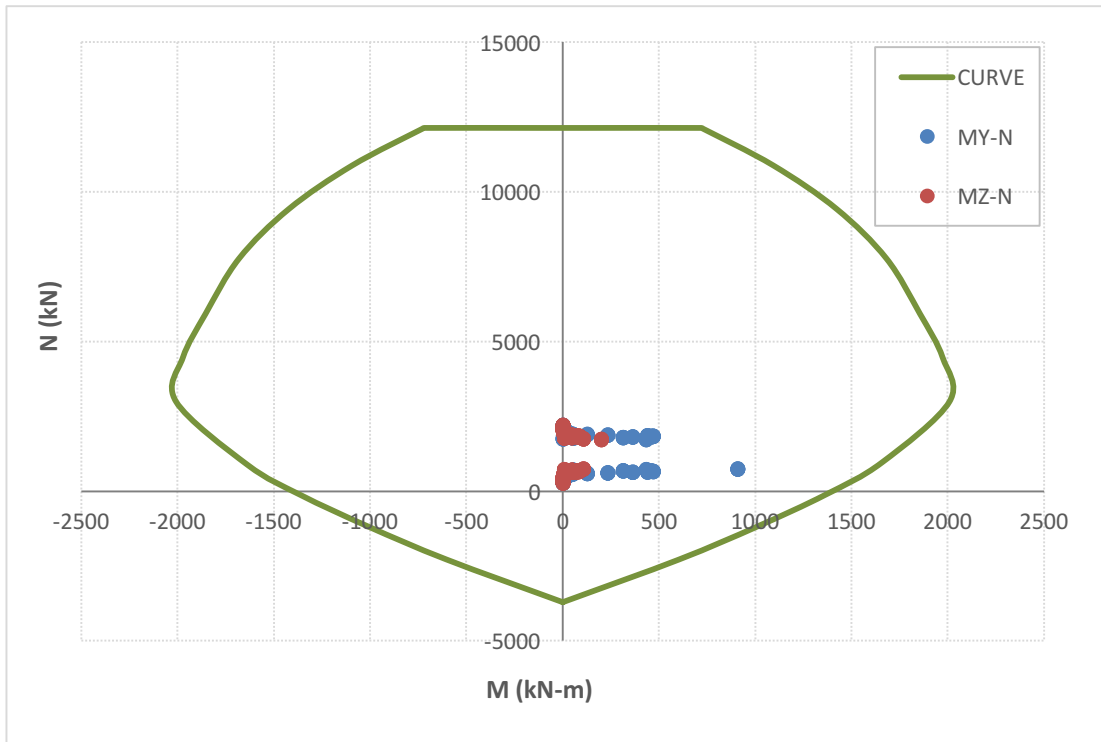


Figure 4.44. Q<sub>10</sub> case pile M-N interaction diagram for Combination 8

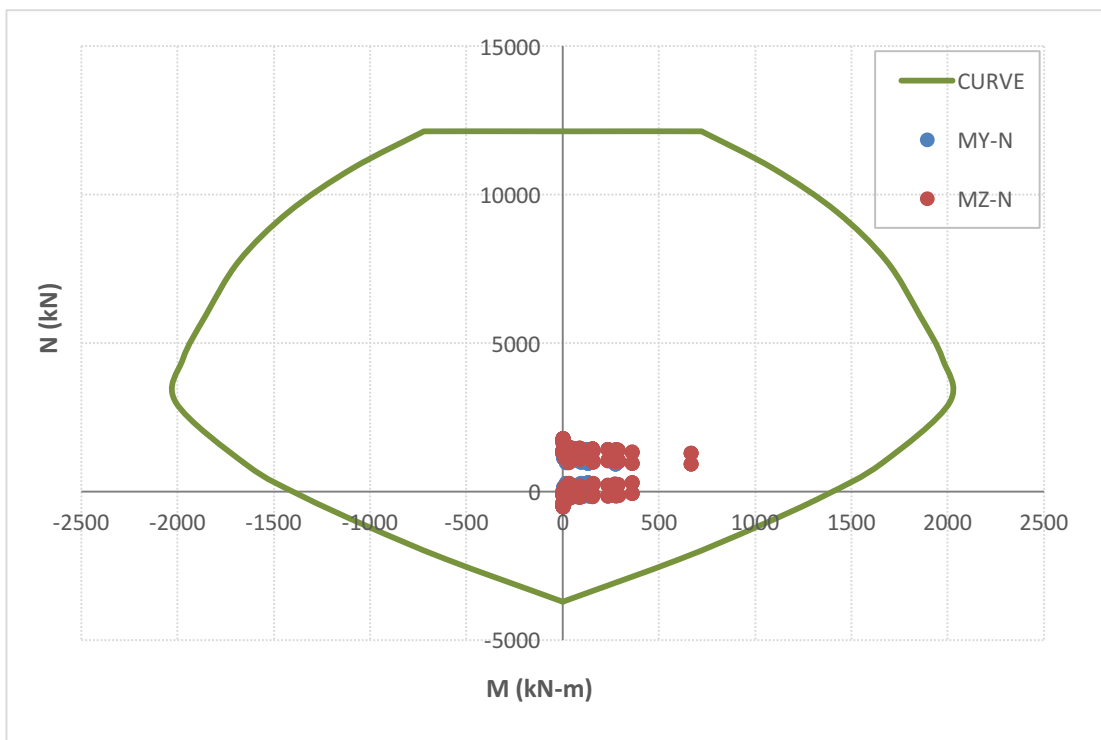


Figure 4.45. Q<sub>10</sub> case pile M-N interaction diagram for Combination 9

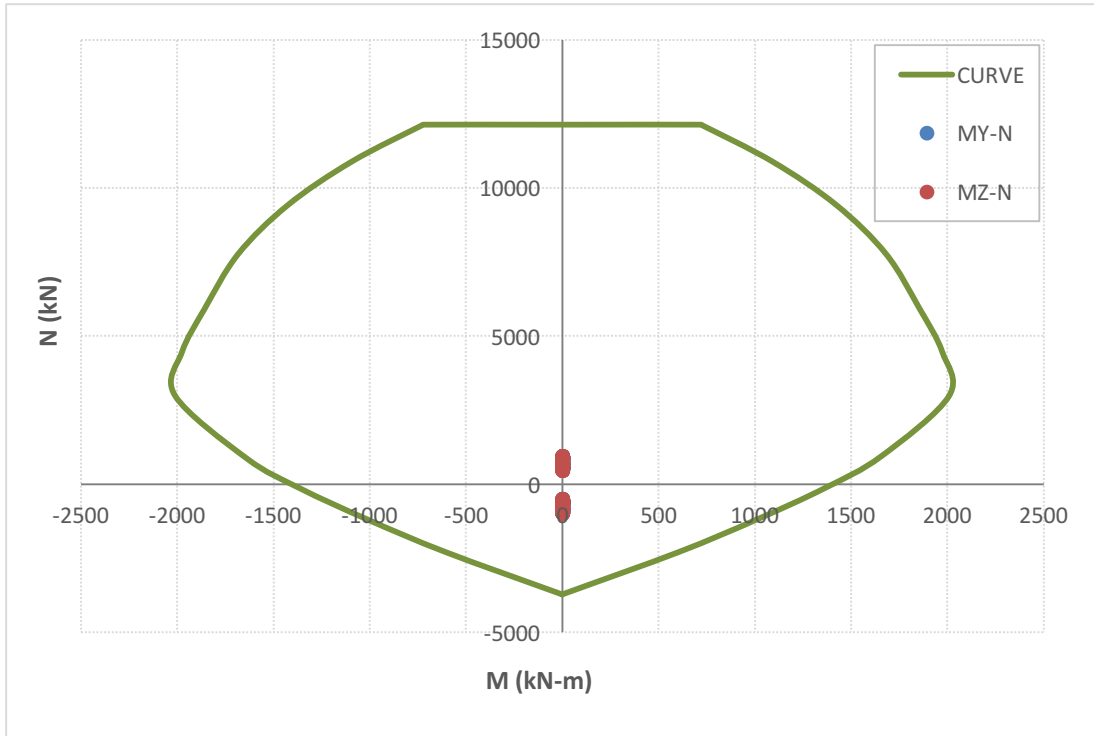


Figure 4.46. Q<sub>25</sub> case pile M-N interaction diagram for Combination 1

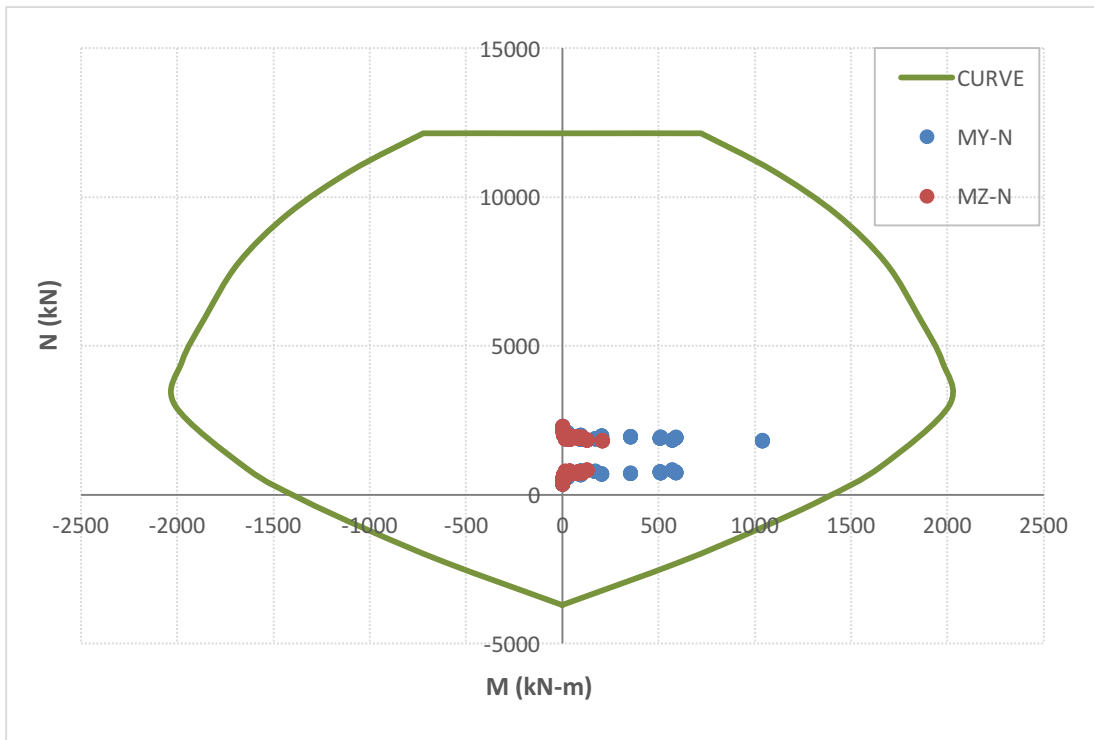


Figure 4.47. Q<sub>25</sub> case pile M-N interaction diagram for Combination 8

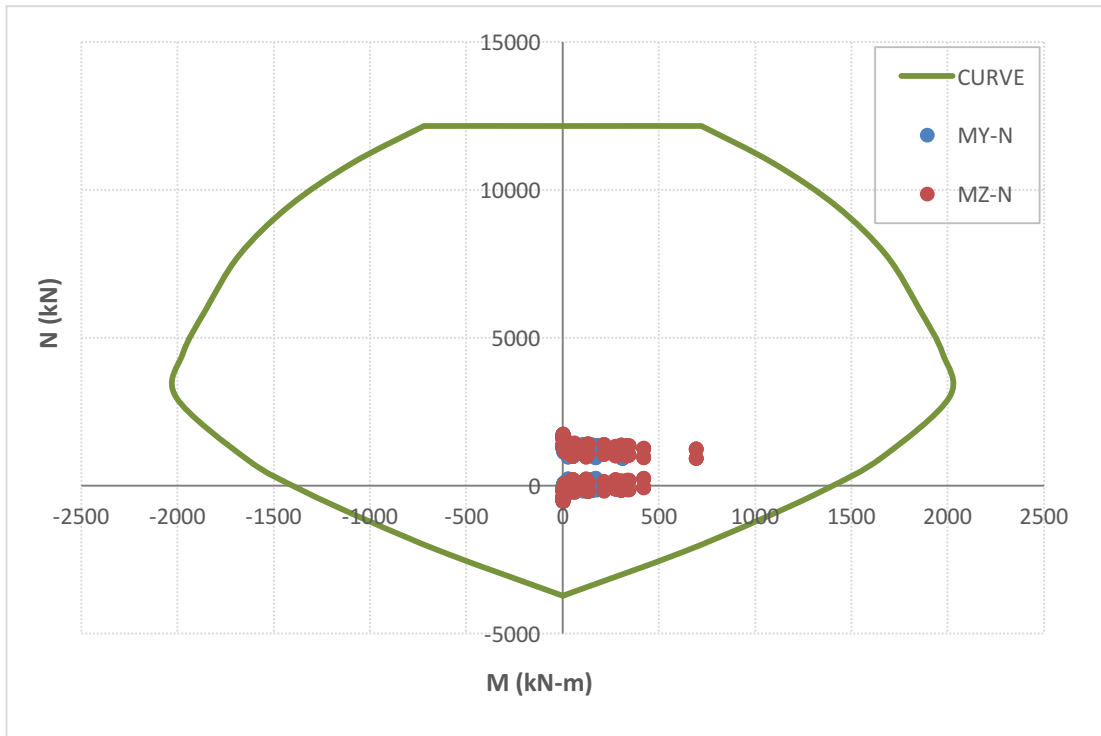


Figure 4.48. Q<sub>25</sub> case pile M-N interaction diagram for Combination 9

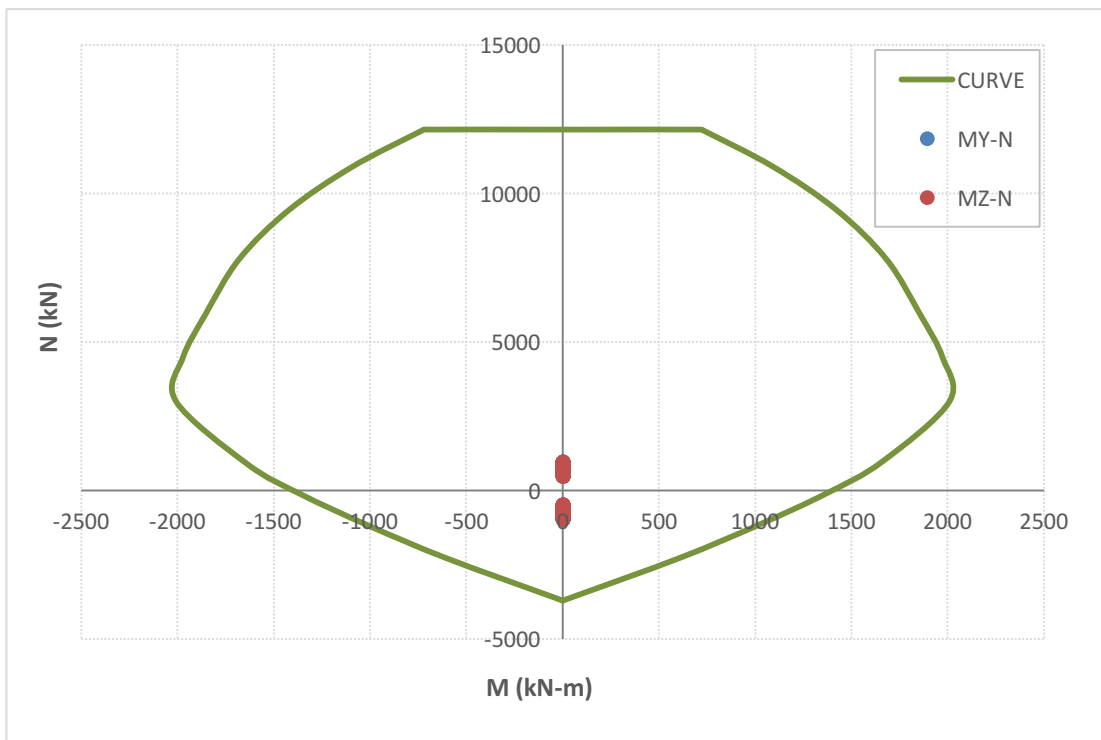


Figure 4.49. Q<sub>50</sub> case pile M-N interaction diagram for Combination 1

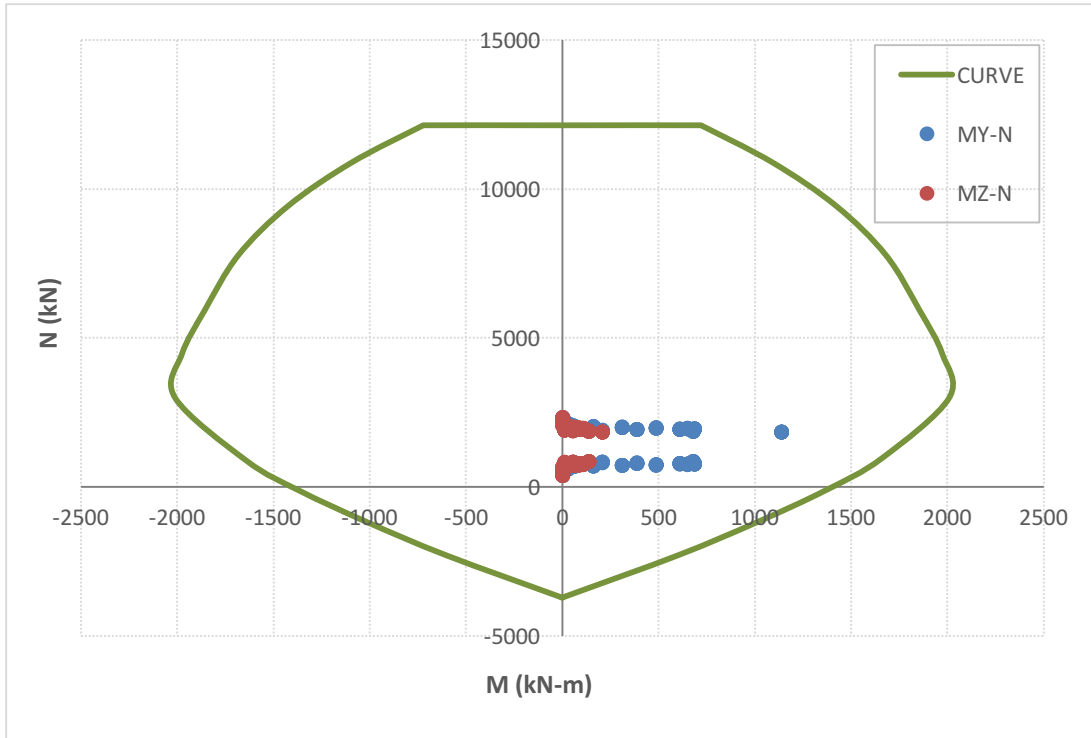


Figure 4.50.  $Q_{50}$  case pile M-N interaction diagram for Combination 8

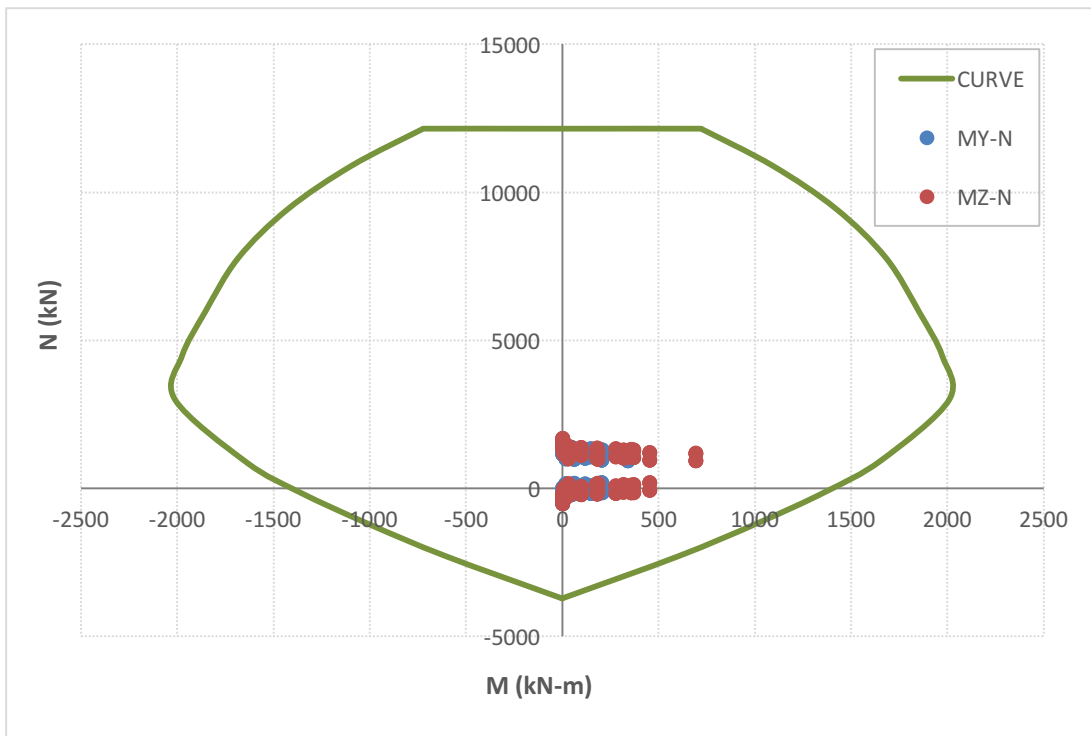


Figure 4.51.  $Q_{50}$  case pile M-N interaction diagram for Combination 9

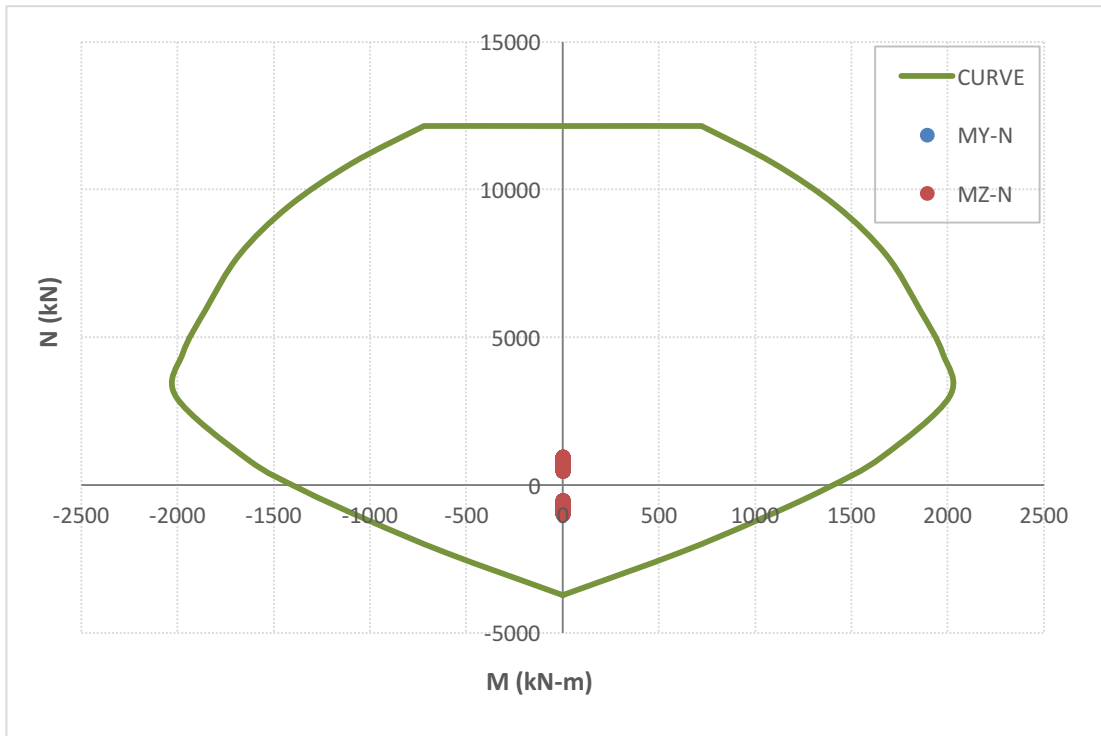


Figure 4.52.  $Q_{100}$  case pile M-N interaction diagram for Combination 1

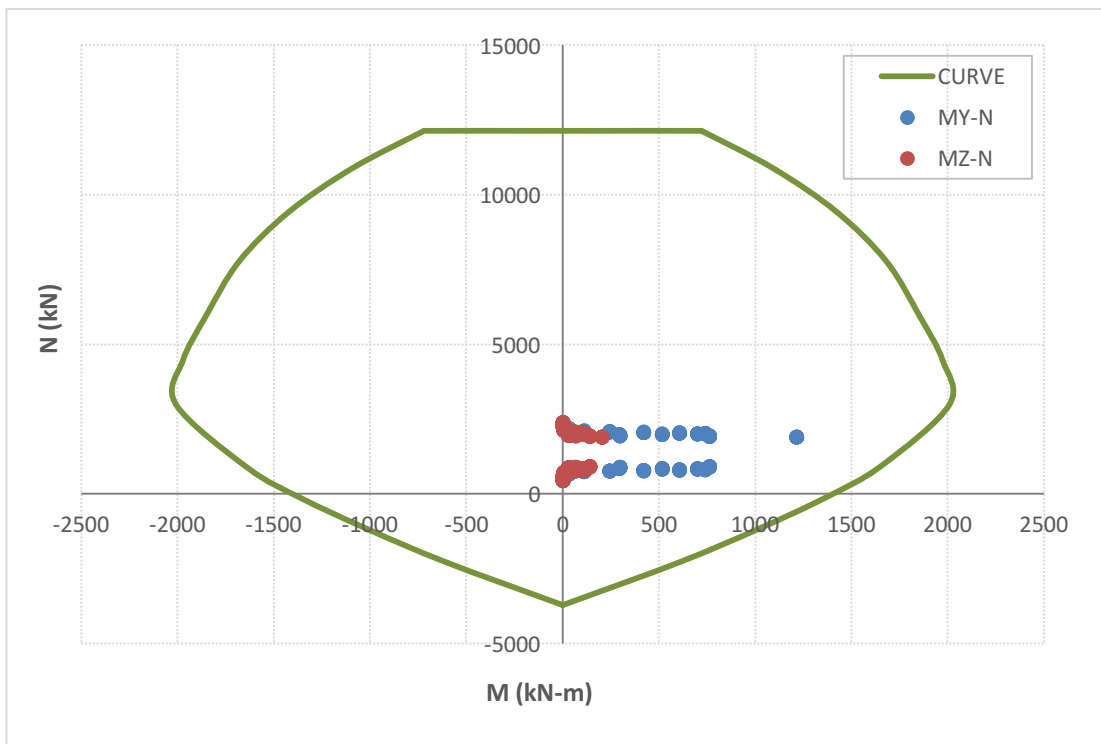


Figure 4.53.  $Q_{100}$  case pile M-N interaction diagram for Combination 8

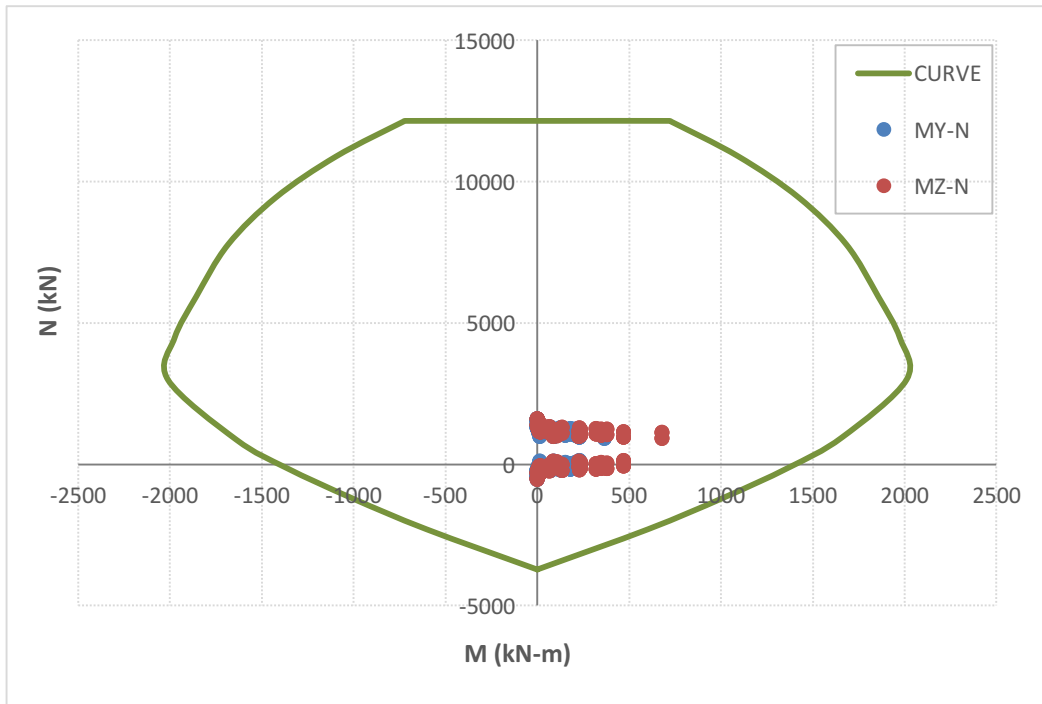


Figure 4.54.  $Q_{100}$  case pile M-N interaction diagrams for Combination 9

When the flexure capacity of the pile is investigated according to Combination 8, it is observed that for no scour case pile reaches 30% of its capacity and for  $Q_{10}$  case this value doubles. For  $Q_{100}$  case, only 68% of pile capacity is used. So, the capacity ratio for  $Q_{10}$  is considered as a critical point. Before this point change in capacity ratio is relatively high whereas it is slightly small afterwards as shown in the Figure 4.55.

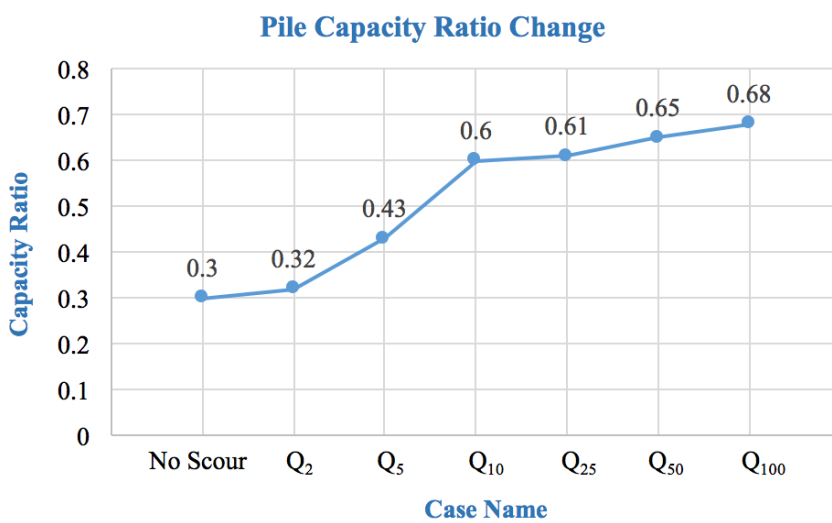


Figure 4.55. Pile flexure capacity change according to discharges

#### 4.4.4 Pile Shear Force Check

Shear capacities of piles are obtained for both directions. For Scenario-1 and Scenario-2, shear force  $F_y$  did not change significantly. On the other hand,  $F_z$ , which acts on weak direction, increases by 20.7% and 23.5% for Scenario-1 and Scenario-2, respectively. The result for Scenario-2 is given in Table 4.23.

According to ACI318-08 Building Code for Structural Concrete (ACI, 2008),

$$\phi V_n = V_u \quad (4.40)$$

where,

$\phi$ = strength reduction factor, 0.9

$V_u$ = factored shear force at the section

$$V_n = V_c + V_s \quad (4.41)$$

where,

$V_c$ = shear strength provided by concrete, kN

$V_s$ = shear strength provided by steel, kN

$$V_c = 0.17\sqrt{f'_c} b_w d = 680 \text{ kN} \quad (4.42)$$

where,

$V_c$ = Nominal shear strength provided by concrete, kN

$f'_c$  = specified compressive strength of concrete, MPa

$b_w$  = width of pile section, cm

$$d = 0.8 D \quad (4.43)$$

Table 4.23. Acted shear forced for both directions  $F_y$  and  $F_z$

<b>Case Name</b>	<b>Shear <math>F_y</math> (kN)</b>	<b>Shear <math>F_z</math> (kN)</b>
<b>No Scour</b>	222.3	310.2
<b>Q<sub>2</sub></b>	234.5	371.9
<b>Q<sub>5</sub></b>	244.1	373.5
<b>Q<sub>10</sub></b>	248.8	374.9
<b>Q<sub>25</sub></b>	263.4	374.4
<b>Q<sub>50</sub></b>	274.6	373.3
<b>Q<sub>100</sub></b>	281.4	372.1

For all cases, shear strength provided by concrete is enough for both directions.  $F_y$  is increased by 18.5% and  $F_z$  is increased by 20.6% for Scenario-1. Therefore, scour did not affect the shear forces on piles significantly.

To conclude, as it can be seen from the result shear capacity, load carrying capacity of the piles and flexure capacity of the column do not make the bridge concerned scour vulnerable. But the flexure capacity of the piles should be examined in detail.

Lack of precautions for scouring or maintenance for scoured bridges increases the moments in piles. Another important point for not taking scour into considerations is the chance of failure for a bridge with a shallow foundation because of the degradation due to scour. Therefore, scour analysis must be conducted and the river bridges must be designed accordingly. For example, piers should be placed on the locations where the flow velocity is low. Furthermore, scour-resistant applications, such as placement of riprap around piers, should be accompanied to the design of river bridges.

## **CHAPTER 5**

### **CONCLUSION**

Scour-based bridge failures are the most common reason among the other failure reasons. Although the earthquake effects are considered in structural designs, it is not enough for scour vulnerable conditions. Also, during structural design process, scour should be taken into consideration, because the possibility of coupled action of both earthquake and scour is high. Although scour-based failures are more common than earthquake based failures, neglecting the scour makes the bridge design vulnerable against dynamic effects. In this study, two span reinforced concrete Banaz Bridge was examined under combined scour and earthquake action for two different soil conditions.

In this study, HEC-RAS software was used for hydraulic analysis and water surface profiles were obtained. Scour depths were calculated by HEC-18 method, which is a well known method in the world. To investigate the seismic performance of the bridge, linear response spectrum analysis was performed. Although this method does not give the exact results, it is a well-accepted method to determine the maximum response. The bridge was evaluated by comparing the moment capacity of column, the pile capacity, the change in pile shear strength and the natural period alteration. The results obtained throughout this study are valid only for the conditions specified and assumptions made. Whenever, input data, structural system, and the site-specific probability distributions change, the results need to be checked accordingly.

It can be concluded that the structural performance of columns improves as more flexibility is obtained at the piles of a scoured bridge, compared to a newly constructed one. On the other hand, pile forces and stability of the foundation system may become more critical in seismic investigation of a scoured bridge. In the investigated cases, the pile load carrying capacity decreased by 1.7% and pile seismic shear forces increased by 20.7% for scoured bridges compared to a non-scoured bridge.

Scour may become more crucial for the foundations constructed on loose sand or soft clay. In that case, pile load capacity may not be enough to carry the superstructure. For the bridge concerned, scouring does not make much difference on bridge safety in terms of load carrying capacity of piles. Since the end bearing resistance is high and skin friction loss, due to scour, is relatively low, the bridge is safe. As it can be seen from the Figures 4.27 and 4.28, skin friction for non-cohesive soil increases linearly up to critical depth,  $L'$ . That is why the soil erosion at the top levels does not make a remarkable difference in skin friction for non-cohesive soils.

Moreover, column moment capacities increase due to flexibility. If the designer is going to neglect the scour, there are two things to discuss. First, it will not be a problem for flexural capacity of the columns. Second, the designer should overdesign the piles, where the piles will not reach up to their 100% of flexure capacity. Although, developing an overdesign factor is not the purpose of this study, in the original form (no scour), pile capacity reaches its 30% for this bridge. the moment acted on piles increases dramatically and for the investigated case, this amount is 169%. The difference of the Figures 4.35 and 4.53 shows the changes in the moment. As a result, if the detailed scour analysis will not be performed, bridge stability becomes questionable when the pile flexure capacity is exceeded.

In this thesis, several aspects of scoured bridges which are imposed to earthquake, were analyzed. For a future study, detailed probabilistic evaluation is recommended.

Although, the probabilistic distribution of earthquake is recommended as poisson distribution, it is known that it depends on the regional properties. Also, flood frequency curves and probability distributions could be obtained for each specific river. Moreover, the bridges that have foundations on weak soil conditions, can be studied for scour and earthquake. For weak soil conditions, bridge stability may be suspicious due to the decrease in pile load carrying capacity. In addition, different analysis types can be conducted, such as nonlinear time history analysis or push-over analysis. Finally, an overdesign factor can be developed for piles and columns if a scour analysis will not be conducted.



## REFERENCES

- AASHTO. (2002). *Standard Specifications for Highway Bridges*. Washington D.C.: American Association of State Highway and Transportation Officials.
- Abdou, I. (1993). *Affect of Sediment Gradation and Coarse Material Fraction on Clear-Water Scour Around Bridge Piers*. Ph.D. Thesis, Colorado State University, Colorado, U.S.A.
- ACI. (2008). *Building Code Requirements for Structural Concrete (ACI 318M-08)*. U.S.A.: American Concrete Institute.
- Alipour, A., Shafei, B., and Shinozuka, M. (2010). Evaluation of Uncertainties Associated with Design of Highway Bridges Considering the Effects of Scouring and Earthquake. *ASCE*, 288-297.
- ANSYS. (2013, November). *ANSYS Mechanical User's Guide*. Canonsburg, U.S.A: ANSYS, Inc.
- API. (1993). *Recommended Practice for Planning, Designing and Constructing Fixed Offshore Platforms - Working Stress Design*. USA: American Petroleum Institute.
- API. (2000). *Recommended Practice for Planning, Designing, and Constructing Fixed Offshore Platforms*. USA: American Petroleum Institute.
- Arneson, L., Zevenbergen, L., Lagasse, P., and Clopper, P. (2012). *Evaluating Scour at Bridges*. U.S.A: U.S. Department of Transportation Federal Highway Administration.
- Banerjee, S., and Prasad, G. (2011). Analysis of Bridge Performance under the Combined Effect of Earthquake and Flood-induced Scour. *ICVRAM and ISUMA*. ASCE (pp. 889-896).

- Birand, A., Ergun, U., and Erol, O. (2011). *CE366 Foundation Engineering 1 Lecture Notes*. Ankara: Middle East Technical University Department of Civil Engineering.
- Brunner, G. (2016). *HEC-RAS River Analysis System User's Manual Version 5.0*. U.S.A: US Army Corps of Engineers Institute for Water Resources Hydrologic Engineering Center.
- CALTRANS-SDC. (2006). *Caltrans Seismic Design Criteria Version 1.4*. U.S.A.: California Department of Transportation.
- Canadian Geotechnical Society. (2006). *Canadian Foundation Engineering Manual*. Canada: Canadian Geotechnical Society.
- Caner, A. (2014). *Unpublished Lecture Notes for CE767 Highway and Railroad Infrastructures*. METU, Department of Civil Engineering, Ankara.
- Computers and Structures Inc. (n.d.). *SAP2000 (Structural Analysis Program)*. Berkley.
- CSiCOL Development Team. (2005). *User's Manual and Technical Reference*. Computers and Structures, Inc. Berkley, California, USA: Computers and Structures, Inc.
- Das, B. (2007). *Principles of Foundation Engineering*. U.S.A.: Global Engineering.
- Davisson, M. (1970). Lateral Load Capacity of Piles. *Highway Research Record*, 104-112.
- ETH. (2009, December 1). *Internal flow features around bridge piers*. Retrieved from [http://www.vaw.ethz.ch/people/hy/archive/hy\\_122\\_flow\\_feature\\_piers](http://www.vaw.ethz.ch/people/hy/archive/hy_122_flow_feature_piers)
- Fioklou, A., and Alipour, A. (2014). Seismic Behavior of Bridges with Deep Foundations under Effects of Scouring. *Structures Congress*. ASCE (pp. 313-323).
- Froelich, D. (1988). Analysis of on-site Measurements of Scour at Piers. *Proceedings of Hydraulic Engineering Conference*. ASCE (pp. 534-539).
- General Directorate of Highways. (2015). *Türkiye Köprü Mühendisliğinde Tasarım ve Yapıma İlişkin Teknolojilerin Geliştirilmesi Teknik Kılavuzu*. Ankara.

- Gunaratne, M. (2013). *The Foundation Engineering Handbook* (Second Edition ed.). CRC Press.
- Hatanaka, M., and Uchida, A. (1996). Empirical Correlation Between Penetration Resistance and Effective Friction of Sandy Soil. *Soils & Foundations* (Vol.36 (4)), 1-9.
- İleri, S. (2016, May 28). *Karşıyaka Köprüsünde Çökme*. Retrieved July 20, 2016, from [http://alacamposta.com/haber\\_detay.asp?haberID=2812&karsiyaka-koprusunde-cokme-meydana-geldi-kullanima.html](http://alacamposta.com/haber_detay.asp?haberID=2812&karsiyaka-koprusunde-cokme-meydana-geldi-kullanima.html)
- Johnson, P. (1992). Reliability-based Pier Scour Engineering. *Journal of Hydraulic Engineering*, 1344-1358.
- Khan, Z. H., and Amanat, K. M. (2014). Riverbed Scouring Effect in Bridge Pile Foundation During Earthquake. *Advances in Soil Dynamics and Foundation Engineering GSP 240*, 343-352.
- LARSA4D Development Team. (2011). *LARSA 4D Reference Manual*. U.S.A: LARSA Inc.
- Melville, B. (1997). Pier and Abutment Scour: Integrated Approach. *Journal of Hydraulic Engineering*(123(2)), 125-136.
- Noshi, H. (1993). *Experimental Study on The Effect of Sediment Gradation and Flow Hydrograph on Clear Water Local Scour Around Circular Bridge Piers*. Colorado State University, Colorado,U.S.A.
- OpenSees Development Team. (2009). Berkley: OpenSees: Open System for Eartquake Engineering Simulation.
- Poulos, H., and Davis, E. (1980). *Pile Foundation Analysis and Design*. Canada: John Wiley and Sons.
- Prakash, S., and Sharma, H. (1990). *Pile Foundations in Engineering Practice*. Canada: John Wiley and Sons.
- Richardson, E. V., and Davis, S. R. (2001). Evaluating Scour at Bridge Piers. *Hydraulic Engineering Circular No:18*.

- Sheppard, D., Zhao, G., and Ontowijjo, B. (1998). Local Scour Near Single Piles in Steady Currents. *ASCE Compendium of Conference Scour Papers (1991 to 1998)* (pp. 371-376). Reston: ASCE.
- Sivrikaya, O., and Tođrol, E. (2006). Determination of Undrained Strength of Fine-Grained Soils by Means of SPT and Its Application in Turkey. *Engineering Geology*, 52-69.
- Skempton, A. (1951). The Bearing Capacity of Clays. *Build. Res. Congress* (p. div I: 180). London: London Inst. Civ. Engrs.
- Sondevir. (2012, April 9). *Köprü Bir Kez Daha Çöktü*. Retrieved from Son Devir Ekonomi: <http://ekonomi.dunyabulteni.net/gundem/65171/kopru-bir-kez-daha-coktu>
- Song, S.-T., Wang, C.-Y., and Huang, W.-H. (2015). Earthquake damage potential and critical scour depth of bridges exposed to flood and seismic hazards under lateral seismic loads. *Earthquake Engineering and Engineering Vibration*, 579-594.
- Sozcu. (2016, July 5). *Ordu'da Sel*. Retrieved July 20, 2016, from Sozcu: <http://www.sozcu.com.tr/2016/gundem/fatsada-sel-1303467/>
- Sturm, T. W. (2009). *Open Channel Hydraulics* (2nd edition ed.). McGraw-Hill Education.
- Tuna, T. (2016, June 18). *Köprü Çökme Noktasında*. Retrieved July 20, 2016, from haberhurriyeti: <http://www.haberhurriyeti.com/kopru-cokme-noktasinda-159293.html>
- Wardhana, K., and Hadipriano, F. (2003). Analysis of Recent Bridge Failures in the United States. *Journal of Performance of Constructed Facilities*.
- Yanmaz, A. M. (2002). *Köprü Hidroliđi, First Edition*. Ankara: Metu Press.
- Yanmaz, A. M. (2014). *Unpublished CE590 Bridge Hydraulics Lecture Notes*. Lecture Note, METU, Department of Civil Engineering, Ankara.
- Yanmaz, A., and Caner, A. (2012). *Çaycuma Köprüsünün Çökmesi Üzerine Görüşler*. Ankara: Türkiye Köprü ve İnşaat Cemiyeti.

Yüksekol, Ü. (2007). *A Simple Assesment of Lateral Pier Response of Standart Highway Bridges on Pile Foundations*. METU, Department of Civil Engineering. Ankara: METU.



# APPENDIX A

## PILE M-N CURVES

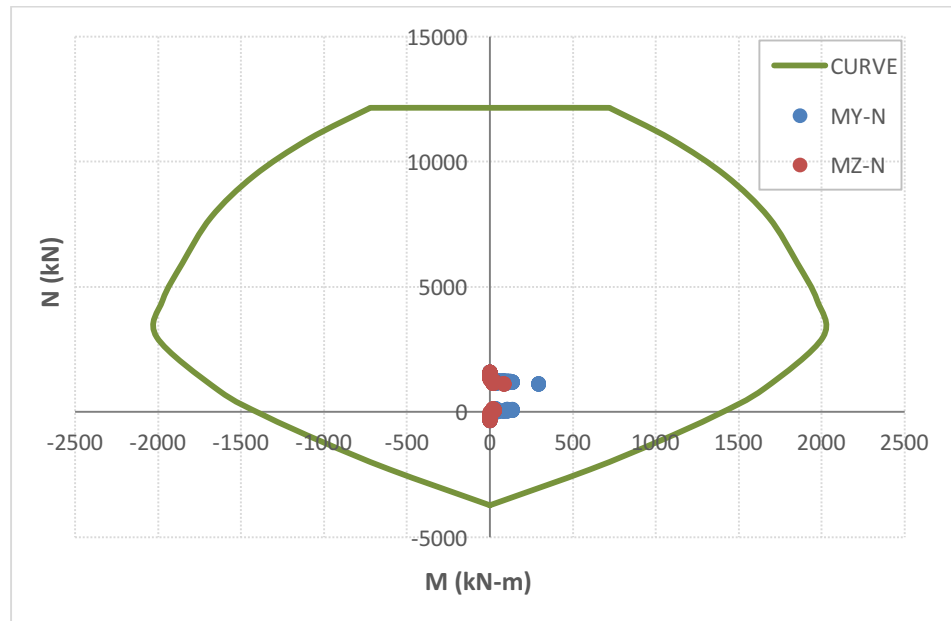


Figure A.1. No scour case pile M-N interaction diagram for Combination 2

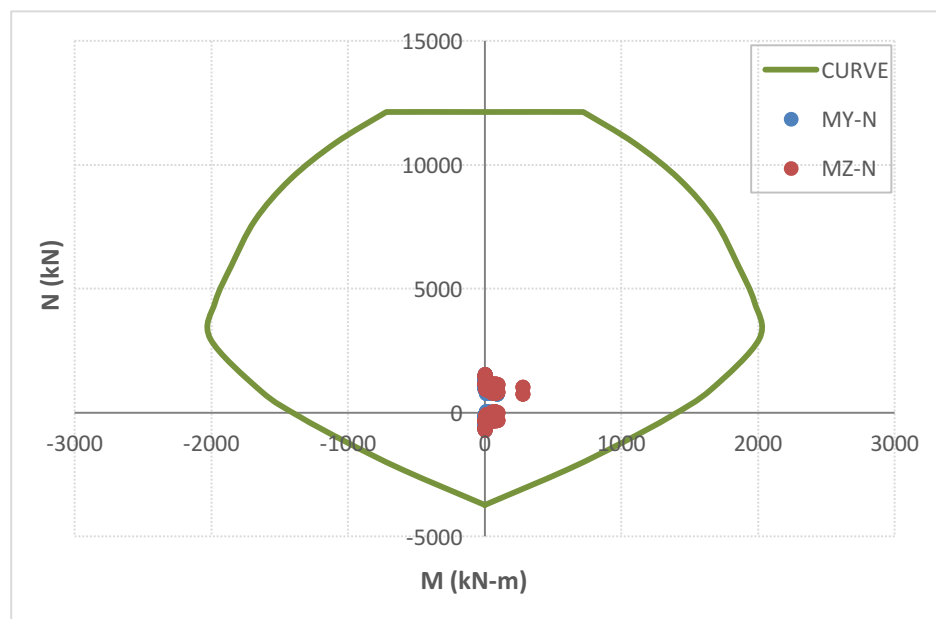


Figure A.2. No scour case pile M-N interaction diagram for Combination 3

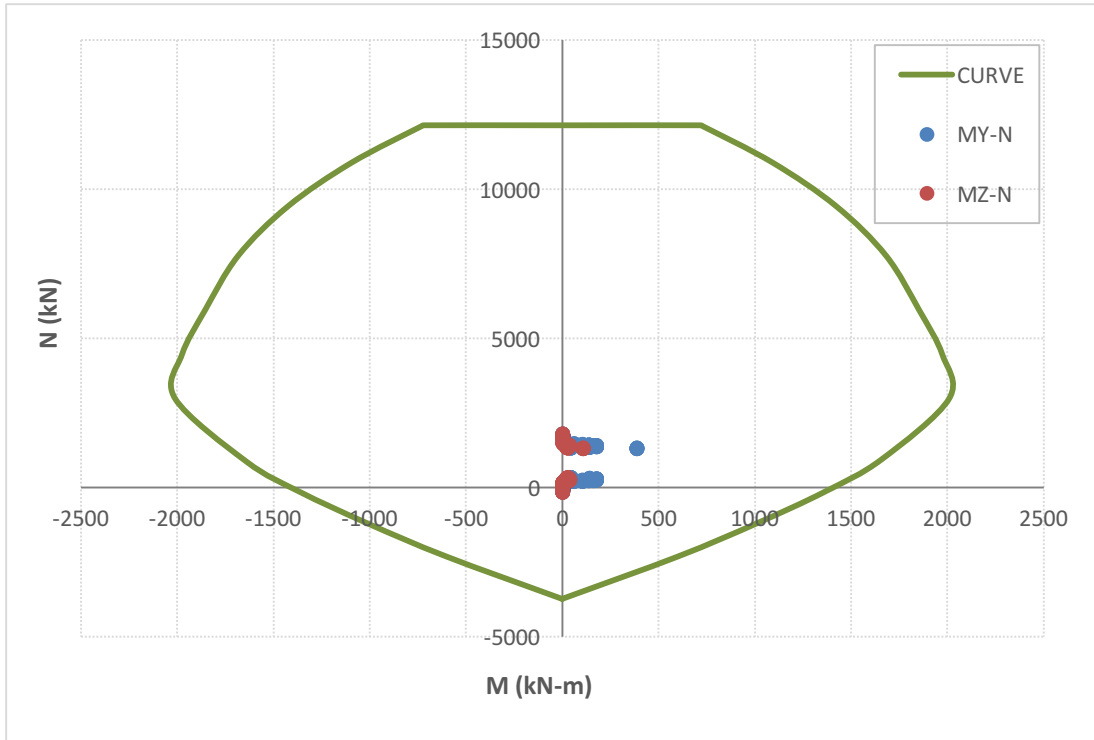


Figure A.3. No scour case pile M-N interaction diagram for Combination 4

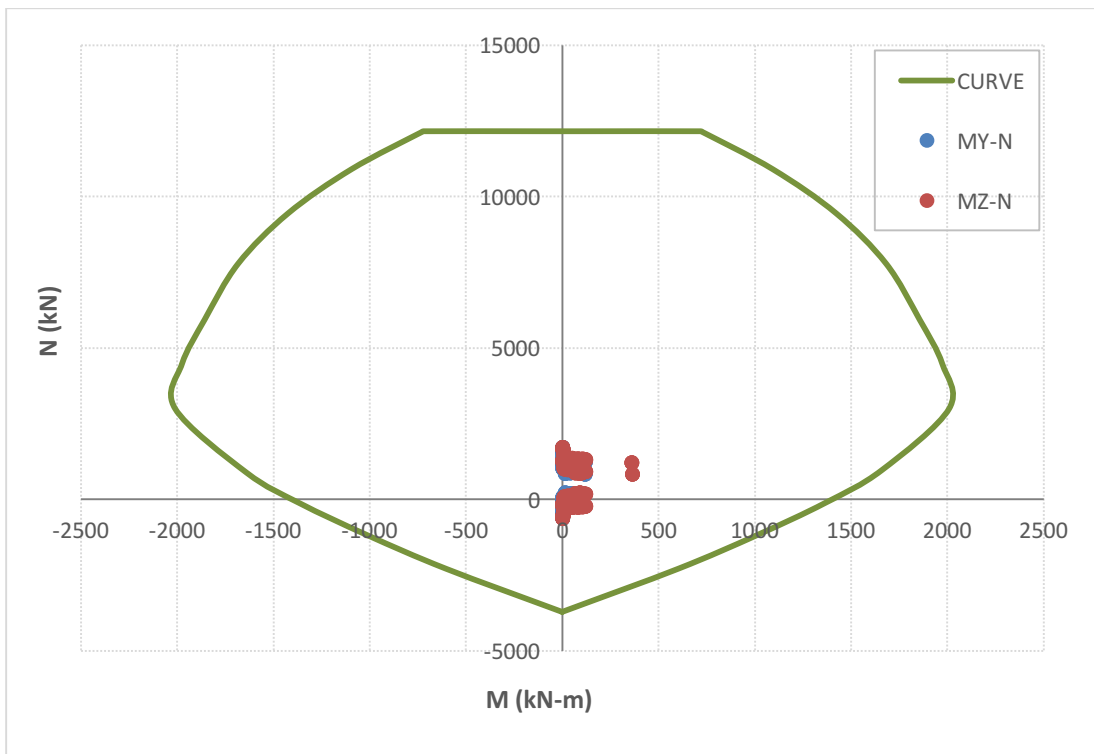


Figure A.4. No scour case pile M-N interaction diagram for Combination 5

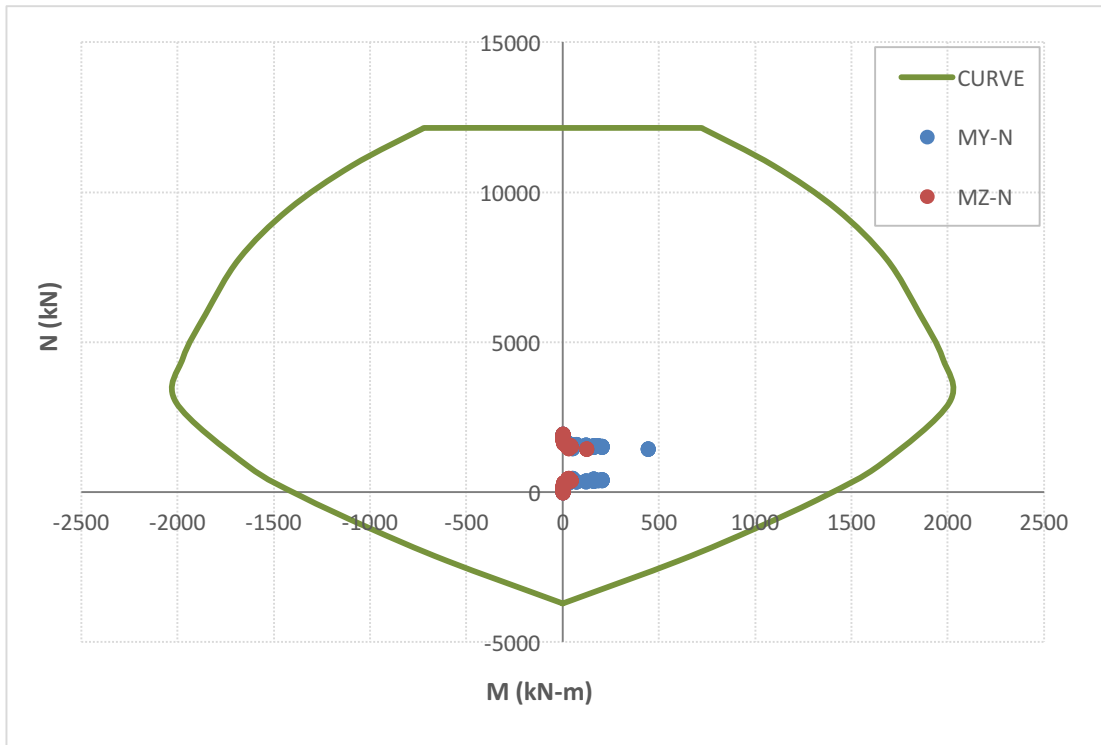


Figure A.5. No scour case pile M-N interaction diagram for Combination 6

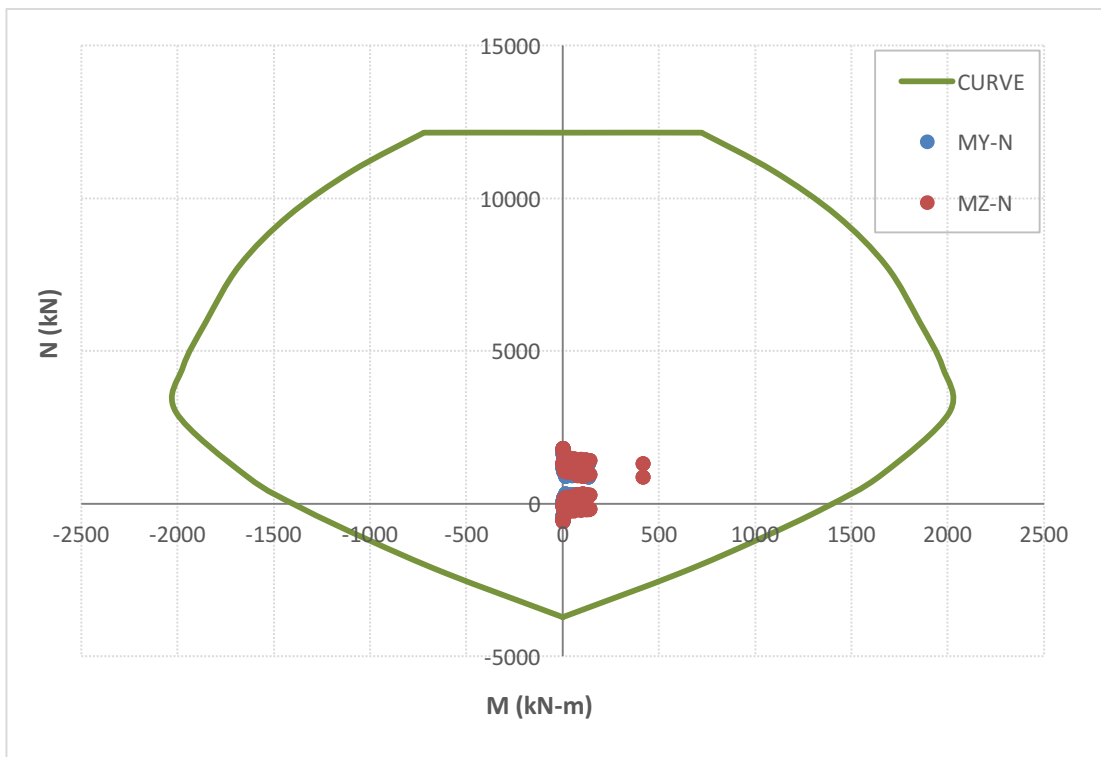


Figure A.6. No scour case pile M-N interaction diagram for Combination 7

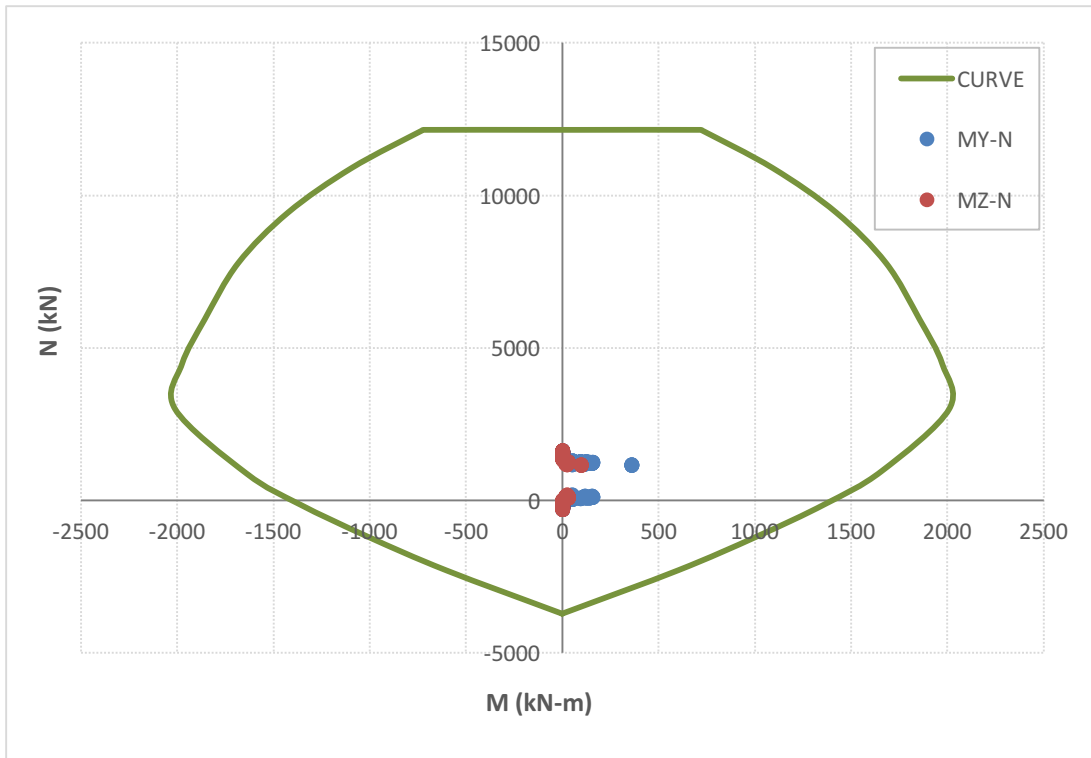


Figure A.7.  $Q_2$  case pile M-N interaction diagram for Combination 2

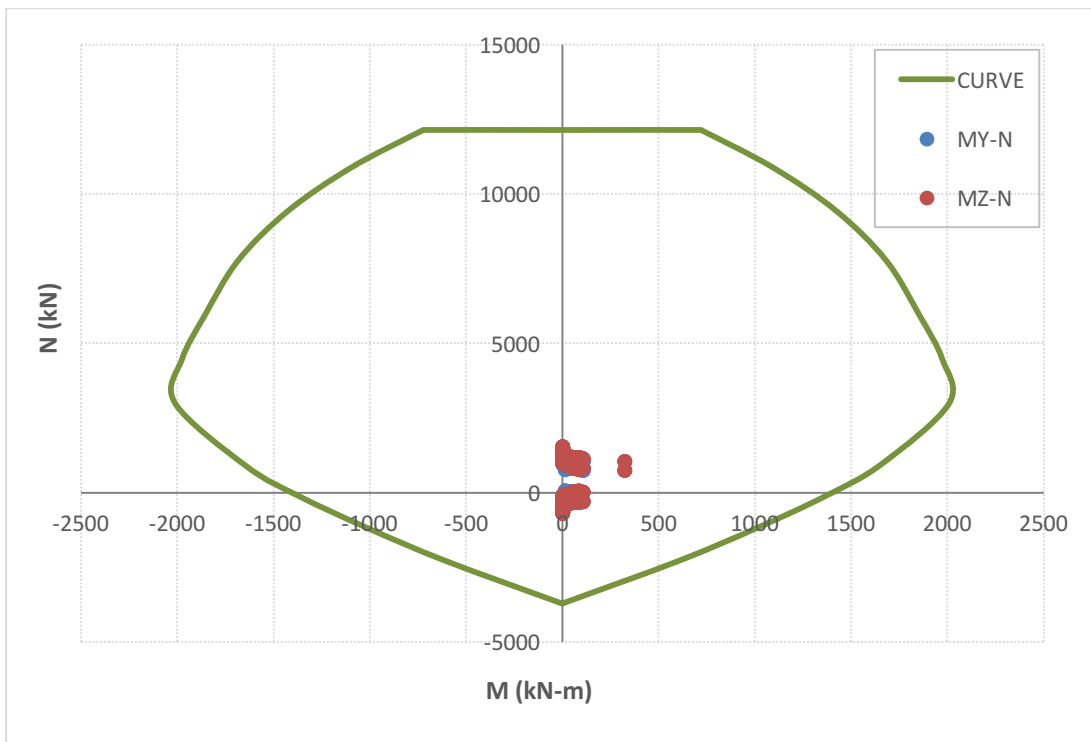


Figure A.8.  $Q_2$  case pile M-N interaction diagram for Combination 3

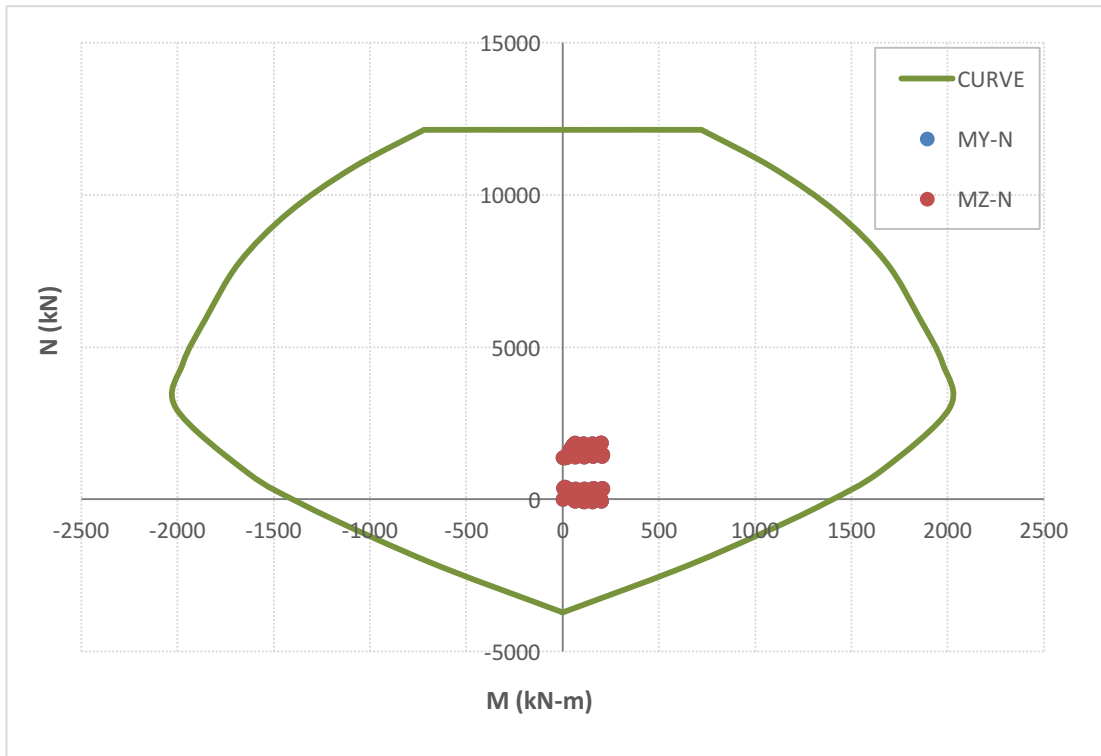


Figure A.9. Q<sub>2</sub> case pile M-N interaction diagram for Combination 4

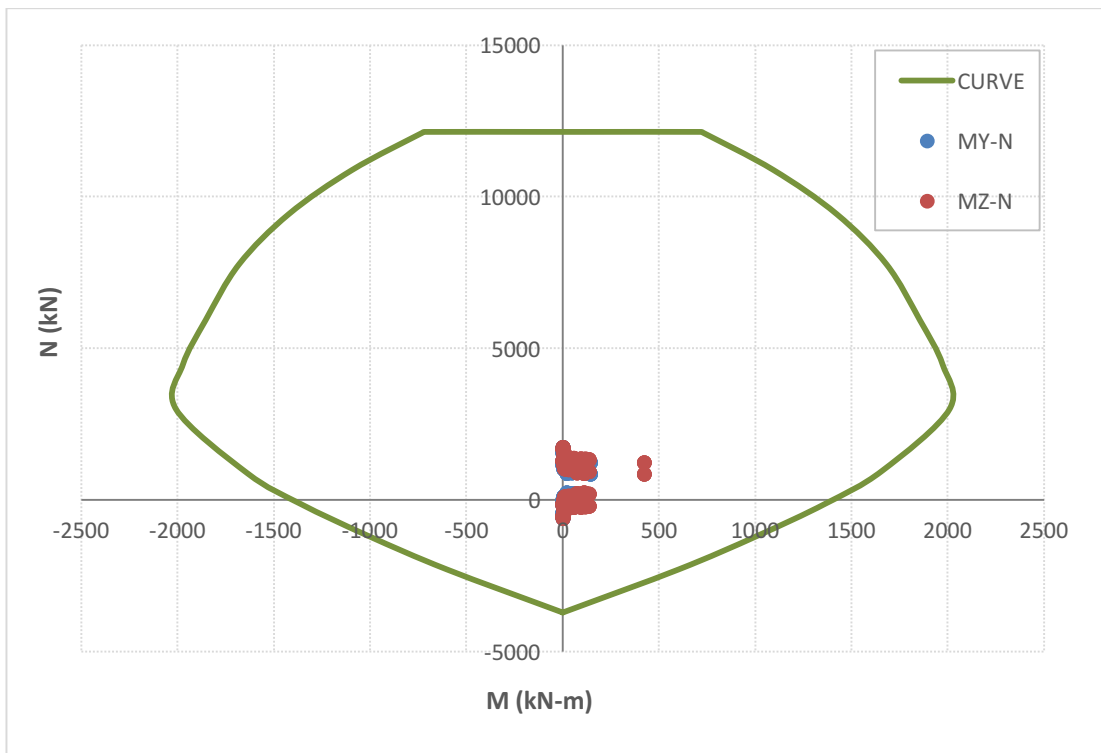


Figure A.10. Q<sub>2</sub> case pile M-N interaction diagram for Combination 5

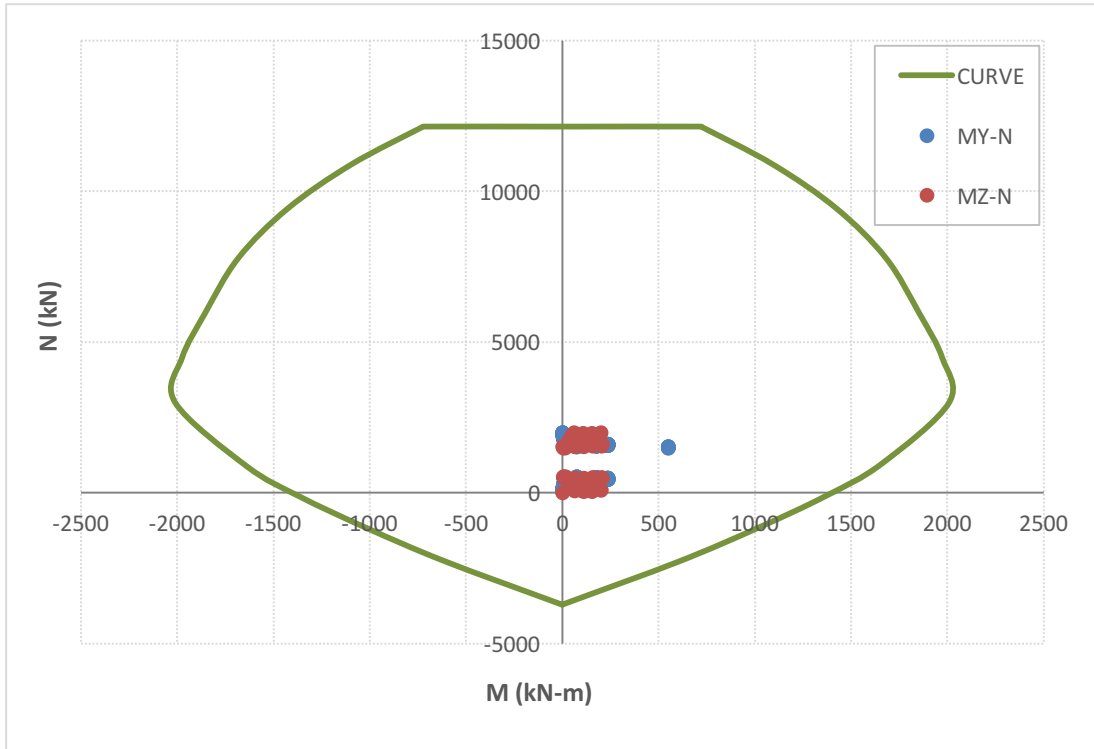


Figure A.11.  $Q_2$  case pile M-N interaction diagram for Combination 6

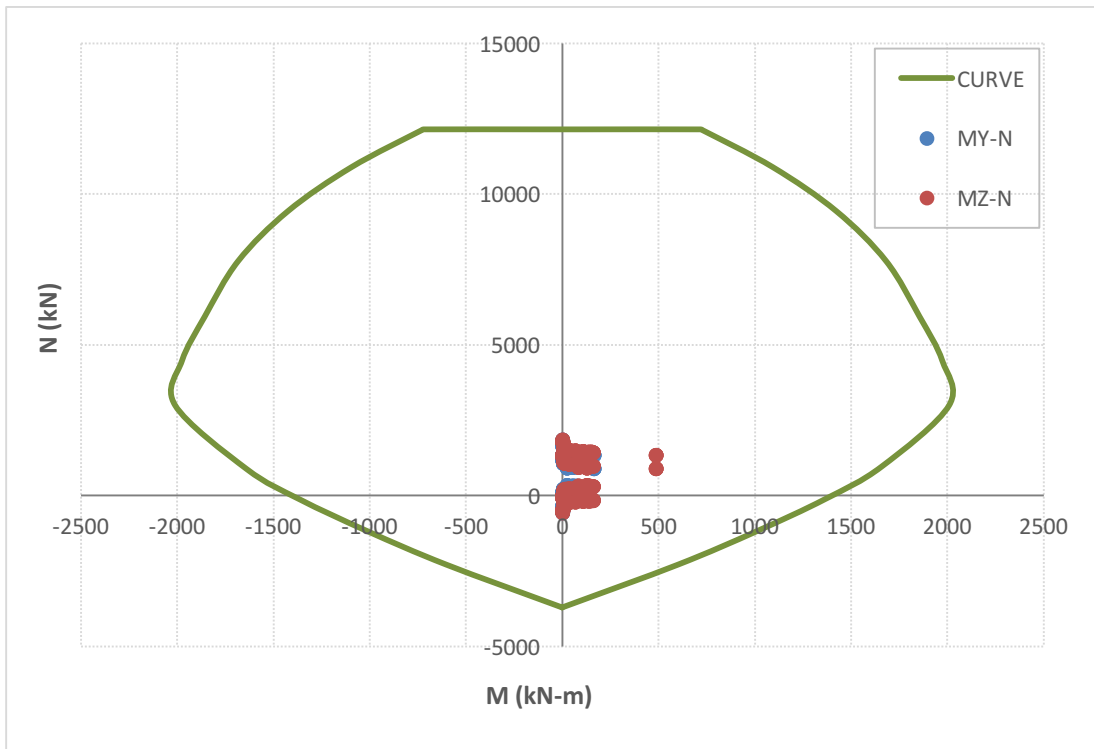


Figure A.12.  $Q_2$  case pile M-N interaction diagram for Combination 7

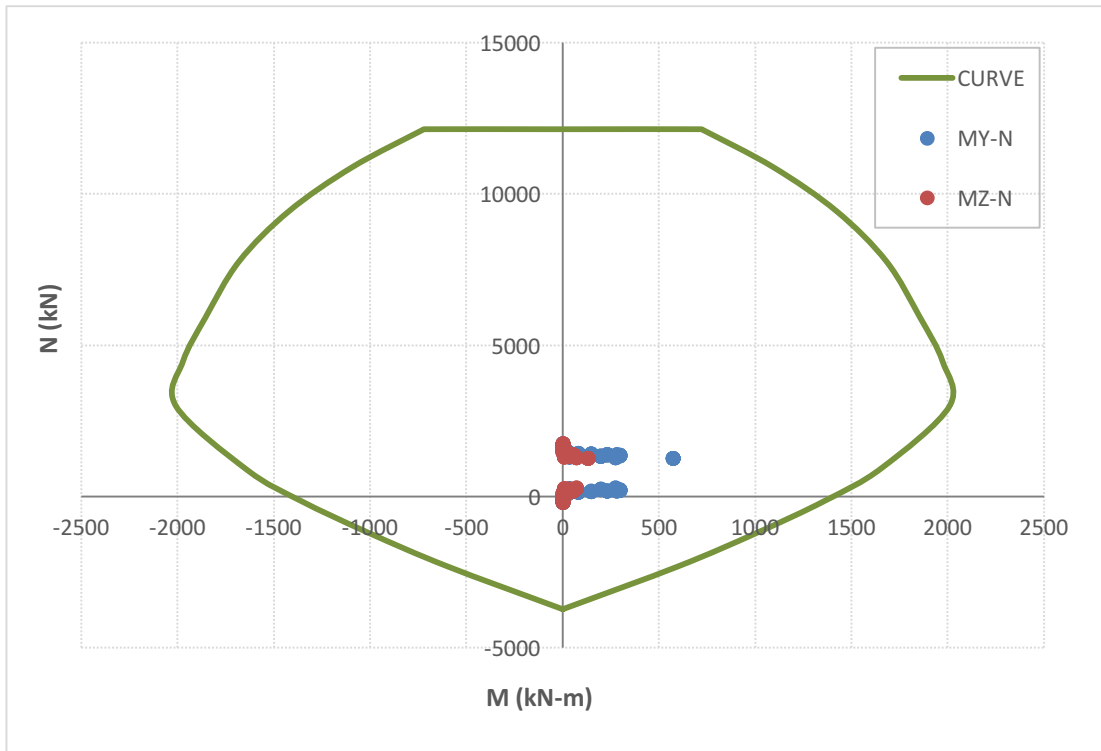


Figure A.13.  $Q_5$  case pile M-N interaction diagram for Combination 2

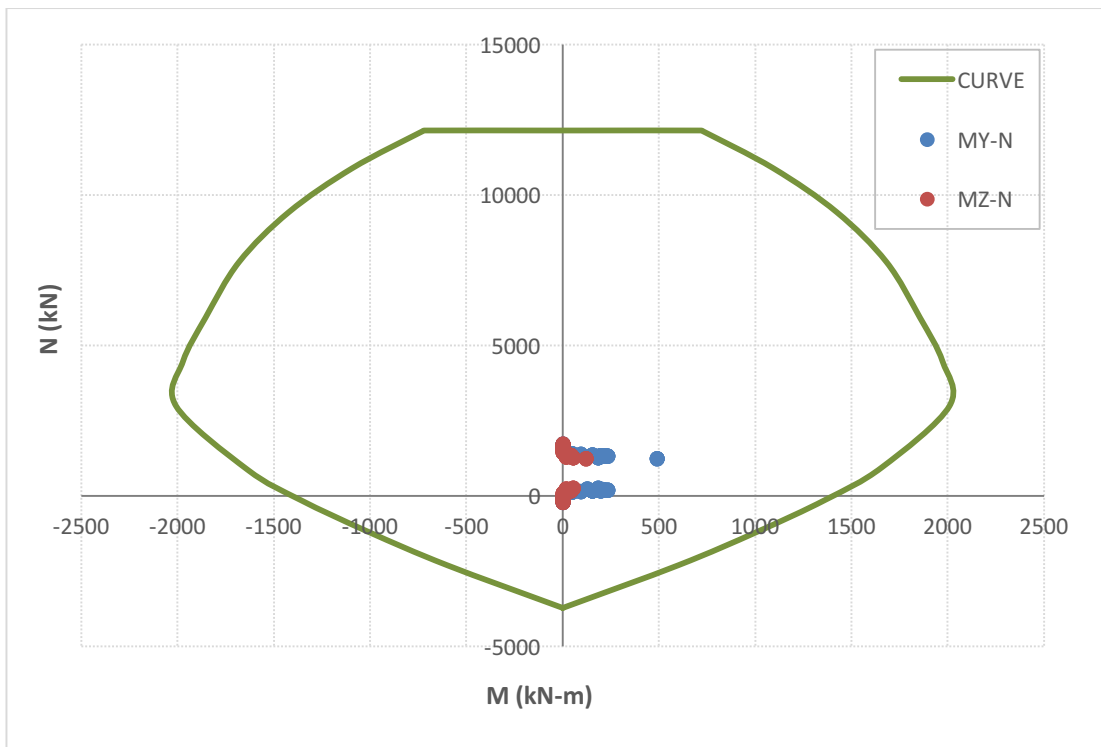


Figure A.14.  $Q_5$  case pile M-N interaction diagram for Combination 3

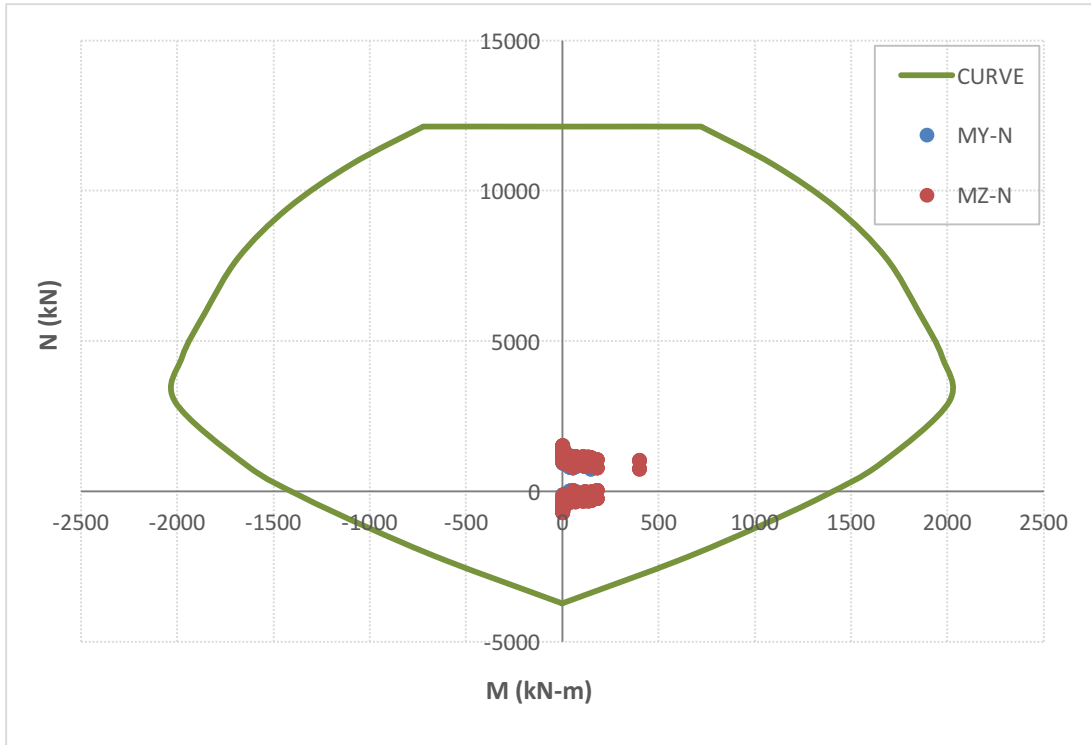


Figure A.15. Q<sub>5</sub> case pile M-N interaction diagram for Combination 4

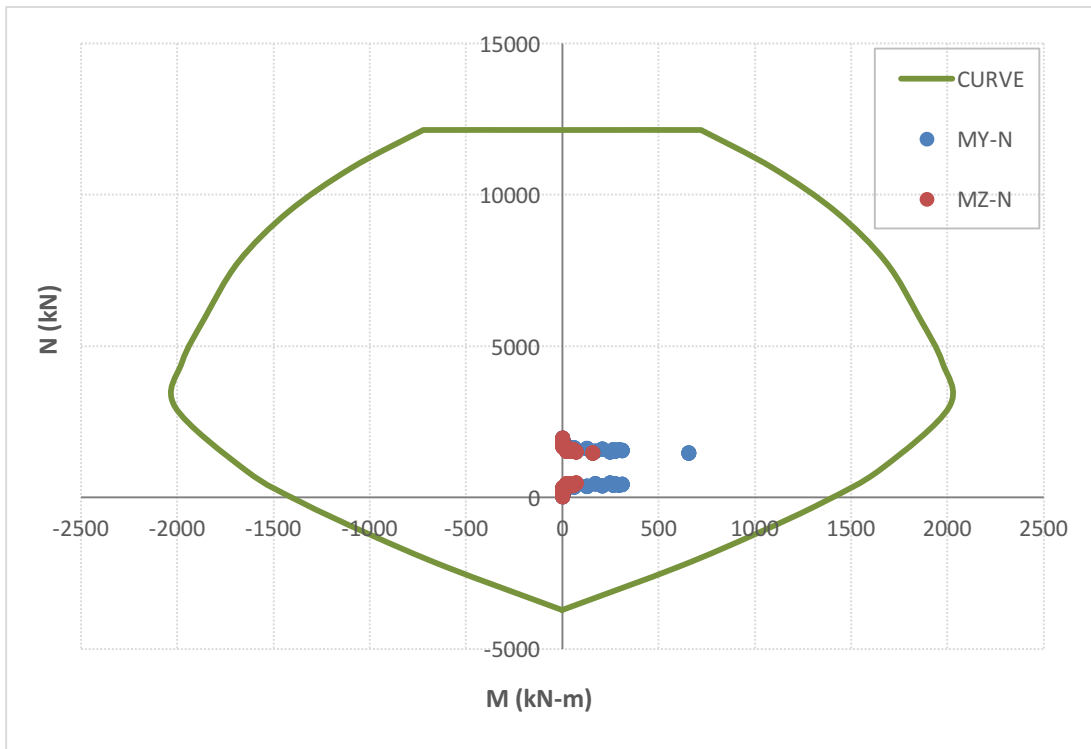


Figure A.16. Q<sub>5</sub> case pile M-N interaction diagram for Combination 5

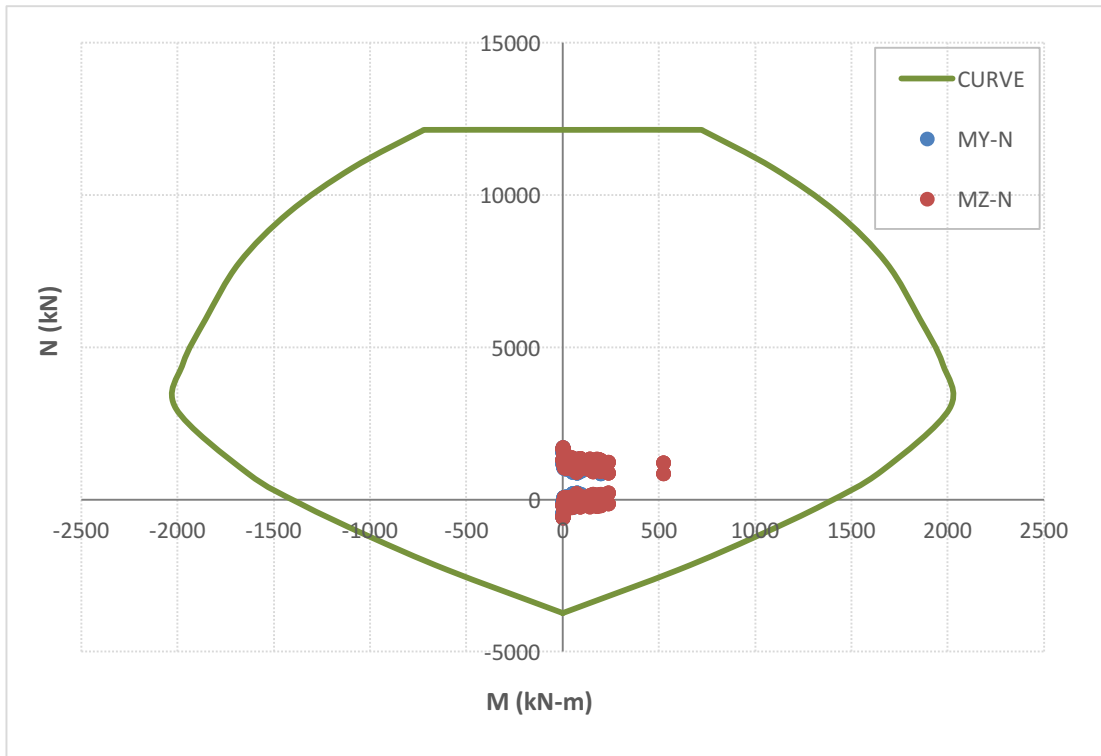


Figure A.17.  $Q_5$  case pile M-N interaction diagram for Combination 6

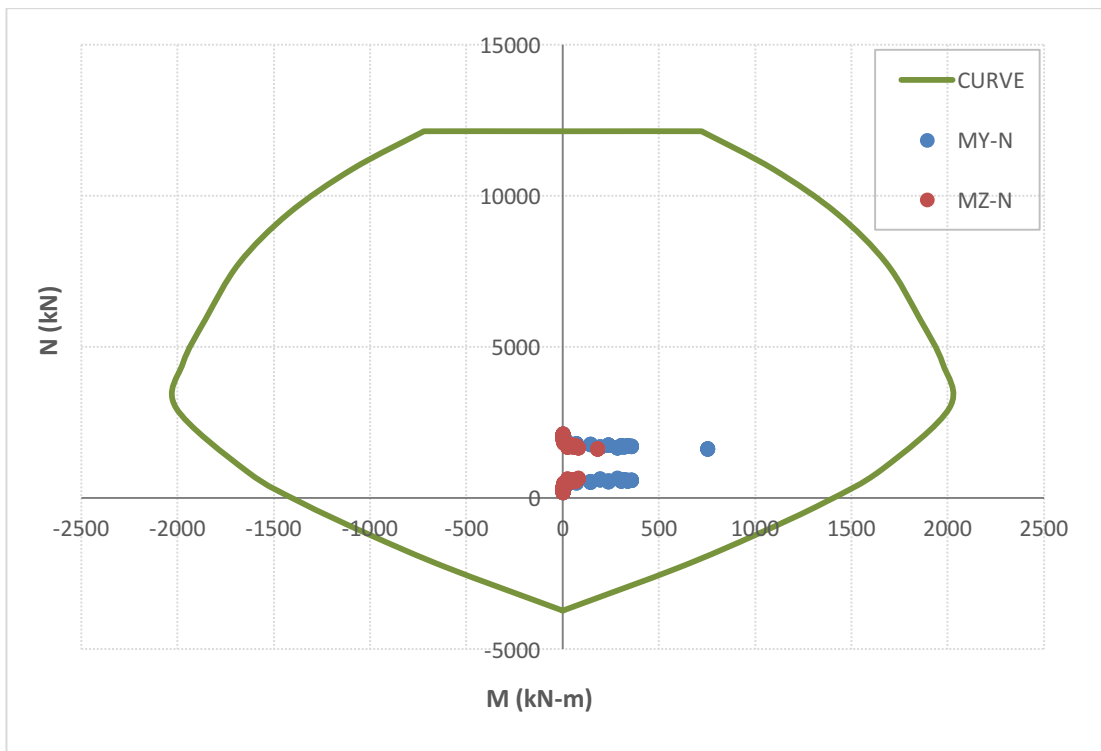


Figure A.18.  $Q_5$  case pile M-N interaction diagram for Combination 7

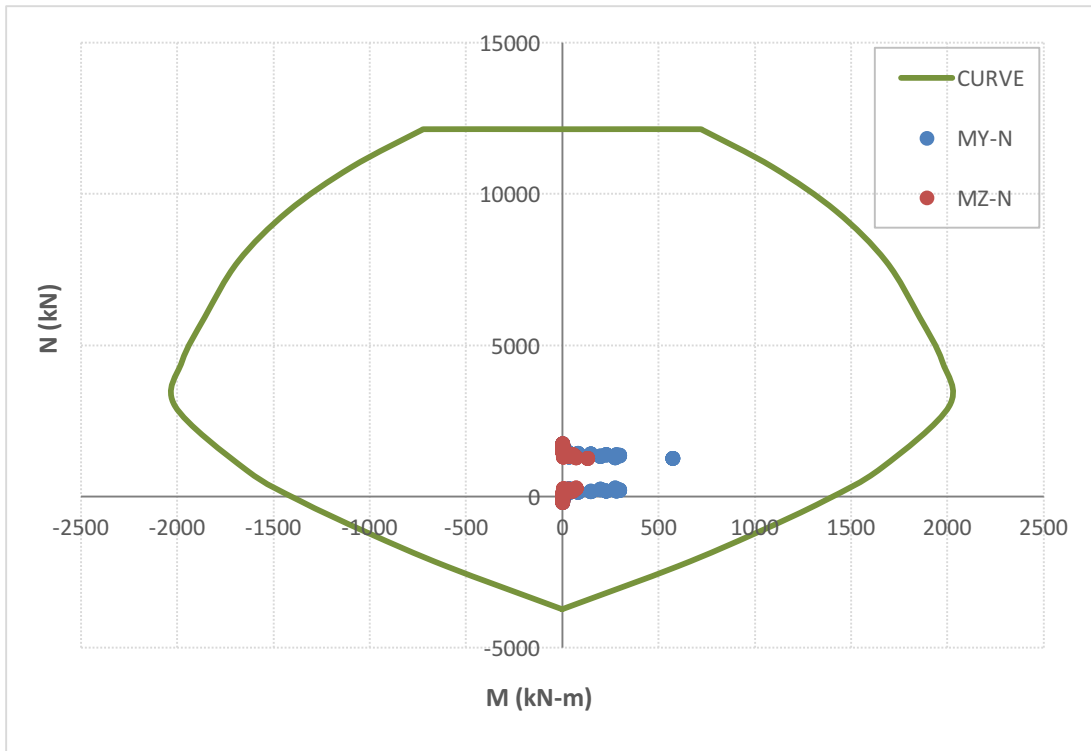


Figure A.19.  $Q_{10}$  case pile M-N interaction diagram for Combination 2

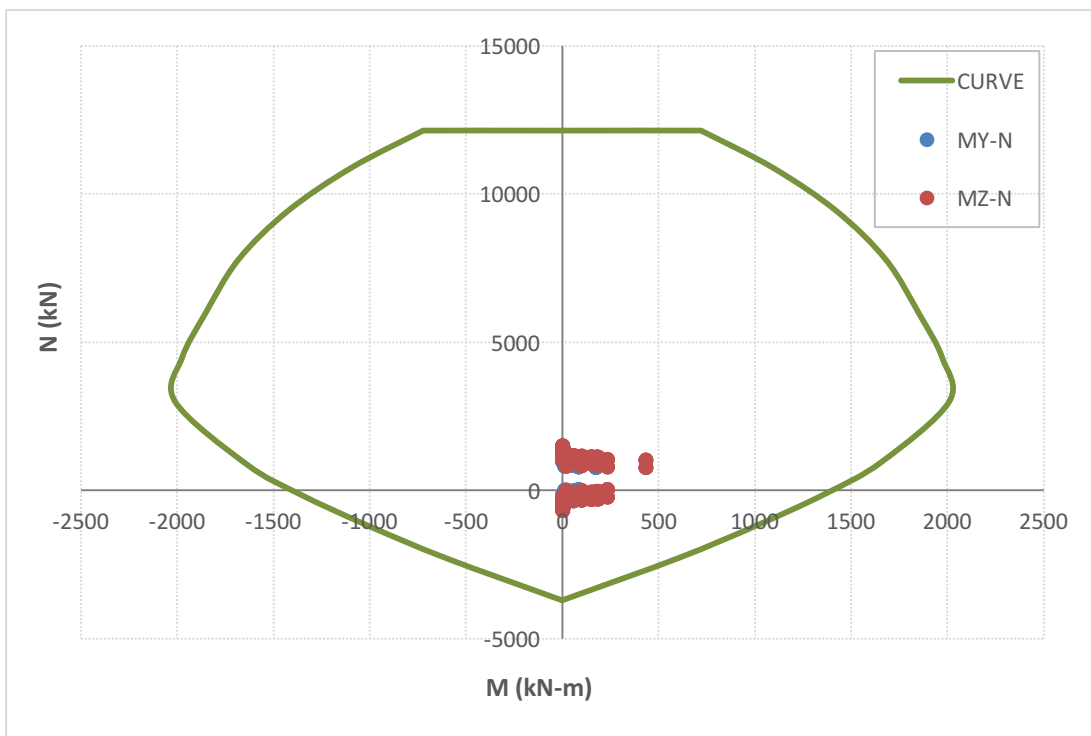


Figure A.20.  $Q_{10}$  case pile M-N interaction diagram for Combination 3

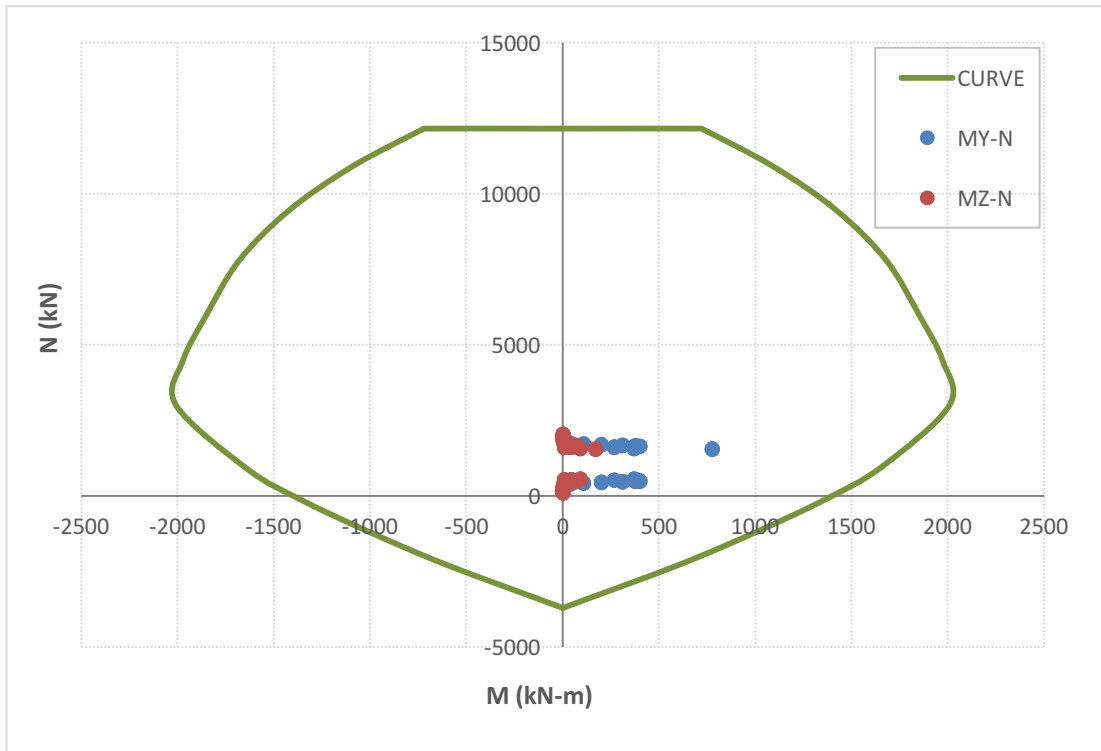


Figure A.21.  $Q_{10}$  case pile M-N interaction diagram for Combination 4

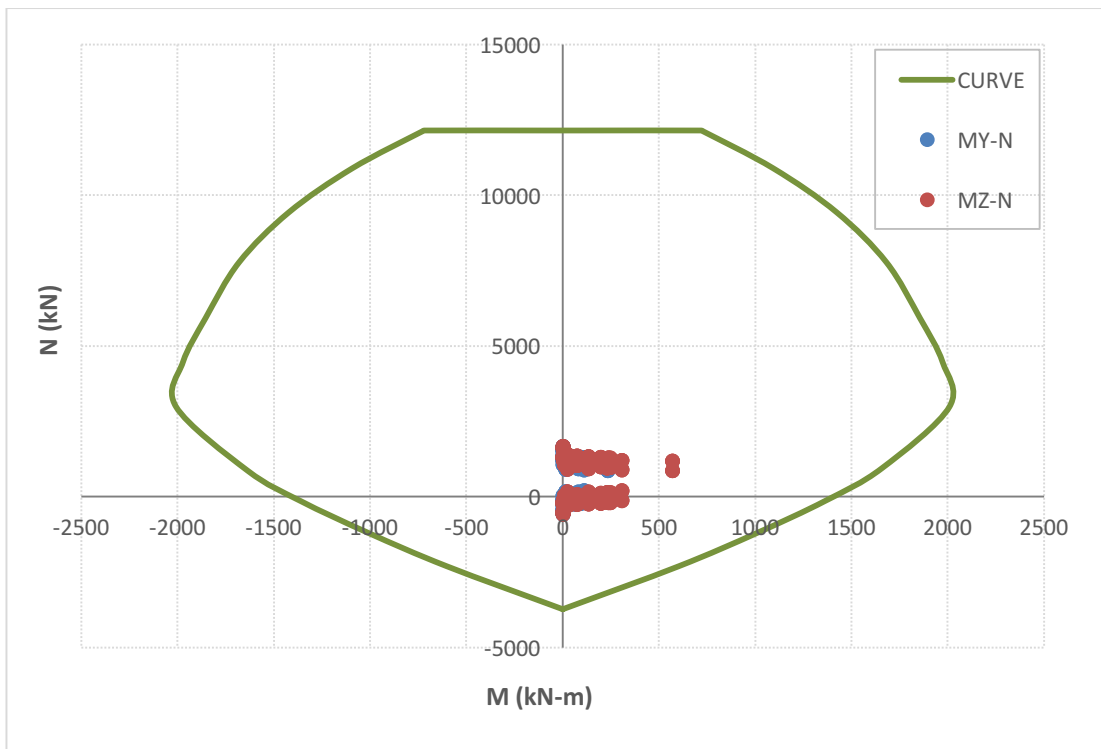


Figure A.22.  $Q_{10}$  case pile M-N interaction diagram for Combination 5

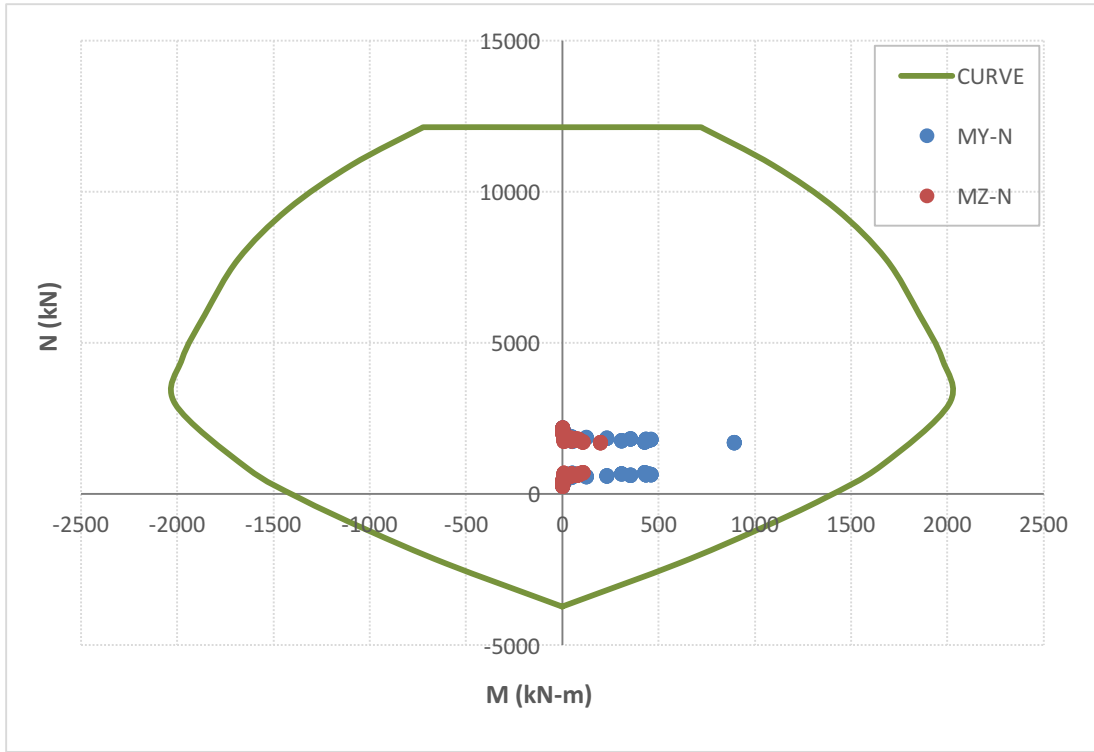


Figure A.23.  $Q_{10}$  case pile M-N interaction diagram for Combination 6

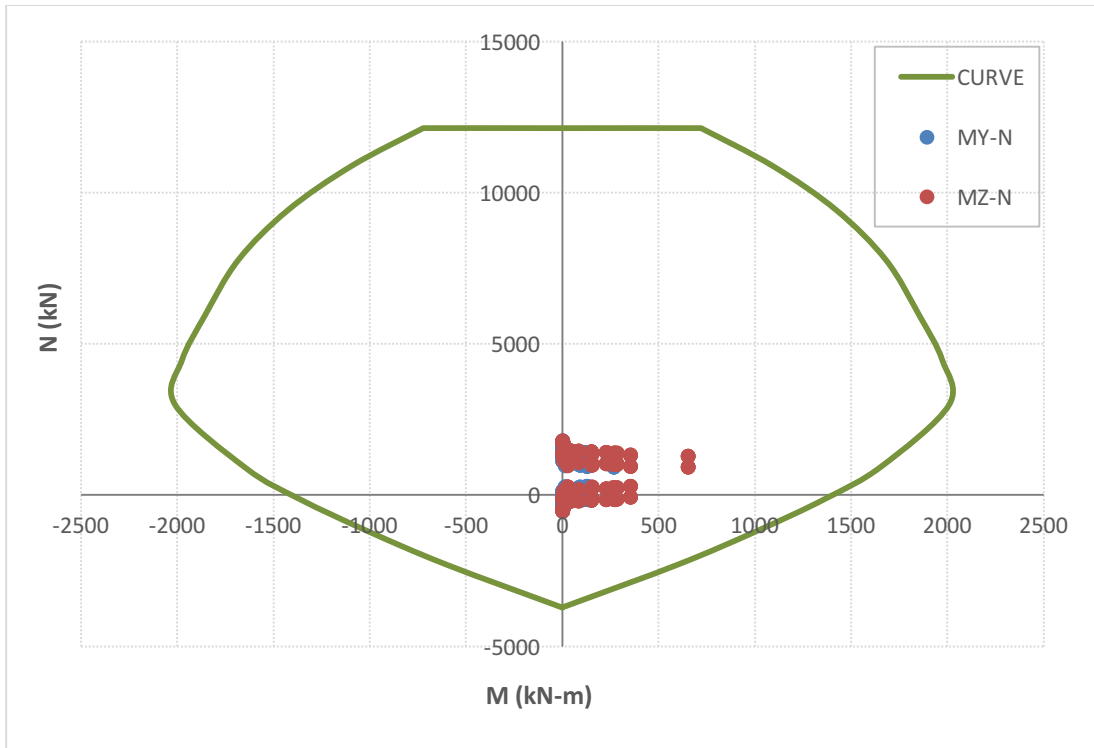


Figure A.24.  $Q_{10}$  case pile M-N interaction diagram for Combination 7

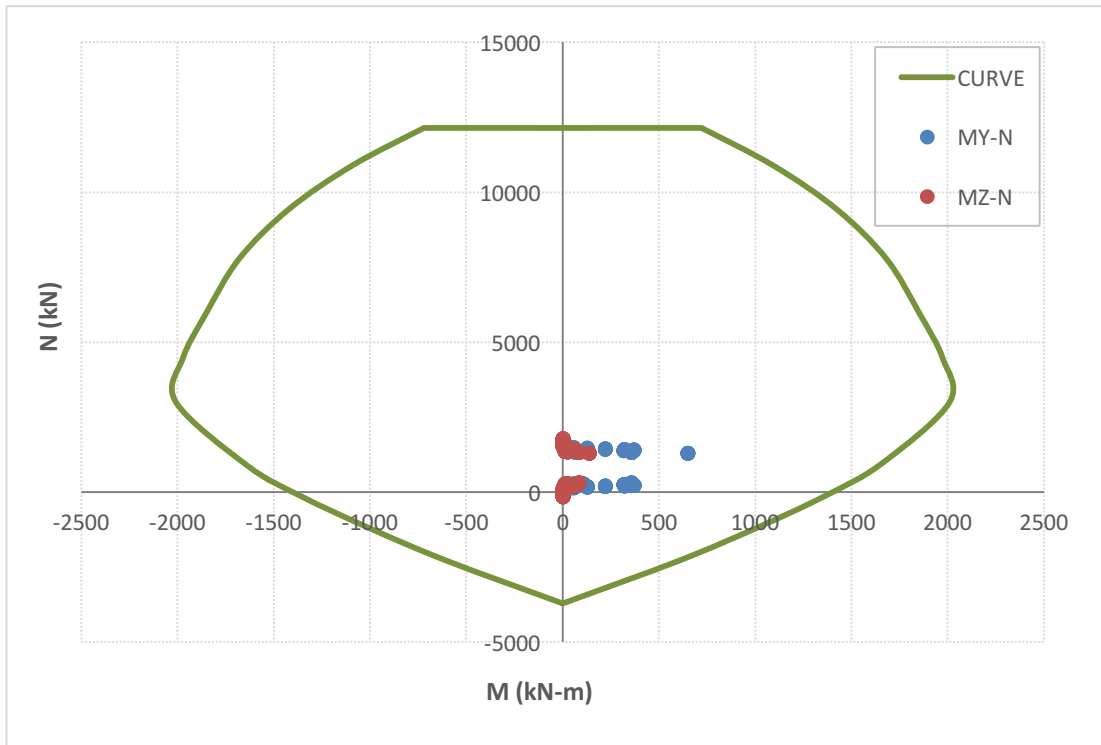


Figure A.25. Q<sub>25</sub> case pile M-N interaction diagram for Combination 2

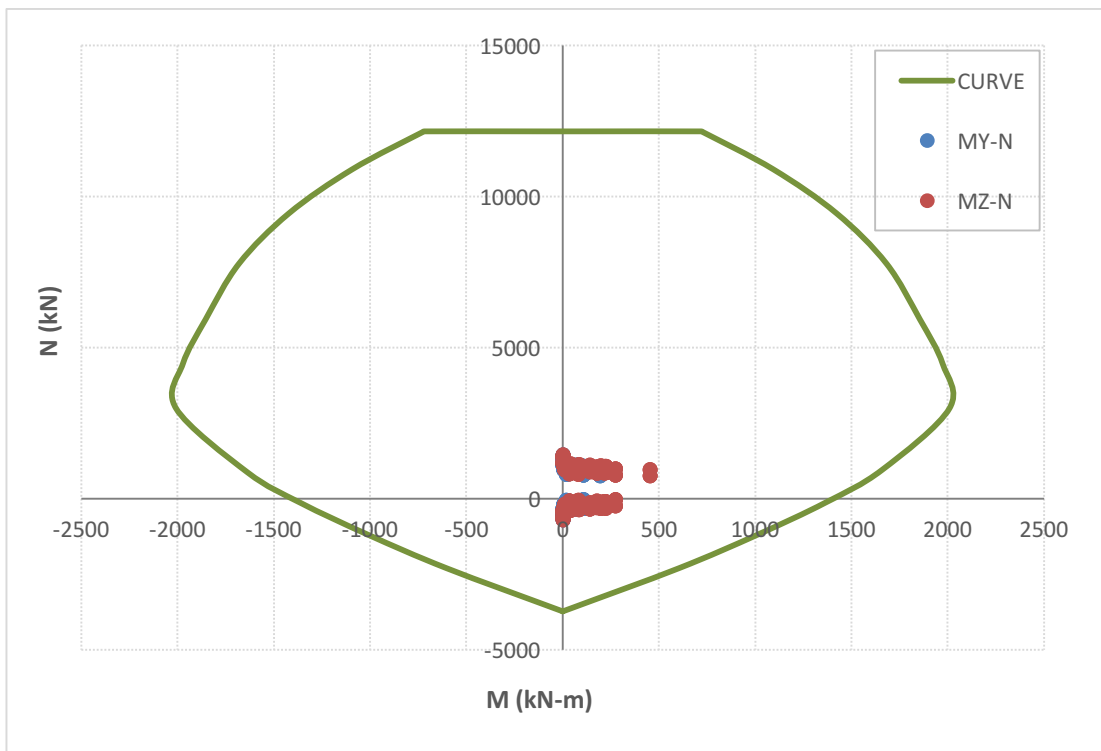


Figure A.26. Q<sub>25</sub> case pile M-N interaction diagram for Combination 3

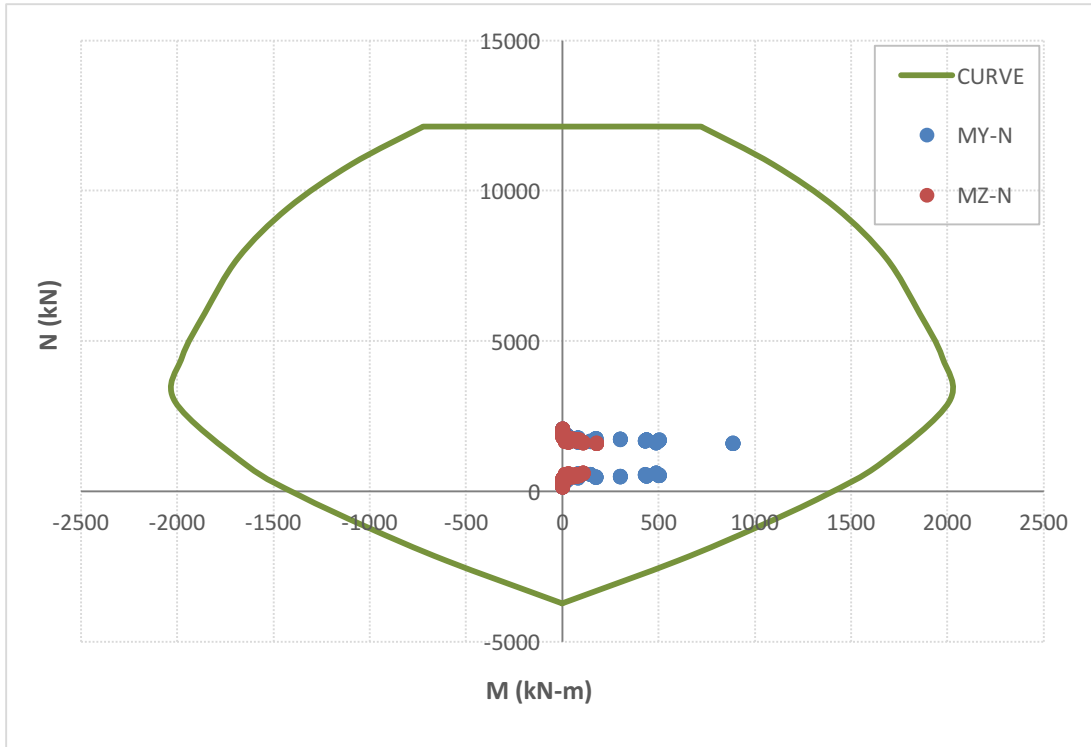


Figure A.27.  $Q_{25}$  case pile M-N interaction diagram for Combination 4

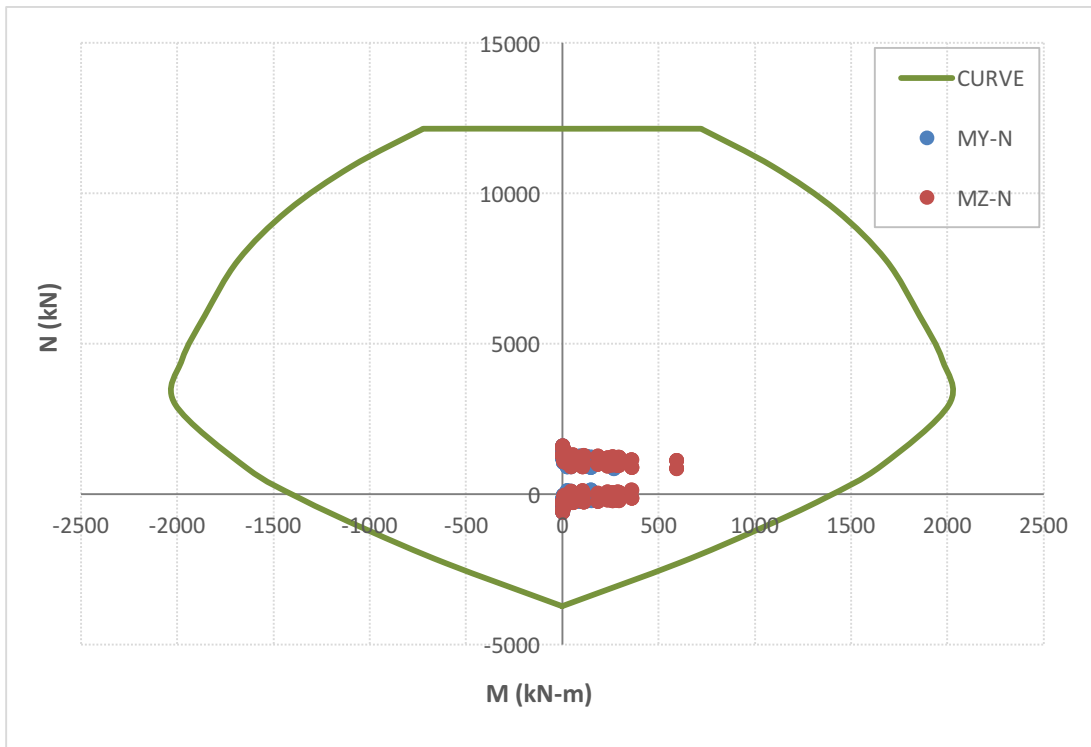


Figure A.28.  $Q_{25}$  case pile M-N interaction diagram for Combination 5

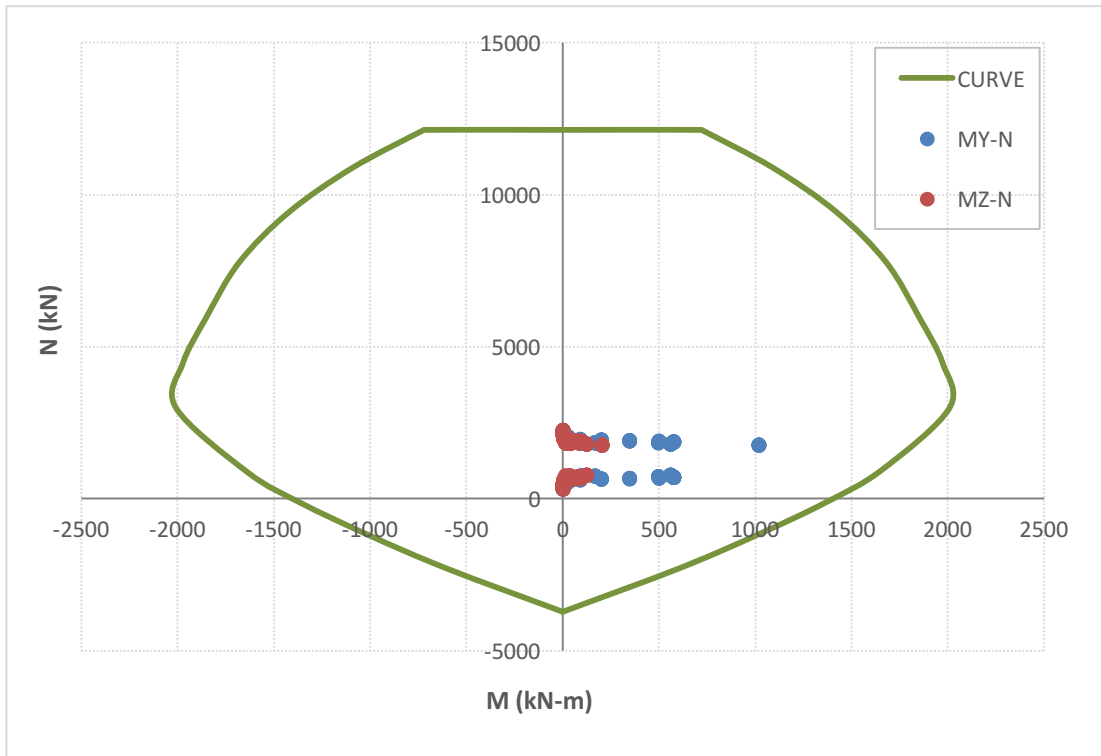


Figure A.29. Q<sub>25</sub> case pile M-N interaction diagram for Combination 6

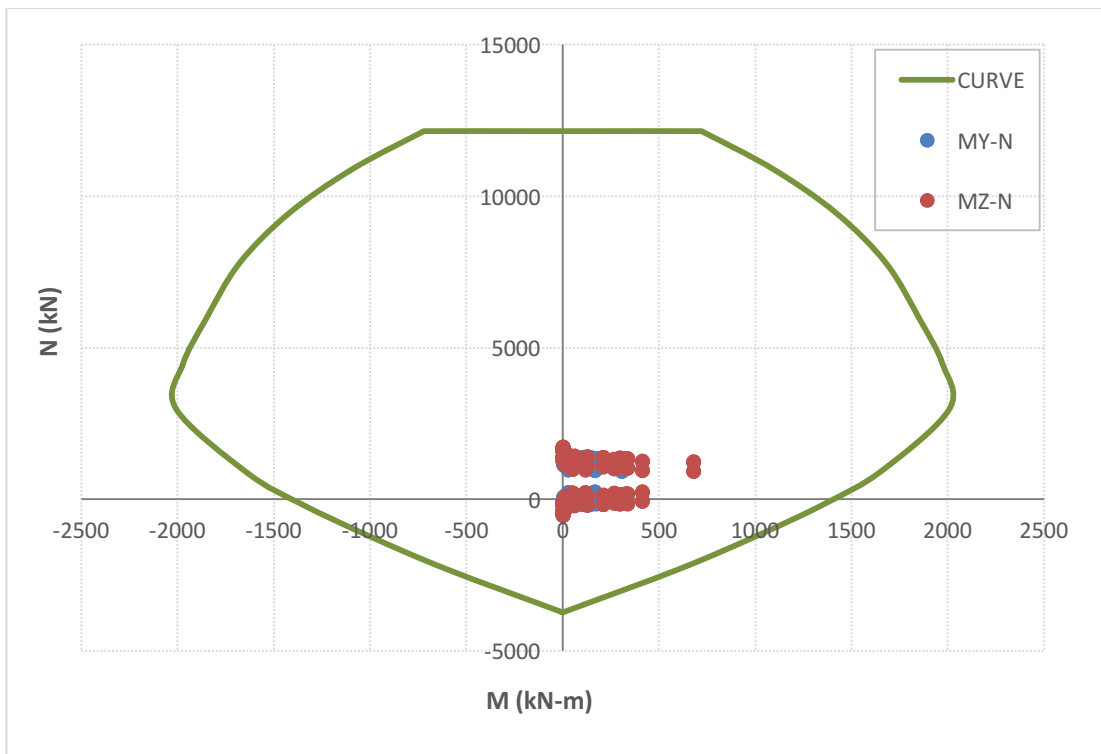


Figure A.30. Q<sub>25</sub> case pile M-N interaction diagram for Combination 7

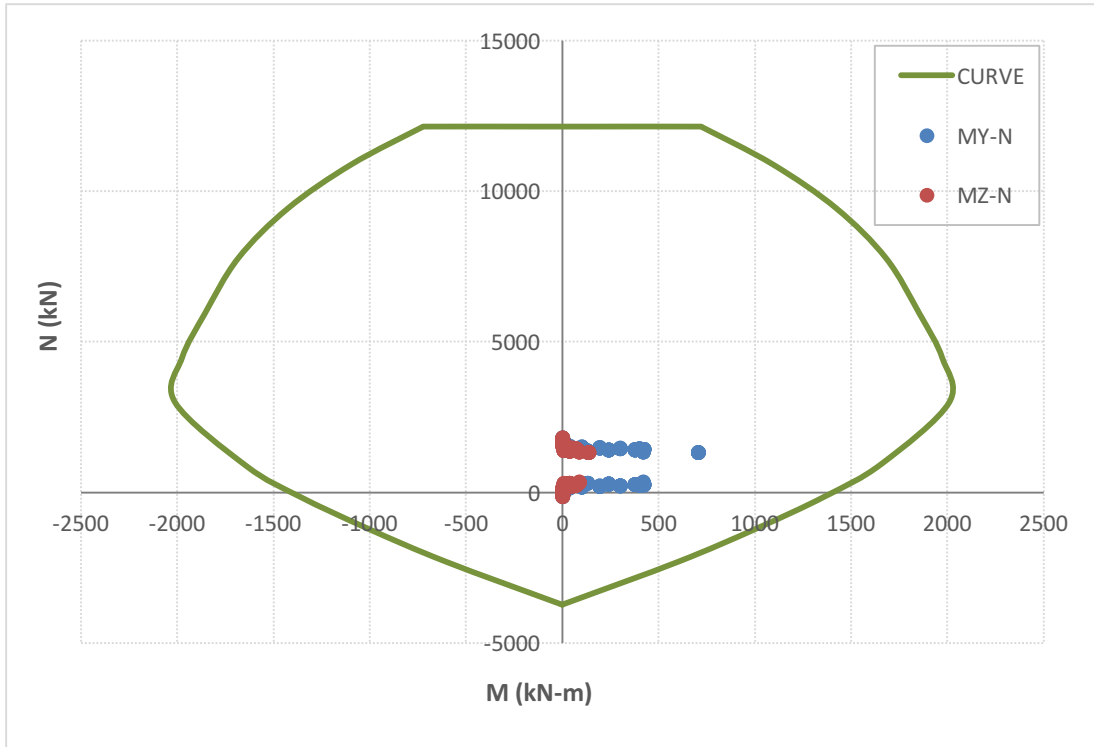


Figure A.31.  $Q_{50}$  case pile M-N interaction diagram for Combination 2

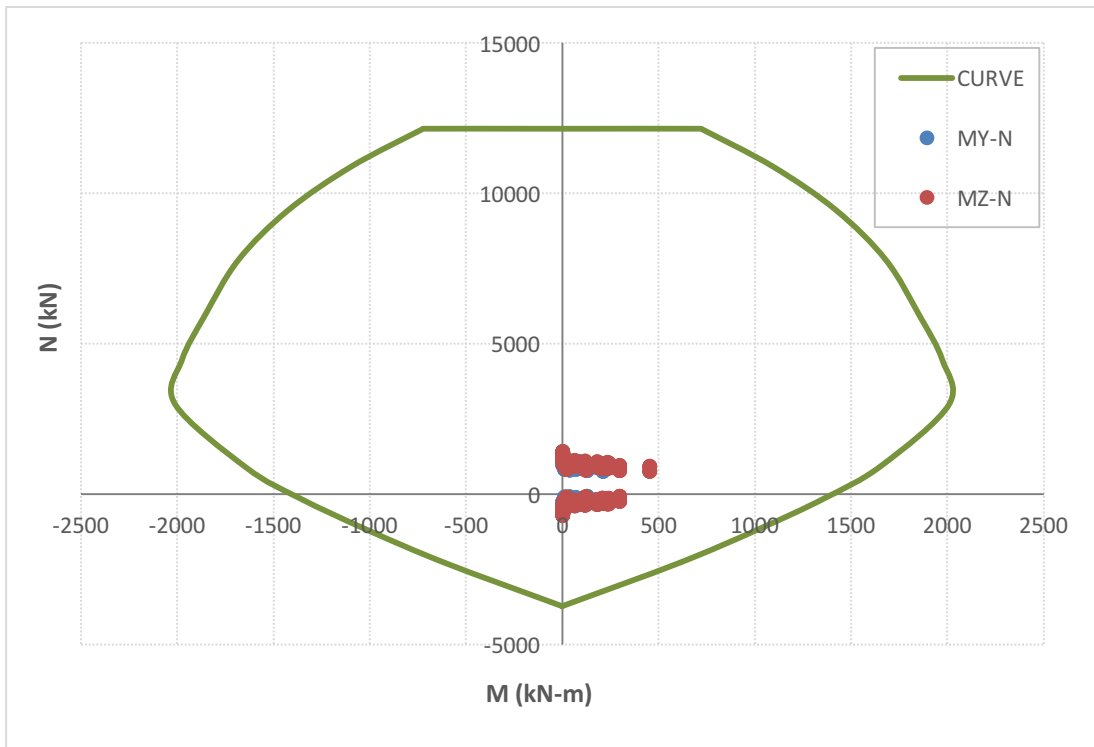


Figure A.32.  $Q_{50}$  case pile M-N interaction diagram for Combination 3

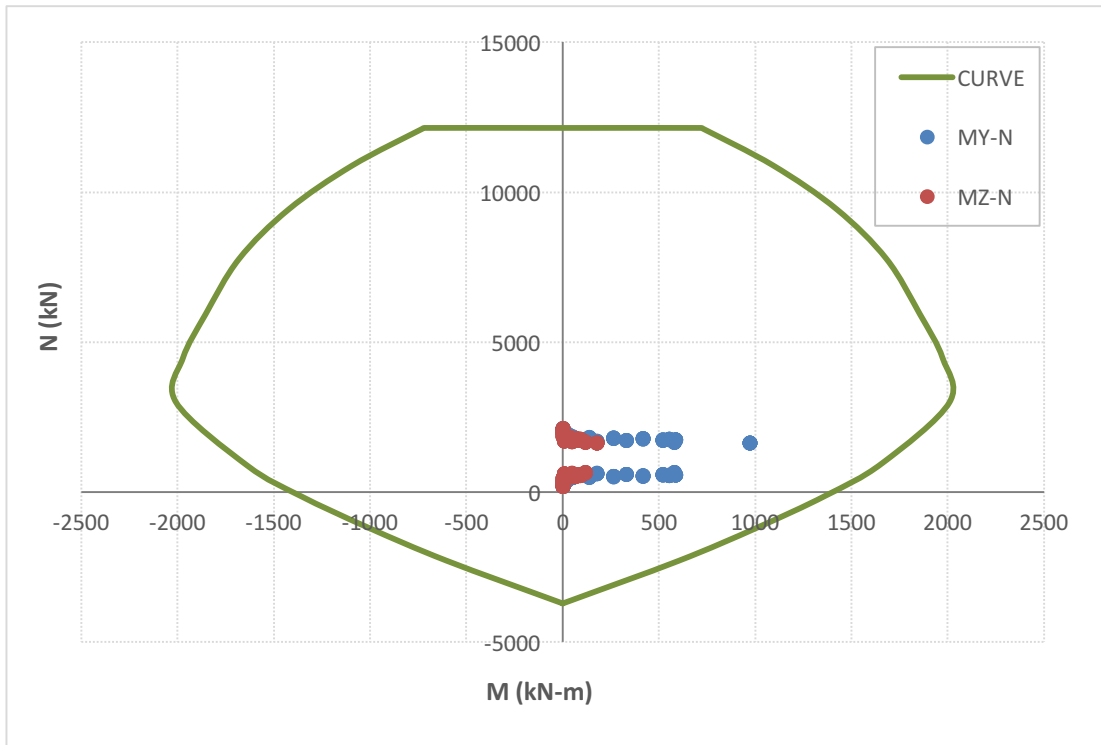


Figure A.33.  $Q_{50}$  case pile M-N interaction diagram for Combination 4

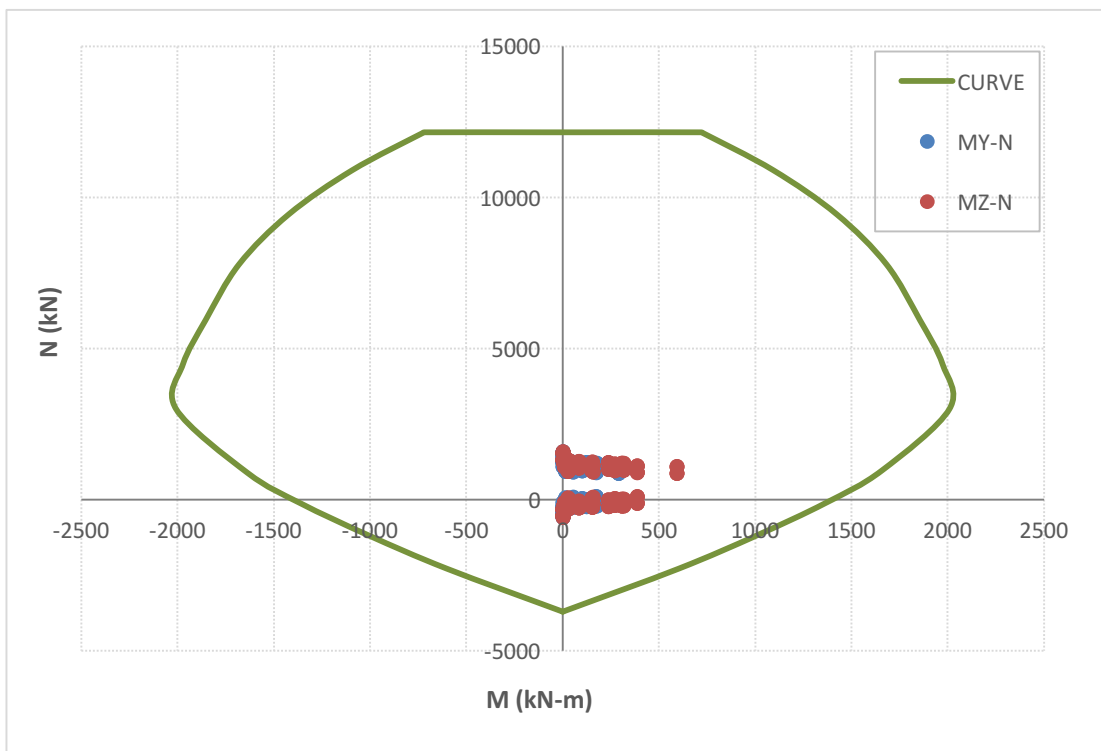


Figure A.34.  $Q_{50}$  case pile M-N interaction diagram for Combination 5

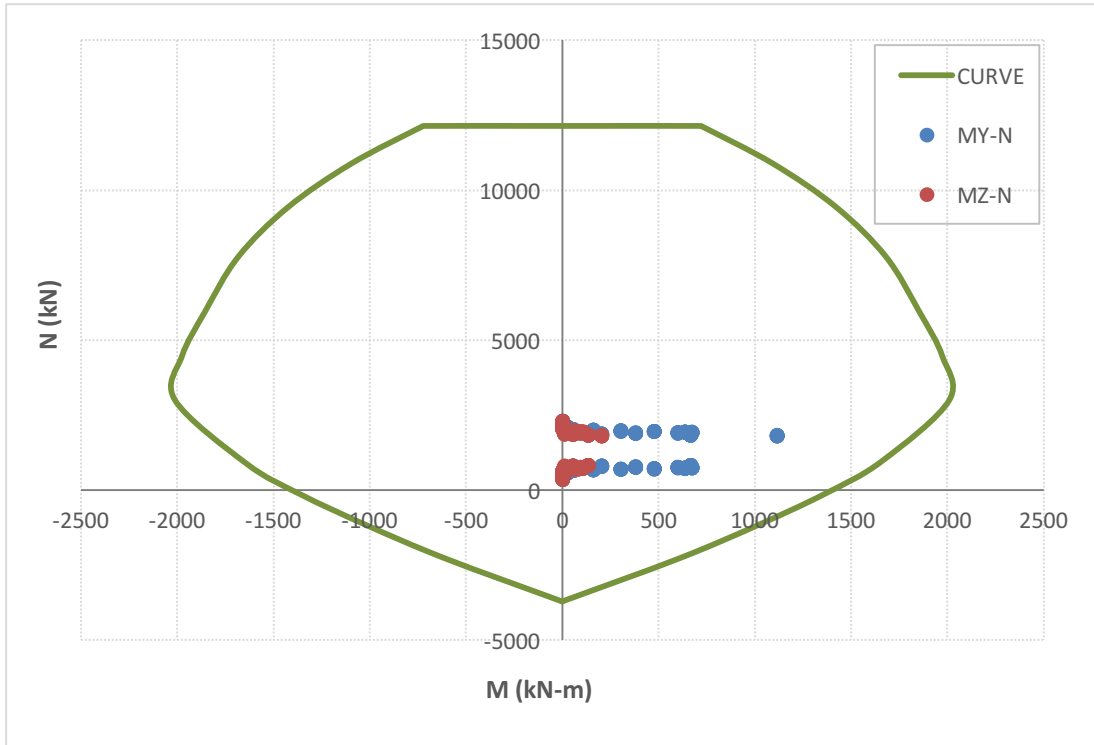


Figure A.35.  $Q_{50}$  case pile M-N interaction diagram for Combination 6

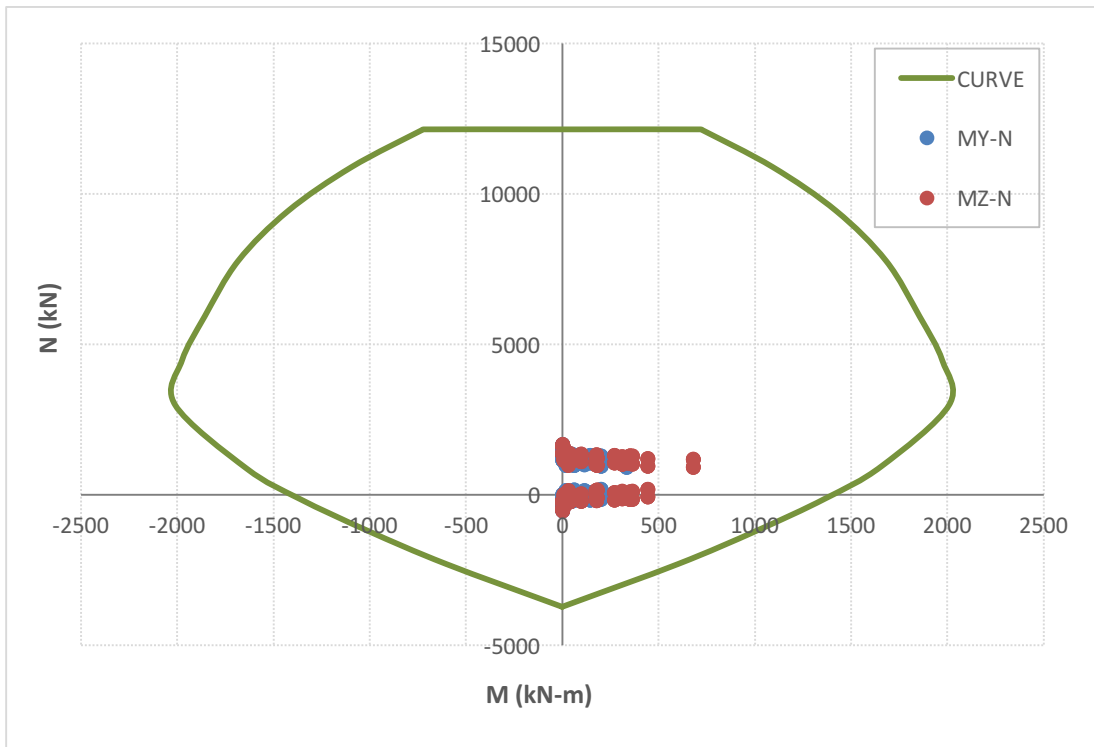


Figure A.36.  $Q_{50}$  case pile M-N interaction diagram for Combination 7

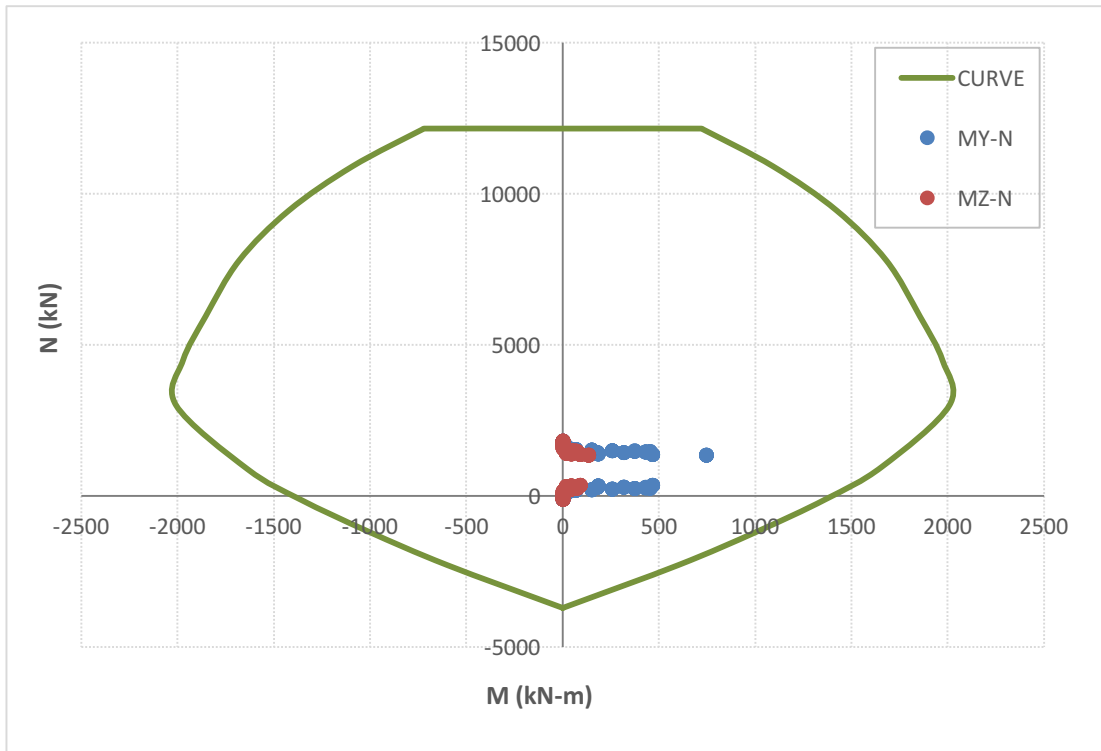


Figure A.37.  $Q_{100}$  case pile M-N interaction diagram for Combination 2

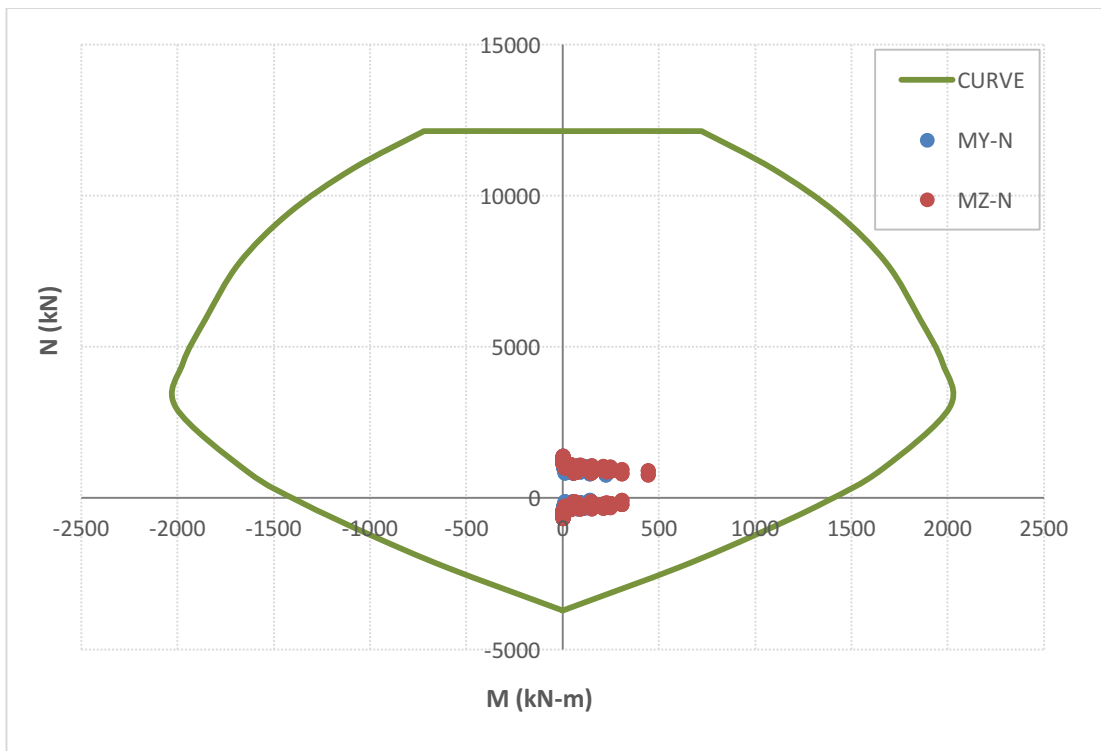


Figure A.38.  $Q_{100}$  case pile M-N interaction diagram for Combination 3

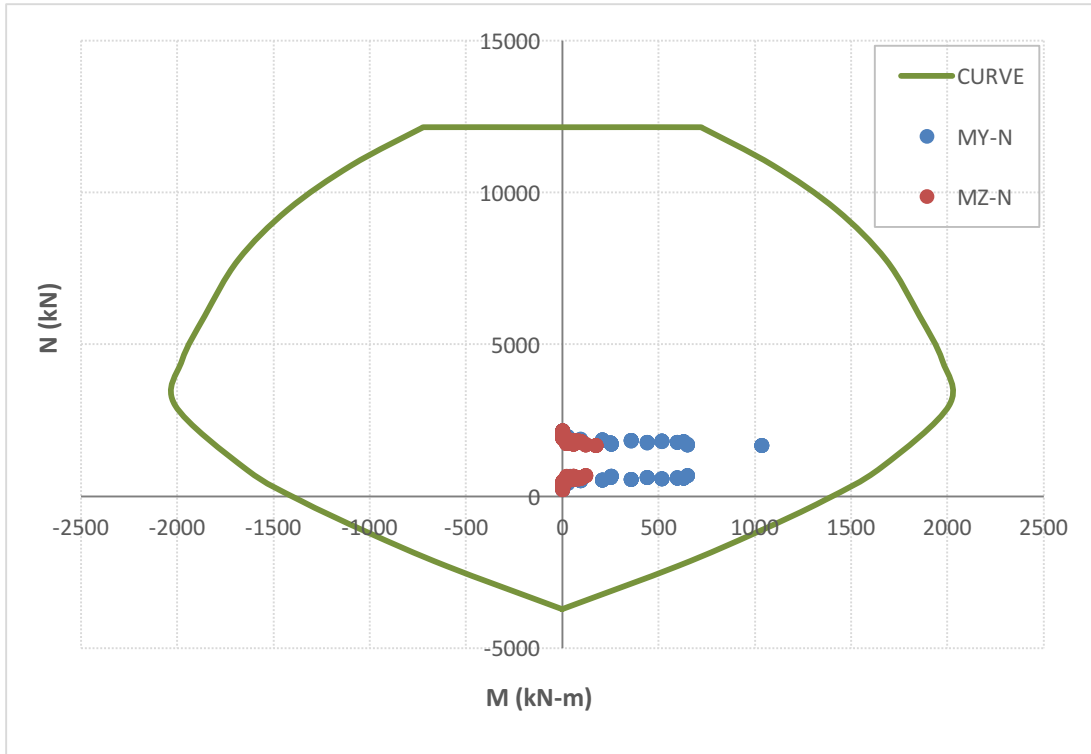


Figure A.39.  $Q_{100}$  case pile M-N interaction diagram for Combination 4

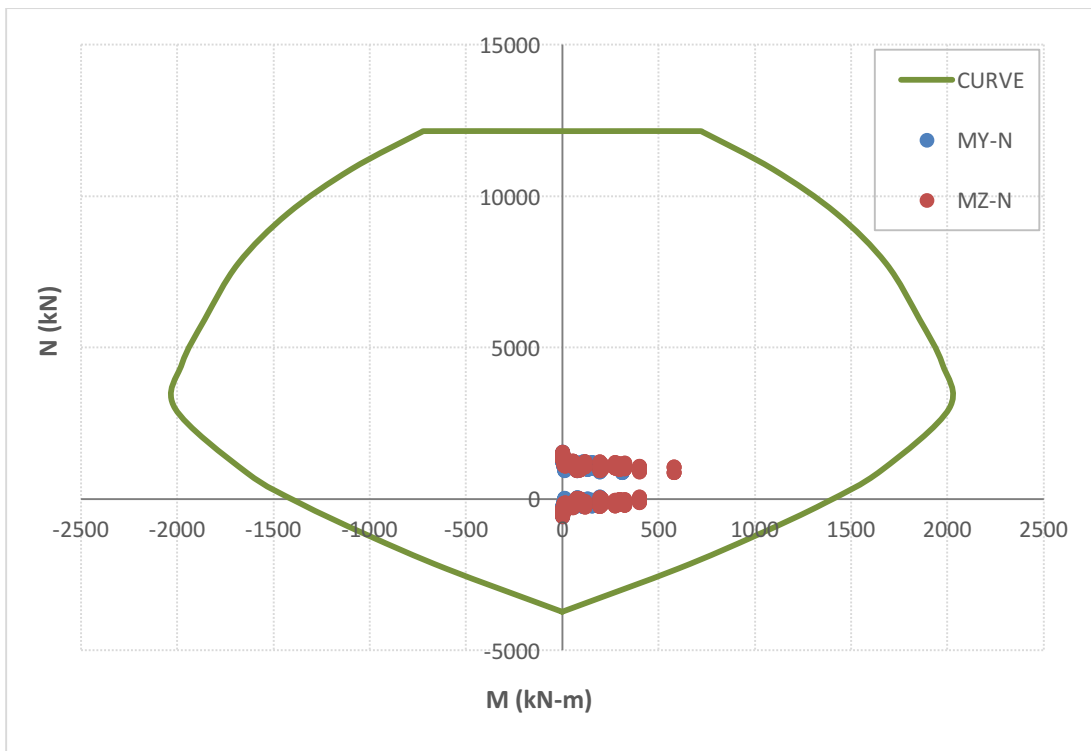


Figure A.40.  $Q_{100}$  case pile M-N interaction diagram for Combination 5

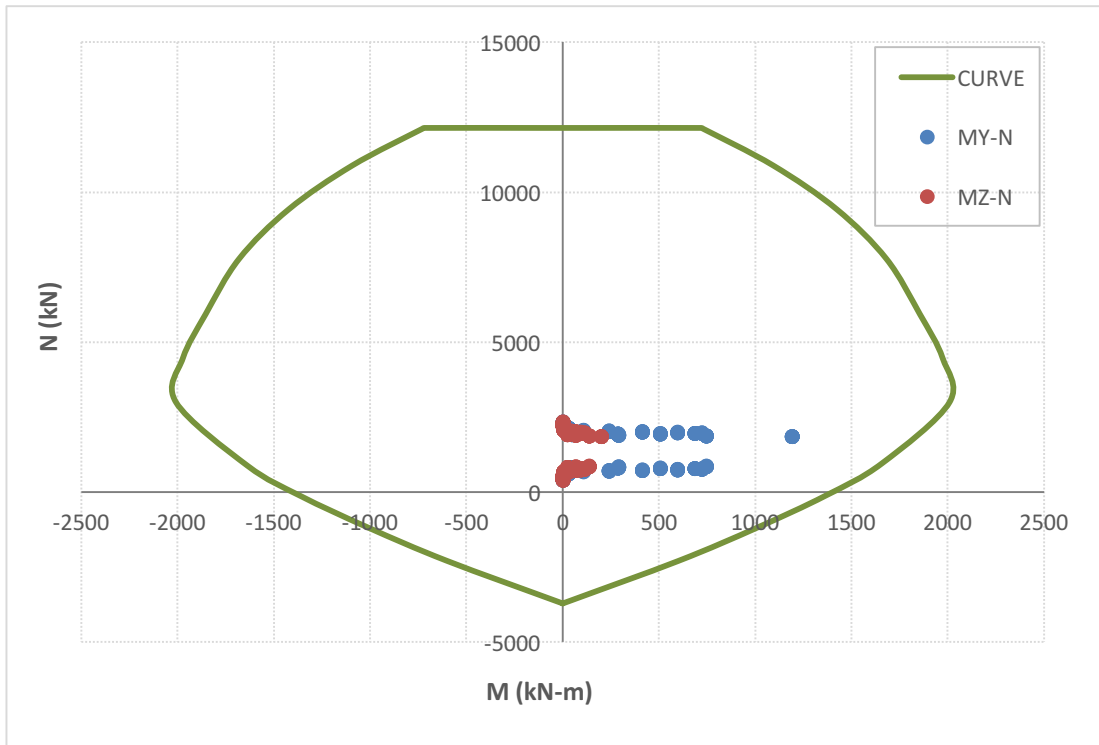


Figure A.41.  $Q_{100}$  case pile M-N interaction diagram for Combination 6

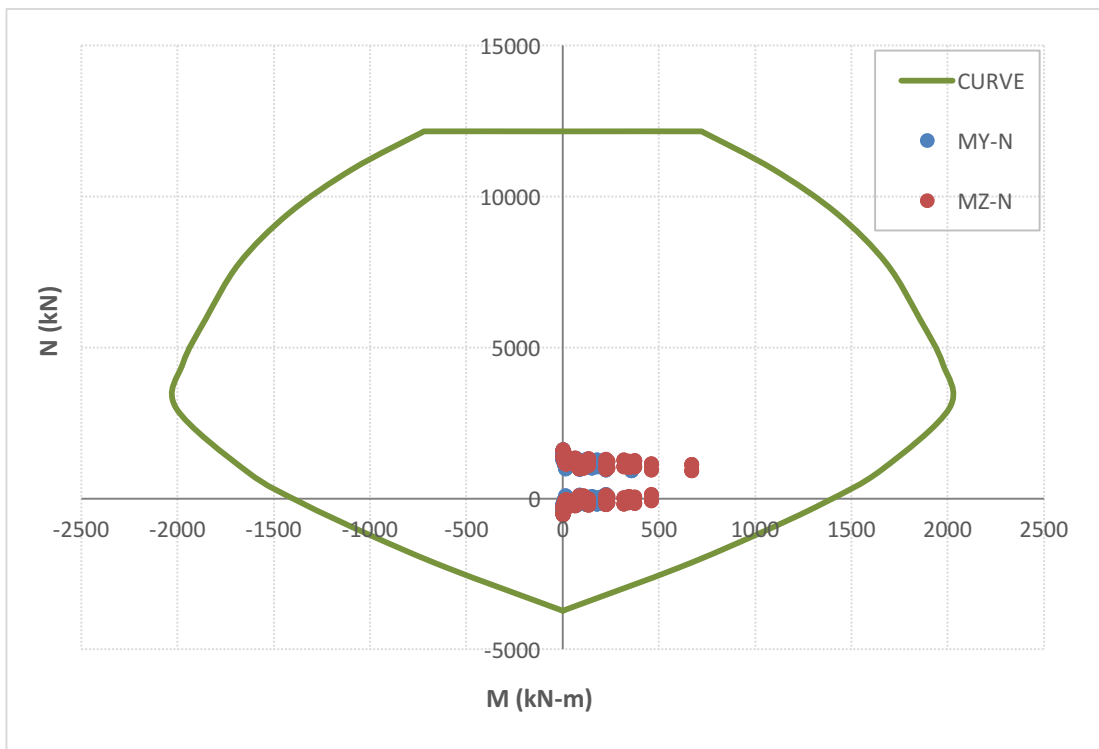


Figure A.42.  $Q_{100}$  case pile M-N interaction diagram for Combination 7